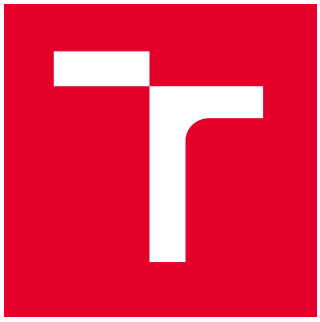

BRNO UNIVERSITY OF TECHNOLOGY

VYSOKÉ UČENÍ TECHNICKÉ V BRNĚ

FACULTY OF ELECTRICAL ENGINEERING AND COMMUNICATION

FAKULTA ELEKTROTECHNIKY
A KOMUNIKAČNÍCH TECHNOLOGIÍ

DEPARTMENT OF BIOMEDICAL ENGINEERING

ÚSTAV BIOMEDICÍNSKÉHO INŽENÝRSTVÍ

MODELLING OF THE HUMAN RESPIRATORY SYSTEM FOR CLINICALLY RELEVANT APPLICATIONS

MODELOVÁNÍ RESPIRAČNÍHO SYSTÉMU ČLOVĚKA PRO KLINICKY RELEVANTNÍ APLIKACE

DOCTORAL THESIS
DIZERTAČNÍ PRÁCE

AUTHOR — Ing. Richard Paštěka, MSc
AUTOR PRÁCE

SUPERVISOR — doc. Ing. Radim Kolář, Ph.D.
ŠKOLITEL

BRNO 2022

ABSTRACT

The increasing incidence of respiratory diseases burdens the world's population and drives major scientific advances in the area of respiratory research. Various models of the human respiratory system are being developed to increase the knowledge and to allow for studies of specific research questions. This thesis aims to establish a physical model of the human respiratory system (xPULM™) that represents an innovative approach to respiratory system behaviour modelling.

To reach this aim, three clinically relevant applications were researched, namely (i) breathing simulation, (ii) patient-ventilator interaction testing and (iii) aerosolised drug delivery. Measurement setups were developed allowing for each application to be tested and evaluated. This process, among other developments, included manufacturing of a physical model of the human upper respiratory tract and the integration of an optical aerosol spectrometer.

The main finding per application is as follows. First, the breathing simulation has been shown to reliably capture flow and pressure changes for a range of tidal volumes and frequencies and to be representative of human breathing. The possibility of using polymer or organic-based lung equivalents is unique and allows for the representation of processes naturally occurring during the human respiration cycle. Second, a new approach to testing patient-ventilator interactions has been introduced. The results show that different asynchronies can be triggered when the simulator is used to represent a patient undergoing assisted mechanical ventilation. Third, the number concentration and size distribution of aerosol particles generated by commonly used dry powder inhalers can be experimentally evaluated during simulations of inhalation and exhalation. This approach proposes an alternative to animal experimentation suitable for applications in aerosol research.

The thesis contains original research that has been presented at international conferences and published in three impact factor journals. The results of this thesis enable further teaching and research activities in respiratory research.

KEYWORDS

human respiratory system modelling, lung simulation, breathing simulation, patient-ventilator interactions testing, aerosolised drug delivery

Author's Declaration

Author:	Ing. Richard Paštěka, MSc.
Author's ID:	134379
Paper type:	Doctoral thesis
Academic year:	2021/22
Topic:	Mechanický plicní simulátor pro účely simulace lidského dýchání

I declare that I have written this paper independently, under the guidance of the advisor and using exclusively the technical references and other sources of information cited in the paper and listed in the comprehensive bibliography at the end of the paper.

As the author, I furthermore declare that, with respect to the creation of this paper, I have not infringed any copyright or violated anyone's personal and/or ownership rights. In this context, I am fully aware of the consequences of breaking Regulation § 11 of the Copyright Act No. 121/2000 Coll. of the Czech Republic, as amended, and of any breach of rights related to intellectual property or introduced within amendments to relevant Acts such as the Intellectual Property Act or the Criminal Code, Act No. 40/2009 Coll. of the Czech Republic, Section 2, Head VI, Part 4.

Brno ....

author's signature*

*The author signs only in the printed version.

ACKNOWLEDGEMENT

I would like to thank the advisor of my thesis, doc. Ing. Radim Kolář Ph.D., and expert advisors FH-Prof. Dr. Andreas Drauschke and FH-Prof. Mathias Forjan, PhD, MSc for their support and valuable comments.

Contents

List of Figures

List of Tables

Introduction

The epidemiological transition is a term referring to a complex and dynamic process of the shift from acute infectious diseases to chronic non-communicable diseases [1], [2]. This transition has already largely occurred in developed high-income countries, where non-communicable diseases accounted for up to 85% of deaths in 2019 [3]. Leading causes are diseases of the circulatory system, respiratory system, and cancer [3], [4]. A rapid epidemiological transition can be observed in many middle-income countries as well [5]. In low-income countries, non-communicable diseases were responsible for more than half of all deaths and their fraction is predicted to further increase with modernisation [1]–[3]. Furthermore, the statistic from countries belonging to the Organisation for Economic Co-operation and Development (OECD) reflects this worldwide trend with the leading causes of mortality being: 30% circulatory diseases (11% ischaemic heart diseases; 7% Stroke), 24% cancers (5% lung cancer, 3% colorectal cancer) and 10% respiratory diseases (4% chronic obstructive pulmonary disease).

Most common respiratory diseases include chronic obstructive pulmonary disease (COPD), asthma, allergic diseases, occupational lung diseases, and pulmonary hypertension [6]. Risk factors such as smoking (in both active and passive form), occupational exposure to dust, fumes and chemicals, and air pollution in general, are among the reasons why the number of patients troubled by respiratory diseases continues to grow [3], [6]. Both asthma and COPD significantly affect a person's ability to breathe and can be effectively treated at the primary care level with aerosol therapy [7]. Symptoms of asthma are often seasonal and usually well reversible with treatment. In comparison, COPD is a progressive disease that can only be slowed down through smart maintenance therapy. According to the Global Asthma Network, up to 339 million people may be affected by asthma worldwide [8]. Furthermore 65 million people globally suffer from mild to severe COPD [9], [10]. Note that the most recently available statistics considered here do not include the effects of the COVID-19 pandemic. According to the estimations, respiratory coronavirus infectious disease, COVID-19, will be among the leading causes of death in 2020 and beyond, increasing the total toll of deaths significantly [3], [4].

Severe cases of respiratory diseases like COPD or COVID-19, can lead to respiratory failure [11]–[13]. Respiratory failure is a serious condition in which the respiratory system fails to maintain adequate gas exchange due to a failure of the lung (gas-exchanging organ) and/or the pump that ventilates the lungs [14]. Affected patients require mechanical ventilation to ensure oxygenation and carbon dioxide clearance [13]. During mechanical ventilation disparity between flow, pressure or volume demands of the patient and the assistance delivered by the mechanical ven-

tilator leads to patient-ventilator asynchrony [15]. These asynchronies are linked with negative physical and mental outcomes such as higher mortality, excessive load on respiratory muscles, lung injury and prolonged ICU stay [15]–[17]. For the reasons described above the testing and minimising of patient-ventilator interactions is a direction currently pursued and explored further in this thesis.

Chronic respiratory diseases are not curable and affect the lungs and airways [18]. These diseases can cause airflow limitation due to airway obstruction, an abnormal inflammatory response of the lungs and other severe problems leading to breathing difficulties [19]. Various forms of treatment that help dilate major airways and increase patients' quality of life are well established [18]. Aerosol therapy is a treatment of choice due to easy drug delivery options, sustained localised action and the possibility of home therapy. The number of drugs delivered in the form of aerosols increases every year because of advancements in aerosol manufacturing and easy-to-use personal inhalation devices [20]. This trend is reflected in growing total worldwide sales of inhalation products [21]. Inhalation therapy devices can be categorised into four main types, including nebulisers, pressurised-metered dose inhalers (pMDI), soft mist inhalers (SMI), and dry powder inhalers (DPI) [22]. Such devices are being continuously developed, evaluated and tested under various conditions. For these reasons, the testing of DPIs is one of the key research topics explored in this thesis.

The statistics regarding respiratory disease covered here might provide a rather negative perspective on the trajectory of human pulmonary health. However, the increasing incidence of respiratory diseases is driving major scientific advances in the area of respiratory research. Various models of the human respiratory system are being developed to increase knowledge and to allow for studies of specific research questions. The common denominator is the effort of the researchers to provide the best possible treatment options for the patients.

Based on the experimental setup, the models used in respiratory research can be divided into four main categories: (1) in vivo (2) in vitro (3) in silico and (4) ex vivo.

In vivo based studies are testing various effects on whole, living organisms such as small animals (e.g. guinea pigs, rats, mice) [23], large animals (e.g. rabbits, pigs, non-human primates) [24] or humans. Animal experimentation has a prominent role in many scientific advancements but presents a challenging ethical dilemma of causing pain and suffering to the animal [25]. By complying with ethical guidelines and good scientific practices the animal welfare and human science principles can be upheld [25], [26].

All modern research endeavours should comply with the principles of 3Rs that were proposed by Russell and Burch [27] in 1959. Namely [28]:

- "a *replacement* of animals in research, which results from an active development of alternatives;"
- "a *reduction* in the number of animals used in experiments;"
- "a *refinement* of laboratory and field techniques to reduce invasiveness and/or to increase the values of the results."

Subsequently, increasing efforts are being invested in the development and validation of alternatives to animal experimentation. These efforts have been instigated by legislative powers like the EU directive on the protection of animals used for scientific purposes (2010/63/EU) and by the growing involvement of the general public [29]. The following paragraphs provide an overview of experimental setups that can be developed in compliance with 3Rs and hence provide alternatives to animal experimentation.

In vitro models can use isolated living components of organisms such as cells or biological molecules for experiments. However, animals and humans are not directly involved, except as donors of biological material [30]. In vitro studies are conducted in a laboratory vessel or elsewhere outside the living body. The latest in vitro models in the field of respiratory research are based on organ-on-a-chip, and microfluidic technologies [31]. Prominent examples include modelling and diagnosis of chronic respiratory diseases [32]–[34], toxicity assessment of various compounds [35], [36] and development of novel drugs [37].

The in silico models (referring to the silicon used for semiconductor computer chips) are utilised to create computer representation of their in vivo counterparts (e.g., organs, systems and processes) [38]. Two breakthroughs facilitating rapid development in the area of in silico based respiratory models can be identified in recent years. The first impulse was the introduction of the respiratory tract model for radiological protection by the International Commission on Radiological Protection (ICRP) [39]. The second catalyst was the advancement of computational fluid-particle dynamics (CFPD) methods [40], [41]. These methods offer a possibility to predict airflow and to localise aerosol particle deposition in the human respiratory tract [42], [43].

The ex vivo models, also called in vitro tissue-based models, include procedures with living functional tissues or organs isolated from an organism and sustained outside the organism in an artificial environment under highly controlled conditions [44]. The ex vivo models allow for tests and measurements that would be difficult to conduct in a living subject under controlled conditions at all times [45]. They provide a valuable resource for translational medicine and are especially suitable for studying the mechanisms of lung injury, lung deposition of inhaled therapeutics on

a regional level, and toxicity tests [23], [46], [47].

Original research presented in this thesis introduces and utilises a model of the human respiratory system xPULM™, that incorporates aspects of in vitro, in silico and ex vivo modelling approaches.

The use of models in respiratory research and the range of their possible applications is growing. For the context of this work the key applications include breathing and lung simulation [48]–[51], education and training of students/health professionals [52]–[54], testing of mechanical ventilators [55]–[57], and aerosolised drug delivery [58]–[61].

Aim of the thesis

This thesis aims to establish a physical model of the human respiratory system (xPULM™) that represents an innovative approach to respiratory system behaviour modelling. To reach this aim, three clinically relevant applications were researched, namely (i) breathing simulation, (ii) patient-ventilator interaction testing and (iii) aerosolised drug delivery. The goals of the thesis consider the available instrumentation at the University of Applied Sciences Technikum Wien. This thesis has been developed as a part of continuous cooperation between the University of Applied Sciences Technikum Wien and the Brno University of Technology. Further cooperation partners include the University of Trás-os-Montes E Alto Douro and the hospital Centro Hospitalar De Trás-Os-Montes E Alto Douro whose engagement allowed for the acquisition of CT examinations from a retrospective clinical trial.

The goals of the thesis are to:

1. Determine the capability of the xPULM™ to reproducibly simulate human breathing patterns. The breathing simulation should be evaluated for a variety of breathing frequencies and tidal volumes while using different lung equivalents (e.g. polymer-based bags, lungs obtained from animals). Modify hardware and software components to advance the model towards anatomically and physiologically realistic breathing simulation.
2. Obtain information from a retrospective clinical trial focusing on realistic human upper airway geometry. Manufacture a physical model of the human upper respiratory tract and implement it into the existing measurement setup. The model should approximate anatomical structures (oral cavity, the pharyngeal region and the first centimetres after the larynx) of a healthy human.
3. Develop, implement and test a measurement setup allowing for simulation of a patient undergoing mechanical ventilation. Determine the undesired interactions occurring between the mechanical ventilator and the simulated patient. Discuss comparability of results to situations occurring in clinical practice.
4. Develop, implement and test a measurement setup allowing for experimental evaluation of dry powder inhalers. Include optical aerosol spectrometry technology to measure the characteristics of inhaled particles. Evaluate the results and discuss their comparability to findings reported in the available literature.
5. Discuss the obtained results in the context of respiratory research. Outline further directions in modelling of the human respiratory system.

Structure of the thesis

This thesis consists of the following chapters: Introduction, Aim of the thesis, Structure of the thesis, 3 main numbered chapters, Conclusion, Further directions & future work, and Appendix A & B .

The Introduction outlines the motivation behind the development of models in respiratory research, summarises the state-of-the-art of human respiratory system modelling and their applications. The core of the dissertation is the original research divided into the following numbered chapters.

Chapter 1 focuses on the evaluation of the xPULM™ and its ability to simulate human breathing patterns. This research was published in the journal Scientific Reports in 2019 [62]. Chapter 2 deals with asynchrony effects originating from a disparity between flow, pressure or volume demands of the patient and the assistance delivered by the mechanical ventilator. This research was published in the journal Applied Sciences in 2021 [63]. Chapter 3 focuses on the experimental evaluation of aerosolised drug delivery with DPIs. This research was published in the journal Pharmaceutics in 2022 [64]. Aerosol particle diameter and particle number concentration of pharmaceutical aerosols generated by four dry powder inhalers were explored under realistic inhalation and exhalation conditions.

Appendix A, presents continuous work regarding breathing simulation research. Reliable breathing simulation is fundamental for applications presented in chapters 1– 3. The comparison of the simulation to spirometry measurements was presented at the international conference EMBEC2017 and published as [65]. The simulations of breathing at rest and artificially ventilated patients were presented at the international conference PDES2018 and published as [66]. The evaluation of waveforms suitable for testing of inhalation devices was presented at EMBEC2021 and published as [67].

Appendix B, summarises findings regarding the experimental assessment of the aerosol particle deposition. These findings facilitated the evaluation of dry powder inhalers provided in chapter 3. The analysis of the xPULM™ for aerosol inhalation test replacement, was presented at the international conference WC10 and published as [68]. The comparison of breathing patterns for aerosol inhalation was presented at the international conference EUSAAT2018 and published as [69]. The changes of particle deposition caused by different breathing patterns were presented at the international conference EMBC2019 and published as [70].

Throughout this thesis, the xPULM™ is referred to either as the "electromechanical lung simulator" or the "human respiratory system model". The latter is used when additional components (e.g., replicas of the upper airways) and software is used to model both the upper and lower human respiratory tract simultaneously.

1 Breathing simulation using polymer and organic human lung equivalents

Abstract

Simulation models in respiratory research are increasingly used for medical product development and testing, especially because in vivo models are coupled with a high degree of complexity and ethical concerns. This work introduces a respiratory simulation system, which is bridging the gap between the complex, real anatomical environment and the safe, cost-effective simulation methods. The presented electro-mechanical lung simulator, xPULM™, combines in silico, ex vivo and mechanical respiratory approaches by realistically replicating an actively breathing human lung. The reproducibility of sinusoidal breathing simulations with xPULM™ was verified for selected breathing frequencies (10-18 bpm) and tidal volumes (400-600 mL) physiologically occurring during human breathing at rest. Human lung anatomy was modelled using latex bags and primed porcine lungs. High reproducibility of flow and pressure characteristics was shown by evaluating breathing cycles (n_{Total}=3273) with highest standard deviation $|3\,\sigma|$ for both, simplified lung equivalents ($\mu_{\dot{V}}$=23.98±1.04 L/min, μ_P=-0.78±0.63 hPa) and primed porcine lungs ($\mu_{\dot{V}}$=18.87±2.49 L/min, μ_P=-21.13±1.47 hPa). The adaptability of the breathing simulation parameters, coupled with the use of porcine lungs salvaged from a slaughterhouse process, represents an advancement towards anatomically and physiologically realistic modelling of human respiration.

Keywords

respiration simulation, biomedical electro-mechanical systems, alternative to animal testing, lung simulation, primed porcine lungs, biomedical engineering education

This chapter is published as:

- R. Pasteka, M. Forjan, S. Sauermann, and A. Drauschke, "Electro-mechanical Lung Simulator Using Polymer and Organic Human Lung Equivalents for Realistic Breathing Simulation," Sci. Rep., vol. 9, no. 1, p. 19778, Dec. 2019, doi: 10.1038/s41598-019-56176-6.

Author contributions statement:

- R.P., M.F., S.S., A.D. designed the experimental setup, R.P conducted the simulation with the mathematical model, R.P., M.F. conducted the experiments, R.P., M.F. processed and analysed the data, R.P., M.F. wrote the manuscript, R.P. prepared figures and tables. All authors reviewed the manuscript.

1.1 Introduction

Animal testing helped catalyse rapid advancement in many areas of medical engineering by providing insights into the complex functionality of living organisms. Nevertheless, ethical and economic concerns have been raised for years [25]. Because of these concerns, the principle of 3Rs (Replacement, Reduction and Refinement) must be followed before including animals into any testing procedure [27], [71]. General consensus dictates to avoid using animal tests whenever reliable and consistent alternatives are available [27]. These efforts have been instigated also by legislative powers e.g. the EU Directive 2010/63/EU [72] and EU regulation 2019/1010/EU [73], which have been formed with the aim of reducing the number of animals used for testing. Hence development and validation of new alternatives to animal testing are encouraged [74].

In medicine, simulation techniques are adopted mainly for equipment testing, treatment planning and medical staff education. Simulation devices comply with the increasing requirements on patient safety and provide educational opportunities in a standardised manner. The field-specific applications of simulation devices are also growing [75]. One of the most important driving forces for the development of models in respiratory research is the increasing incidence of pulmonary disease amongst the world's population. Deeper insight into the respiratory process would increase development potentials for respiratory care devices and treatment techniques. The latter is particularly important with a growing portion of the population suffering from obstructive and restrictive pulmonary diseases [76]. The Organisation for Economic Cooperation and Development (OECD) has reported, that 6.1% of the population in Europe aged 15 years or older suffers from asthma. The chronic obstructive pulmonary disease (COPD) further affects 4.0 % of the same population group according to the EU wide health survey [77]. The ability of a person to breathe is negatively influenced by both asthma and COPD, thus, significantly affecting the quality of life. The modelling of the affected organs in the human body is a state of the art method to extend the knowledge through specific tests.

Depending on the experimental measurement setup the respiratory models can be divided into in vivo models, in vitro testing procedures, in silico models and mechanical lung simulators. The first category covers in vivo measurement setups employing laboratory animals or human probands during testing. The complex systemic response of the organism to the particular event which is nearly impossible to simulate otherwise can be obtained using such techniques [23]. According to the 3R principle [27], [71],in vivo studies should be limited and replaced by alternative approaches whenever applicable.

Representing the second category of in vitro techniques is the emerging field

of microfluid based lab-on-chip technology. This technology commonly focuses on specific layers of cell cultures and their various interactions on a cellular level. Simultaneously, up to four cell types may be included. Lung-on-chip technology provides valuable insides about the toxicity of tested substances and in virology studies [78]. The third category of in silico models currently in use is based on the mathematical simulation of general transport equations [79]. Adjustments of the in silico models according to individual airway geometries and adaptability of initial and boundary conditions can provide information about the physical airflow field in sub-millimetre areas [80], [81]. The fourth category of mechanical based respiratory models, in general, simulate human breathing process by volume displacement within defined compartments. The compartments used vary depending on the focused problematic and can include electro-mechanically driven syringes, bellows systems or pneumatically driven cylinder systems. The volume displacement can be driven by an external device, most commonly a medical ventilator, or by simulator's active components e.g. servo-motors. [52], [82], [83] The mechanical models can in general accurately control simulation parameters (tidal volume, respiratory rate, etc.) making a simulation of the breathing patterns physiologically authentic. Additionally, they can offer an inexpensive alternative to in vivo animal testing approaches, due to the wide range of usable components [84]. More sophisticated mechanical models are able to represent anatomical structures of the human respiratory system via the inclusion of realistic lung equivalents and simulate further physiologically occurring respiratory processes such as pleural depression. Moreover, various pathological conditions such as airway obstructions can be flexibly simulated by introducing resistor components. Experimental measurements with mechanical simulators are used as a basis for validating numerical models of the respiratory system, medical product development and aerosol inhalation studies. Additional application fields include teaching and practical training of students and medical staff for the use of medical ventilators. [48], [54], [85], [86]

Further optimisations of mechanical simulators should consider the respiratory physiology for simulation and modelling purposes. The basic respiratory flow parameters which shall be considered, depending on the accuracy of the simulation, are the breathing frequency (f), tidal volume (V_{T}), inspiratory flow rate ($\dot{V}_{\mathrm{INS}}$), expiratory flow rate ($\dot{V}_{EXP}$), inhalation time (T_{INS}), exhalation time (T_{EXP}) and breath-holding time (T_{HOLD}) [87], [88]. Taking these parameters into account, the respiratory airflow can be characterised as a periodic, time-dependent function of an incompressible, viscous media [88].

In this work, the electro-mechanical lung simulator xPULM™ is used. The underlying concepts and functional evidence with previous generations of the lung simulator have been described by David et al. and Forjan et.al [89], [90]. Based on

these results xPULM™ as used in this work, was developed. The bellow system described in [90] was again used as a driving mechanism of the volume displacement during the simulation replacing a piston-cylinder system [89]. The xPULM™ additionally includes changes of the operating system, control software and hardware. In previous generations, as described in [89], the computational power of the integrated PC influenced the chosen breathing parameters like frequency and tidal volume. In order to meet the highly demanding and complex boundary conditions of a realistic breathing simulation, a real-time acquisition and processing unit was now implemented as a major change. This development stage allowed to further optimize the already well-established methodology of mechanical breathing modelling. The simulation options, therefore, include measurements with different lung equivalents, adjustable tidal volumes and breathing frequencies. The xPULM™ control software of this version is implemented on a real-time data processing unit making the simulation parameters independent of the computational power of the connected PC. For legal reasons, it was necessary to rename the new model to xPULM™. This paper aims to introduce the electro-mechanical lung simulator xPULM™ in first applications in respiratory research, teaching and training. Design, development and final realisation of the xPULM™, closely following the 3R principles, are described. The functionality of the simulator is demonstrated by reliable and reproducible simulation of breathing patterns with various respiratory simulation parameters. The main distinguishing feature of xPULM™, in comparison to other respiratory models, is the capability of measuring breathing characteristics with the inclusion of simple or complex replicas of human lungs. Modelling of respiratory simulation processes is thereby moved closer to anatomically realistic lung simulation. Potential application, impact and deployment of the simulator in e.g. testing, teaching and research applications are outlined in the discussion. A video clip, recorded during measurements with primed porcine lungs, highlighting the simulation process is uploaded as a part of the submission.

1.2 Matherials & Methods

1.2.1 Mathematical model of the simulator

The electro-mechanical simulator is based on a mathematical model of the entire system, as shown in Fig. 1.1. The governing equations were first derived by Solc et al.[91]. The basis of the mathematical model is a simulation of the thoracic chamber and a lung equivalent both approximated by pneumatic cylinders in Fig. 1.1A.

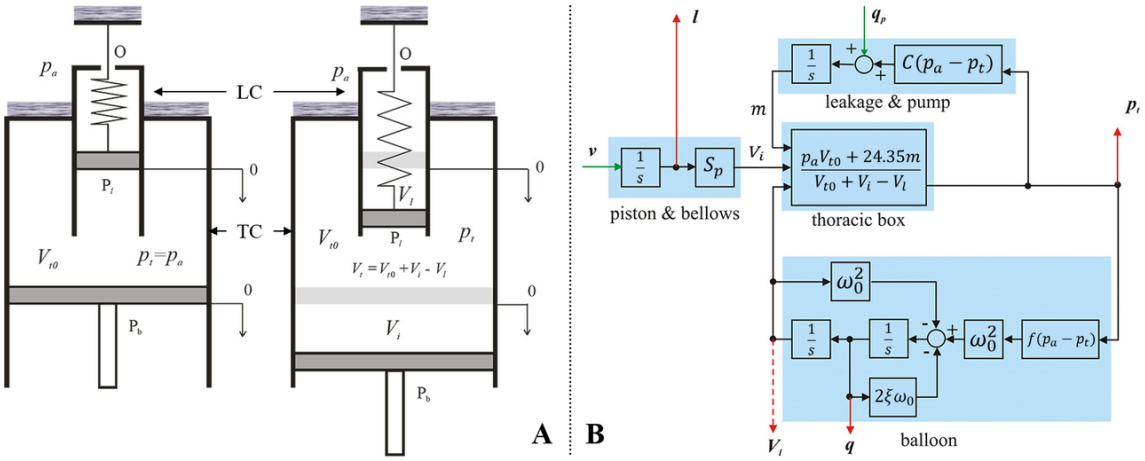

Fig. 1.1: The mathematical model of A) an electro-mechanical simulator with a thoracic chamber TC and a lung cylinder LC as a simulation basis including the observation parameters of volume V and pressure p inside TC and LC. B) The simulation scheme of the simulator including the modelled components of 'piston & bellows' (with the cross-sectional area S_p), the 'thoracic box' (with the atmospheric pressure p_a), the volume of the thoracic V_t, the initial volume of the chamber V_{t0}, its added volume V_i, the corresponding lung volume V_l and - assuming the ideal gas equation - the function of a leakage flow m, a model for 'leakage & pump' (with leakage constant C depending on the pressure difference between atmospheric pressure p_a and pressure in the thoracic chamber p_t) and the behaviour of the lung equivalent as a 'balloon' (with its dynamic properties characterised by eigenfrequency ω_0 and damping coefficient ξ) (based on and adapted from [91]).

The volume of the thoracic chamber can be expressed as:

$$V_t = V_{t0} + V_i - V_l \tag{1.1}$$

where V_t [dm^3] is the volume of the thoracic chamber, V_{t0} [dm^3] is the initial volume of the thoracic chamber, V_i [dm^3] is the volume added by the movement of the piston P_b and V_l [dm^3] is the volume of the lung equivalent. The position of the piston is controlled by its velocity. Therefore, the volume added to the thoracic box by the movement of the piston P_b depends on the velocity of the piston v [dm/s] and the cross-sectional area of the piston S_p [dm^2]:

$$\frac{\partial V_i}{\partial t} = S_p v \tag{1.2}$$

The ideal gas law can be utilised to state the relation between V_t and the pressure inside the thoracic chamber p_t [kPa]:

$$p_t V_t = nRT \tag{1.3}$$

where n [mol] is the amount of gas, R= 8.31 J mol^{-1} K^{-1} is the universal gas constant and T= 293.15 K is the absolute temperature. The final formula expressing the relationship between volume and pressure inside the thoracic chamber is derived based on the following assumptions: (I) Pressure in the thoracic chamber and in the lung equivalent is equal to the atmospheric pressure at the beginning of the breathing cycle $p_t \cdot V_t = p_a \cdot V_{t0}$, (II) the thoracic chamber cannot be considered perfectly airtight and the leakage flow is represented by the function m, and (III) the temperature of the air is presumed to be constant 20 °C. Taking into account the listed assumptions, converting pressure units to [bar] and using equation (1.3) and equation (1.1) yields:

$$p_t = \frac{p_a V_{t0} + 24.35m}{V_{t0} + V_i - V_l} \tag{1.4}$$

The time rate of leakage is expressed as:

$$\frac{\partial m}{\partial t} = C(p_a - p_t) = Cp_v \tag{1.5}$$

where C [mol s^{-1} bar^{-1}] is the leakage constant and p_v [bar] is the vacuum in the thoracic box. To compensate for the leakage, a vacuum pump q_p was included as a further component into the lung simulator. The last step in deriving the complete mathematical model of the lung simulator is to describe the behaviour of an artificial lung equivalent (balloon). Taking the already introduced lung cylinder as the basic modelled of a lung equivalent, the relation between the volume of the lung equivalent V_l [dm^3], the compliance of the lung equivalent C_l [dm^3/bar] the damping coefficient ξ, the eigenfrequency ω_0 [rad/sec] and the vacuum in the thoracic chamber p_v [bar] is:

$$\frac{\partial^2 V_l}{\partial^2 t} + 2\xi\omega_0 \frac{\partial V_l}{\partial t} + \omega_0^2 V_l = \omega_0^2 C_l(p_v) \tag{1.6}$$

where both the damping coefficient ξ and the eigenfrequency ω_0 characterise the dynamic behaviour of the elastic balloon.

The initially abstract mathematical description of the model and the underlying processes of volume and pressure changes during respiration were captured and simulated as an interaction of electric and mechanical components. Test measurements have shown [91] good correspondence between the mathematical model and mechanically realised simulator for both, square and sinusoidal input signals. The shape of the sinusoidal waveform essentially correlates with the simplified flow pattern of human spontaneous breathing at rest [92]. The fundamental theoretical assumptions could thus be confirmed and served as a basis for the development of the current version of the simulator.

1.2.2 The electro-mechanical lung simulator - xPULM™

This chapter introduces the physical construction, sensory equipment and components interconnections of the electro-mechanical lung simulator, xPULM™. The simulator has been developed to replicate physiologically realistic human respiration cycles. The entire setup of xPULM™, with main components highlighted, is shown in Fig. 1.2. The main functionalities include the capability of performing a breathing simulation with changing flow profiles of breathing patterns (sinusoidal), adaptability of simulation parameters (frequency and tidal volume), and the exchangeability of lung equivalents (artificial or organic-based). The mechanical simulator is designed to allow both active and passive respiratory simulation. The term active means that the lung model can be operated to simulate a spontaneously breathing human lung. In contrast, the term passive refers to the ability of the lung simulator to act as a mechanically ventilated human lung, for example using medical ventilators, regardless of their configuration.

The construction of the simulator has been inspired by the functionality of the

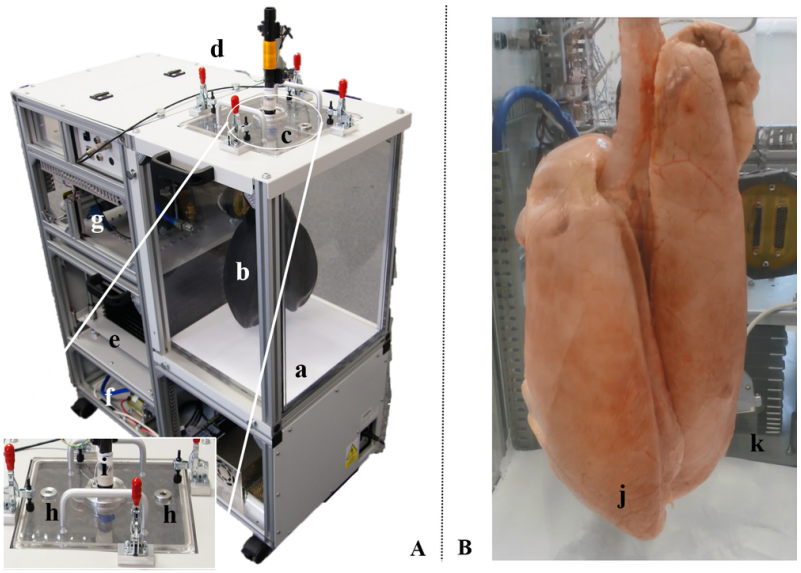

Fig. 1.2: xPULM™ simulator A) with a) the thoracic chamber, b) latex bags as lung equivalents, c) interoperable lid, d) airflow sensors e) the respiratory drive system – realised as bellows system for pressure change generation in the thoracic chamber, f) the motor with the vacuum pump and g) the real-time FPGA based control unit. The zoomed-in picture of the interoperable lid shows h) the connector ports for the organ nutrition circuit (arterial and venous connection) and i) the distal end of the simulated trachea, used for connecting the aerosol measurement system. Thoracic chamber B) housing j) a primed porcine lung ventilated with the movement of the k) bellow system.

human respiratory system under physiological conditions. The key concept for the inflow and outflow of air into the lungs is the result of the pressure gradient between the atmosphere and the thoracic cavity that was integrated into the lung simulator. Therefore, analogies can be found between the main components of the simulator and functional elements of the human respiratory system. An overview of the simulator setup, depicted in Fig. 1.3, consists of a respiratory-drive system, the rigid thoracic chamber and an aluminium housing frame. In this construction, the thoracic chamber is the central part of the simulator setup. It houses the chosen lung equivalent and mimics the pressure condition of the thorax in the human body. Moreover, the sensors for monitoring pressure, temperature and humidity changes during simulation are included there. The thoracic chamber is produced out of a transparent Polymethylmethacrylate (PMMA) hosting a total volume of 61 L. This construction allows the simulation process and lung equivalent status monitoring. This feature is particularly useful in training and education.

The lung equivalent is connected to the removable square shaped lid of the thoracic chamber via a threaded connection. Interchangeability of lung equivalents, representing the human lower respiratory tract, is one of the essential elements for anatomically realistic breathing simulation with xPULM™. The thoracic chamber can house any chosen lung equivalent constricted only by the maximum volume of the chamber. The structurally simplest equivalent used is an elastic bag (made of latex or silicone), which may vary in volume, form and elastic properties. Depending on the intended simulation, either a single bag may be used or - to achieve a higher degree of approximation to human physiological values - two bags connected via a y-shaped piece may be included. Symmetrical as well as asymmetrical setups of the lung equivalent are possible. As such, any medically relevant lung volume and capacity can be simulated including typical values from small children to adults. For an anatomically more realistic simulation of the human lung, specifically focusing on the internal structure of the lung tissue, a porcine lung may be introduced into the setup instead of polymer-based bags. Thereby the complex inner structures and branching of the respiratory tract from bronchi to the terminal bronchiole are present. This includes bends, bifurcations, and series of cartilage ring supporting the trachea from the inside. Additionally, high humidity levels ($\approx 99\,\%$ RH), normal in human lungs, comparable lung capacity (3–6 L) and division into lung lobes are represented by using the porcine lungs. Fine structures within the alveolar duct may be occluded due to the preservative process which leads to tissue adhesion especially in the lowest regions of the respiratory tract. Gas exchange is not retained when using a chemically preserved porcine lung. From the construction point of view, the thoracic chamber is connected to the bellows system and the vacuum pump via a separate flange. The airflow created by the vacuum pump is measured by the uni-

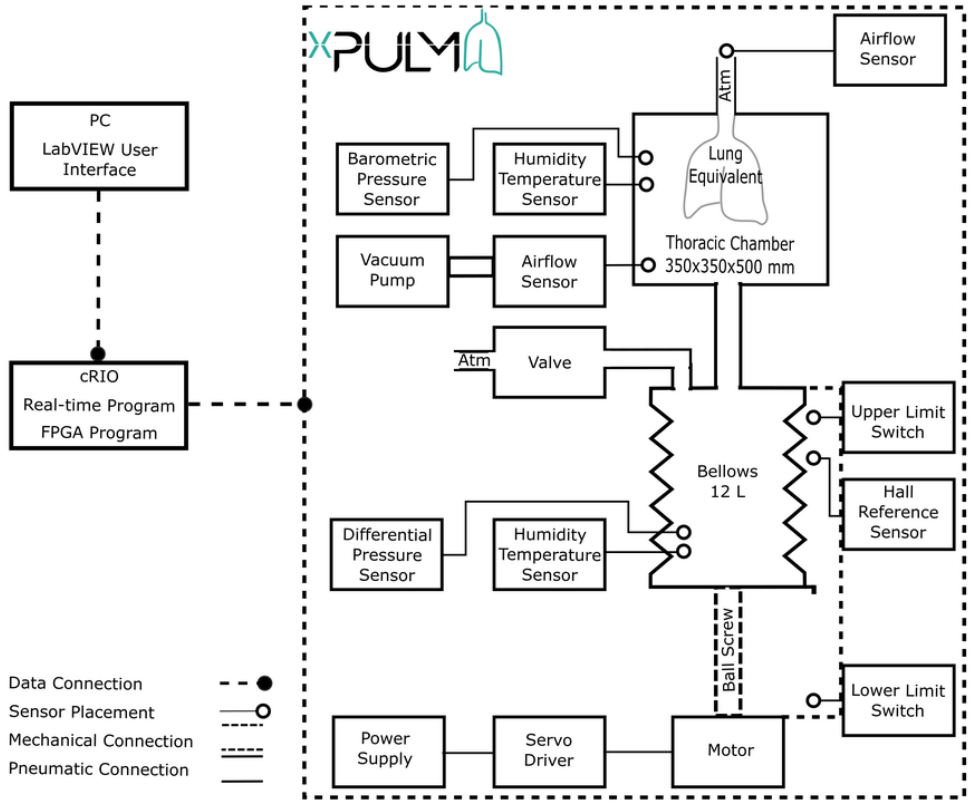

Fig. 1.3: Overview of the xPULM™ simulator components. This schematic includes interconnection and placement of the simulator main components and sensory equipment for flow, pressure and temperature measurements. All electronic components are connected to the cRIO data acquisition unit. Readings from the sensors are processed by LabVIEW based xPULM™ control software (Real-time and FPGA program). Simulation parameters can be adjusted using the User Interface running on a dedicated PC.

directional airflow sensor AWM5104VN (Honeywell, USA). The vacuum pump has been introduced into the setup of the xPULM™ system to achieve similar conditions to the anatomical environment of the human lung, where the organ is attached to the thoracic cage via the pleural liquid and thereby stretched to an extended position constantly. The alterations of the airflow during breathing pattern simulation with xPULM™ is not caused by the vacuum pump operation. On the contrary, the task of the vacuum pump is to maintain negative pressure inside the thoracic chamber, to counter leakages and to ensure that the inflexion points of the lung tissue are reached throughout the simulation cycle. Subsequently, the incorporated pressure control keeps the lung equivalent from completely collapsing at any point in time during the breathing simulation. The vacuum pump evacuates the thoracic

chamber with a peak flow of 5 L/min reaching the maximal negative pressure of −30 hPa (in relation to the atmospheric pressure). To protect the lung equivalent and bellows system from damage the magnetic coil valve is opened in case of excessive negative pressure ($p_t < -25$ hPa). This leads to pressure equalisation between the atmosphere and the thoracic chamber. The range of negative pressure values during simulations depends heavily on the used lung equivalent and can be set as a parameter in the xPULM™ control software. The simulation of respiratory patterns with the xPULM™ is achieved by the movement of the bellows system mimicking exertion of the diaphragm and intercostal muscles during the respiratory cycle. The lower end of the respiratory drive system is movable while the upper part is stationary, fixed to the housing frame of the simulator. Mechanically, the respiratory drive system is realised by a ball screw connected to the movable bottom part of the bellows on the one side and on the other side with a motor via a threaded connection, Fig. 1.3. A brushless AC servomotor turns the ball screw and the rotatory motion is subsequently transferred to a vertical movement of the bellows system. The range of motion of the entire respiratory drive system is 23.5 cm generating a maximal peak flow of ±130 L/min. Thus, it is guaranteed that any normally occurring physiological or pathological respiratory flow patterns can be simulated. The bellows are protected against potentially damaging over-extension by two mechanical switches. The switches are secured at the simulator housing frame and toggled whenever the upper or lower limit position is reached. Movement can be performed only away from the activated limit position switch. Additionally, the bellow system range of movement is limited in the control software. Furthermore, the signal from a hall sensor serves as a reference point and is used to calculate the initial bellow position during the simulation initialisation procedure. Similarly to the movement of the diaphragm in a human body, motion of the bottom part of the bellows downwards causes the inflation of the lung while the return to the initial position leads to the deflation of the lung. Consequently, the volume displacement in the thoracic chamber manifests as inhalation (extension) and exhalation (compression) of the lung. Physiologically occurring intrapulmonary pressure gradient is accordingly present in the model and leads to the airflow in- and out of the lung equivalent. The in-line airflow through the simulated trachea is measured, using two high precision, unidirectional, temperature compensated airflow sensors AWM720P1 (Honeywell, USA) which are mounted on top of the simulated trachea.

To be able to process the data received from the sensors and to dynamically react on condition changes in real-time, the xPULM™ simulator is equipped with the embedded industrial data processing and acquisition unit cRIO (National Instruments, USA). This unit consists of a real-time controller 9024 running the xPULM™ real-time program and a reconfigurable FPGA (Field Programmable Gate Array) chassis

9114 which is flashed with the xPULM™ FPGA program. The chassis includes I/O modules providing direct connectivity with the simulator sensory equipment. Measurement data of the flow, pressure, temperature and humidity within the thoracic chamber as well as in the surrounding environment can be monitored during the breathing simulation process. The surrounding environment is of specific relevance if aerosols are applied to the inhaled gas mixture. Signals from the sensors are retrieved by the xPULM™ Control Software and subsequently transferred to the real-time program for further processing. Generation of impulses controlling motor movement, valve state and vacuum pump performance is based on the recorded values from sensors and set simulation parameters. The breathing pattern, respiratory rate, tidal volume and pressure inside the thoracic chamber can be controlled via the LabVIEW based User Interface. Besides, the flow and pressure characteristics are plotted during the entire simulation runtime. Bidirectional information exchange between both software components provides effective and fast means of breathing simulation control. The simulator was realised with an FPGA-based unit and can, therefore, function as a stand-alone embedded system. The breathing simulation process is controlled without further intervention by the user, which corresponds to the intended general modular and flexible design of the simulator.

The human breathing simulation process is performed under Continuous Rotation Controlled (CRC) mode. For purposes of the CRC control algorithm, any breathing pattern is transformed into a vector of corresponding motor rotation values. Subsequently, motor control impulses matching the desired flow value are generated. Therefore the simulation follows a predefined set of motor rotations without further regulatory inputs from the flow or pressure sensors. For this reason, the volume of the air exchanged during in-/ex-halation phases of a breathing pattern simulation may vary based on the properties of the lung equivalent used. Hence providing the option of investigating the effect of high or low lung compliance and influences of other mechanical properties under steady breathing effort.

1.2.3 Sinusoidal respiratory simulation

Simulation parameters are chosen to represent physiological values, where a breathing rate (f) of 12–18 breaths per minute (bpm) is assumed physiological and a tidal volume (V_T) of 500 mL is a typical standard for breathing at rest [93].

Parameters of breathing simulations with the mathematical model

The mathematical description as given in chapter 1.2.1, models the behaviour of the electro-mechanical simulator during breathing simulations. The mathematical model was implemented in Simulink (MathWorks) environment and supports

Tab. 1.1: Overview of the Simulation parameters and their combinations used during the measurements with xPULM™.

Simulation Parameters Settings - xPULM™	
Breathing Patterns	Sinusoidal in CRC simulation mode
Lung Equivalent	2x3 L latex bags, Primed porcine lungs
Frequency	10, 12, 15, 18 bpm
Tidal Volume	400, 450, 500, 550, 600 mL
Initial Pressure	0 hPa (Latex), -6 hPa (Porcine)
Duration	2 min
Repetition	3

simulation with adjustable parameters for pressure condition of the surrounding environment, input sinusoidal piston movement profile, leakage flow and balloon-like lung equivalent properties. Following simulation settings of the mathematical model are used for a comparison with the physical version of the xPULM™ simulator P_a= 1 bar, V_0= 61 L, S_p= 2.7 dm, ω_0=48.3 rad/sec, C= 0.2 mol s^{-1} bar^{-1} and dynamic properties of the lung equivalent ξ= 35, C_l= 500 dm^3/bar or 0.5 L/hPa.

Parameters of the breathing simulations with xPULM™

The simulation process is controlled, including breathing parameters settings for each measurement trial, by the xPULM™ control software. Sinusoidal breathing pattern simulation under CRC mode was tested. Artificial lung equivalents and primed porcine lungs were included in the measurement setup. In the first step, a simplified model of the human lung was realised by two 3 L latex bags. In a second step a higher level of approximation to the more complex structure of human lung was ensured by performing the breathing simulation cycles with primed porcine lungs. Porcine lungs were obtained from a slaughterhouse process. Measurement experiments, each lasting 2 minutes and repeated three times, were performed for all combinations of pulmonary equivalents with different respiratory rates and tidal volumes. The applied set of simulation parameters is summarised in Tab. 1.1.

The measurements were carried out with an external exhaust air system to realise stable environmental conditions. The following values of the external environment were recorded during the measurements relative air humidity 40–55 %RH, temperature 19–21 °C and atmospheric pressure 900–1050 hPa.

Airflow and pressure characteristics during the simulation in CRC mode were recorded for:

- Sinusoidal breathing pattern with two 3 L latex bags in parallel mount.
- Sinusoidal breathing pattern with primed porcine lungs.

Time normalisation of repetitive cycles

Recorded airflow characteristics of sinusoidal breathing pattern in CRC operation mode were analysed separately for the used lung equivalents, the combinations of breathing frequencies and tidal volumes. Individual respiratory cycles, including in-/ex-halation period, were isolated and time normalised from the raw airflow dataset. Incomplete breathing cycles were discarded from further processing. Time normalisation of repetitive breathing periods includes isolation of the respiratory cycle by finding corresponding intersections of analysed airflow signal with zero isolines. The original time scale is converted to a percentage of a respiratory cycle ranging from 0 % to 100 %. Time normalisation allows the comparison of repeatable events at any given point in time across all breathing periods. The time normalisation technique is particularly helpful while comparing events that occur with varying frequency or contain different amounts of data samples.

1.3 Results

1.3.1 Evaluation of the breathing simulations

At first flow and pressure outputs of the mathematical model are compared with the characteristics measured during sinusoidal breathing simulations with xPULM™ in Fig. 1.4. Subsequently, additional measurements with xPULM™ are evaluated to access simulated breathing pattern reproducibility under various conditions. Testing and evaluation of the sinusoidal breathing pattern measured with xPULM™ includes 20 measurement trials representing changes of five tidal volumes (V_T= 400–600 mL) at four breathing frequencies (f= 12–18 bpm). The results are separated into categories based on the changing breathing simulation parameter and summarised in terms of airflow and pressure characterisation for latex bags in Fig. 1.5, for porcine lungs in Fig. 1.6 and for statistical indicators of cycle reproducibility in Tab. 1.2. Data with the same simulation parameters have been analysed and evaluated together as one large data set. Breathing cycles have been isolated and evaluated. Mean breathing cycles, as well as standard deviation, have been calculated based on interpolated and time normalised data sets. The standard deviation of $|3\,\sigma|$ of the isolated breathing cycles has been included to highlight the variation of all breathing signals over time. High reproducibility of flow and pressure characteristics was shown by evaluating breathing cycles (n_{Total}= 3273) with the highest standard deviation $|3\,\sigma|$ for both, simplified lung equivalents in a form of a latex bag ($\mu_{\dot{V}}$= 23.98 ± 1.04 L/min, μ_P= - 0.78±0.63 hPa) and primed porcine lungs ($\mu_{\dot{V}}$=18.87±2.49 L/min, μ_P= -21.13±1.47 hPa).

1.3.2 Comparison of the simulation to the mathematical model

The comparison of the predictions of the established mathematical model and the measured flow and pressure characteristics are both based on the use of a balloon as lung equivalent. In case of the mathematical model a balloon with compliance of 0.5 L/hPa has been used, whereas the included lung equivalent was represented by two 3 L latex bags. The comparison is represented in Fig. 1.4 and shows a 30 s simulation period with a flow range of ±18 L/min (mathematical model), +16.7 L/min to −17.5 L/min (measured) and a pressure range of +0.5 hPa to −1.4 hPa (mathematical model), +0.8 hPa to −1 hPa (measured). Flow, as well as pressure values, differ in amplitude with −0.5 L/min and 0.3 hPa during exhalation, 1.3 L/min and −0.4 hPa during inhalation respectively. The results show a clear alignment of flow and pressure dependencies for both, mathematical and measured characteristics.

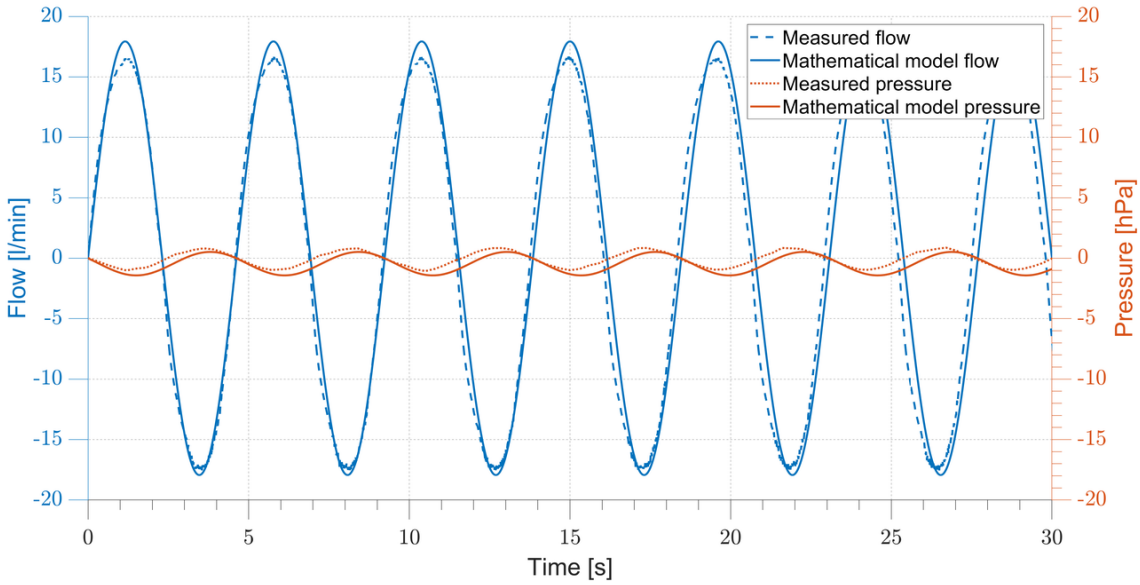

Fig. 1.4: Comparison of the Mathematical model and the xPULM™ breathing simulation for flow and pressure characteristics for sinusoidal breathing pattern with frequency 13 bpm, tidal volumes 500 mL using two 3 L latex bags in parallel mount as a lung equivalent.

1.3.3 Breathing simulation with the artificial lung equivalent

Analysed airflow characteristics for sinusoidal breathing pattern simulation using latex bags exhibit standard deviation from the mean airflow waveform of $|3\,\sigma|$ below 1 L/min for all measured breathing frequencies and tidal volumes. The standard deviation from the mean flow increases slightly with higher breathing frequencies and

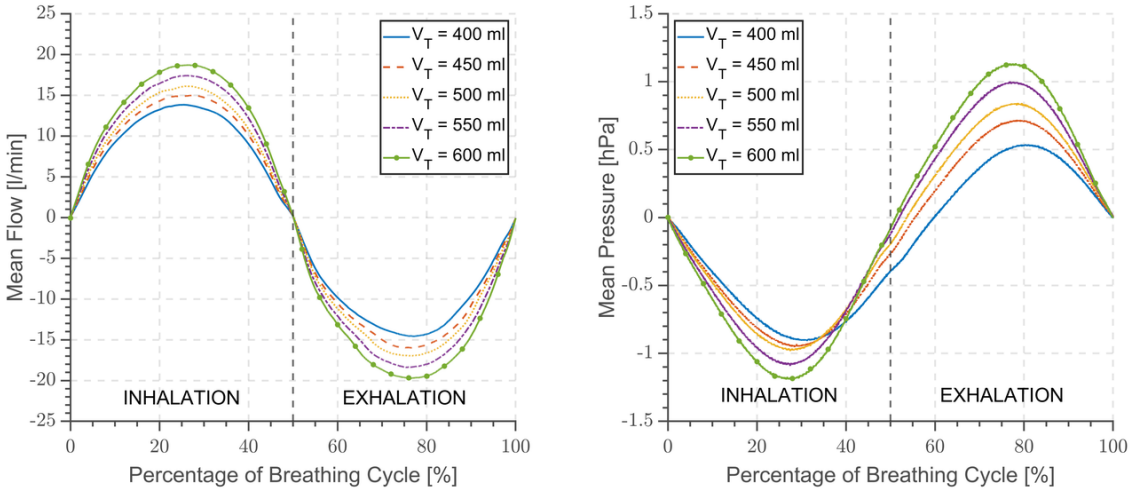

Fig. 1.5: Airflow and pressure characteristics for sinusoidal breathing pattern with frequency 12 bpm, tidal volumes varying from 400–600 mL using two 3 L latex bags in parallel mount as a lung equivalent. The x-axis is normalised in the percentage of breathing cycle where 100 % is equivalent to a period of 5 s.

for greater tidal volumes, reaching the maximum value of 1.04 L/min for $f = 18$ bpm and $V_T = 600$ mL. The differences between mean peak inspiratory and expiratory flows increases with growing breathing frequency. The difference of 7.74 L/min for $V_T = 600$ mL is highest between breathing frequency of 10 bpm and 18 bpm. A similar trend can be observed in the mean peak expiratory values where the maximal difference is 8.05 L/min for the identical simulation parameters.

Corresponding pressure changes inside the thoracic chamber are characterised by the standard deviation of $|3\,\sigma|$ below 0.7 hPa at the local maxima for all measured breathing frequencies and tidal volumes. Cycle-to-cycle differences are not dependent on the simulation parameters settings of frequency and tidal volume as their standard deviation does not vary greatly ($|3\,\sigma| < 0.5$ hPa). Breathing frequency-dependent increase of the differences between peak inspiratory and peak expiratory pressure corresponds with the results obtained from the airflow sensors. The mean inspiratory pressure difference of -1.20 hPa and the mean expiratory pressure difference of 0.72 hPa respectively was measured between breathing frequency of 10 bpm and 18 bpm for $V_T = 600$ mL. Sinusoidal shape of airflow and pressure characteristic is maintained for all measured combinations of tidal volumes and frequencies. Simulation results for volumes varying from 400–600 mL and frequency 12 bpm are depicted in Fig. 1.5. The in-/ex-halation breathing phase lasts the same time duration resulting in an expected inspiration-to-expiration ration (I : E) of 1 : 1. Peak inspiratory flow is reached at 25 % and the peak expiratory flow at 75 % of the breathing

cycle. The pressure inside the thoracic chamber oscillates between ±1.5 hPa during the sinusoidal breathing cycle simulation. The calculated compliance value for the used latex bags is $|C_{\text{Latex}}| = \Delta V/\Delta P = 0.5\,\text{l}/1\,\text{hPa} = 0.5\,\text{L/hPa}$ at peak inspiratory pressure.

1.3.4 Breathing simulation with the primed porcine lungs

The standard deviation of $|3\,\sigma|$ below 6 L/min was recorded while using the primed porcine lungs as a model representing the human lungs. Increase of a difference between individual cycles can be found under the conditions of low breathing frequencies (f = 10 bpm and 12 bmp) and small tidal volumes (V_{T} = 400 mL and 450 mL). This trend is inverse to the simulation conducted with the latex bags. On the contrary, the difference between mean peak inspiratory and expiratory flow exhibits the same characteristic for both used lung equivalents. The maximal difference for peak inspiratory flow is 9.91 L/min and 10.95 L/min for peak expiratory flow between breathing frequency of 10 bpm and 18 bpm for V_{T}= 500 mL, as shown in Tab. 1.2.

Pressure changes recorded with the primed porcine lungs have a standard deviation of $|3\,\sigma|$ under 1.5 hPa for all measurement trials. The expiratory peak pressure is below the atmospheric level, preventing the alveolar regions of the lung from collapsing during the breathing cycle. The shift of the mean peak inspiratory

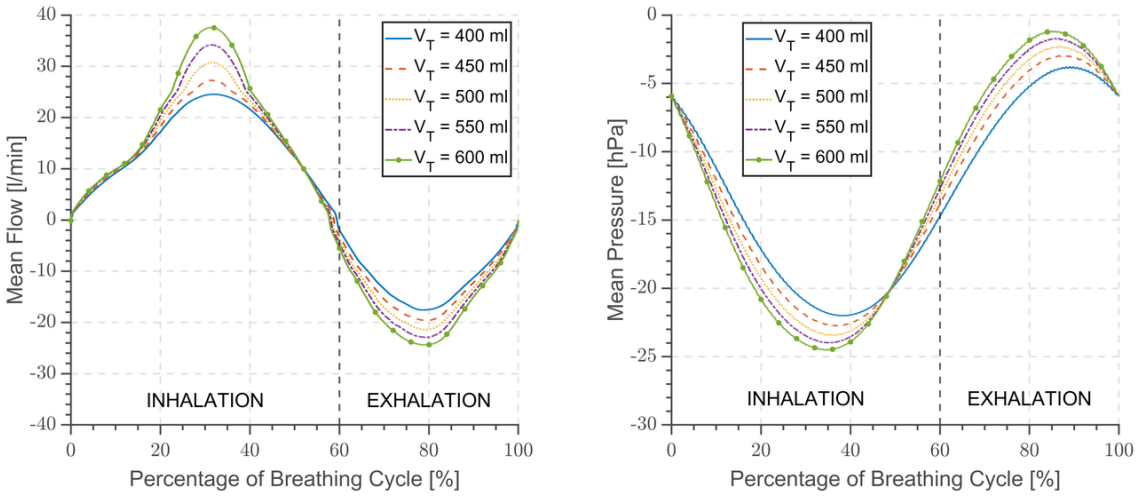

Fig. 1.6: Airflow and pressure characteristics for sinusoidal breathing pattern with frequency 12 bpm, tidal volumes varying from 400–600 mL using primed porcine lungs obtained from a slaughterhouse process. The x-axis is normalised in the percentage of breathing cycle where 100 % is equivalent to a period of 5 s.

pressure towards negative values compensates the elastic properties of the porcine lungs naturally causing them to stay in a collapsed state. Increase of the simulated tidal volume leads to the decrease of the mean peak inspiratory pressure and concurrently causes a rise of the mean peak expiratory pressure. The complex inner structure, the low compliance due to partly collapsed alveolar regions during exhalation, and the dynamically changing elastic properties of the primed porcine lungs are the reasons for a higher standard deviation of flow and pressure in comparison to the breathing simulations conducted with latex bags. The influence of these parameters is especially noticeable during low volume and frequency simulations when the initial deflation of the tissue originally extracted from the living organism has to be overcome. The state of the extracted porcine lung plays an important role during simulations as any tissue impairment introduces an additional source of leakage. The flow and pressure characteristics are highly reproducible, despite the influence of the tissue properties, and deviate only to a maximum of 2.49 L/min and 1.47 hPa. An overview of the airflow and pressure characteristics during breathing simulation results for both lung equivalents is given in Tab. 1.2. However, the simulation with porcine lungs includes many advantages, such as an anatomically accurate approximation of the human lung and its humid inner environment. Moreover, porcine lungs have a comparable lung capacity and are divided into lung lobes. The calculated compliance value for the included primed porcine lung is $|C_{\text{Porcine}}| = \Delta V/\Delta P = 0.5\,(l)/-23.5\,\text{hPa} = 0.02\,\text{L/hPa}$ at peak inspiratory pressure.

Tab. 1.2: Overview of the evaluated measurements of Sin mode breathing for all tested frequencies and corresponding tidal volumes including number of analysed cycles and statistical indicators for cycle reproducibility.

Sinusoidal breathing pattern in CRC mode; two 3l latex bags; Primed porcine lungs															
Set breathing frequency [bpm]	Set tidal volume [mL]	Analysed breathing cycles [-]		Mean peak inspiratory flow [L/min]		Mean peak expiratory flow [L/min]		$\lvert 3\,\sigma \rvert$ from mean flow [L/min]		Mean peak inspiratory pressure [hPa]		Mean peak expiratory pressure [hPa]		$\lvert 3\,\sigma \rvert$ from mean pressure [hPa]	
		Latex	Porcine	Latex	Porcine	Latex	Porcine	Latex	Porcine	Latex	Porcine	Latex	Porcine	Latex	Porcine
10	400	60	60	12.24	22.08	-12.56	-13.44	0.69	2.47	-0.78	-22.76	0.43	-4.74	0.63	1.45
	450	60	60	12.95	24.34	-13.72	-16.74	0.53	2.08	-0.83	-23.54	0.50	-3.23	0.20	0.85
	500	60	60	13.95	25.78	-14.92	-18.24	0.75	2.31	-0.86	-23.88	0.62	-2.54	0.19	0.67
	550	60	59	15.20	29.98	-16.06	-20.27	0.76	2.10	-0.90	-24.34	0.73	-1.78	0.20	0.67
	600	59	59	16.24	32.86	-17.01	-21.53	0.71	2.24	-0.96	-24.64	0.81	-1.46	0.19	0.72
12	400	72	72	13.82	24.51	-14.58	-17.56	0.64	2.09	-0.91	-22.01	0.55	-3.73	0.21	0.90
	450	72	72	15.31	27.30	-16.34	-19.63	0.62	2.10	-0.96	-22.76	0.72	-2.91	0.20	0.72
	500	72	71	16.45	30.85	-17.34	-21.42	0.67	2.29	-0.98	-23.44	0.85	-2.27	0.19	0.71
	550	71	71	17.75	34.23	-18.75	-22.94	0.75	2.18	-1.09	-23.99	1.00	-1.69	0.18	0.80
	600	71	70	18.87	37.57	-19.95	-24.39	0.66	2.49	-1.20	-24.53	1.14	-1.15	0.18	0.73
15	400	90	90	16.11	26.66	-17.09	-19.49	0.81	0.87	-0.93	-21.39	0.87	-2.21	0.21	0.59
	450	90	90	17.49	30.53	-18.40	-21.46	0.84	0.92	-1.05	-22.25	0.97	-2.02	0.21	0.64
	500	90	88	18.96	32.74	-19.97	-22.88	0.65	1.32	-1.22	-22.64	1.12	-1.68	0.18	0.67
	550	89	88	20.31	36.88	-21.45	-24.81	0.64	1.06	-1.41	-23.18	1.25	-1.17	0.19	0.74
	600	89	88	21.65	39.28	-22.78	-26.72	0.72	1.61	-1.62	-23.51	1.41	-1.10	0.21	0.74
18	400	108	108	18.21	29.42	-18.84	-21.44	0.72	1.40	-1.14	-21.13	0.99	-3.17	0.21	1.47
	450	108	107	19.81	33.73	-20.62	-23.53	0.80	1.54	-1.39	-22.25	1.12	-2.40	0.20	0.77
	500	107	107	21.40	37.02	-22.14	-25.11	0.76	1.29	-1.61	-22.77	1.29	-1.58	0.20	0.65
	550	107	106	22.76	39.77	-23.51	-28.65	1.01	1.48	-1.87	-23.22	1.43	-0.98	0.19	0.63
	600	107	105	23.98	42.77	-24.61	-32.48	1.04	1.53	-2.16	-23.69	1.53	-0.40	0.21	0.67

1.4 Discussion

The xPULM™ simulator in its current stage includes a bellows system as a driving force for volume displacement, instead of a rigid cylinder piston system as presented by Forjan et al.[89]. Due to its real-time data acquisition and processing capabilities this setup redefines the simulation options which were supported to a limited extent by the previous models [90]. These capabilities are enhanced by replacing the computational power of an integrated PC by a stand-alone real-time processing and acquisition unit. Moreover, the newly developed xPULM™ control software has been tailored to the real-time environment. The boundary conditions of the chosen input signal, in this case, a sinusoidal pattern, are inherently causing the corresponding flow profile of a given frequency and tidal volume. The results presented in this paper, therefore, include flow and pressure measurements over complete sinusoidal breathing cycles with latex bags as shown in Fig. 1.5 and porcine lungs as shown in Fig. 1.6. The measurements represent range of V_{T}= 400–600 mL and f= 10–18 bpm as summarized in Tab. 1.2.

1.4.1 Mathematical representation of the xPULM™

The mathematical representation of this electro-mechanical lung simulator has been revised and the simulation parameters adapted to fit the conditions of the measurements. The predicted flow and pressure curves of the mathematical model deviate slightly from the measured values. This can be explained by the fact that the mathematical model represents an optimal situation, meaning ideal conditions. Additionally, leakages within the pneumatic system, including the thoracic chamber and the bellows system, are causing behavioural changes of the introduced lung equivalent. This effect can be seen when inspecting the inhalation phase (Fig. 1.4), where a higher difference between mathematically modelled and measured peak inspiratory flow can be observed. Additionally, the higher pressure difference, driving the respiratory process, of the mathematical model results in higher peak flows during exhalation.

1.4.2 Measurement with the latex bags

The latex bags represent a simplified artificial equivalent of human lungs as they contain no inner structure and have a defined volume. Complex tree-like branching of the primary bronchi, typical for the human lungs, is expressed by the main bifurcation separating the latex bags into a left and a right lung. However, such representation assumes both symmetrical bifurcation and lung lobes. In comparison to the human lung, the resistance of a polymer-based bag as lung equivalent is

negligible. The resistance of the simplified simulated respiratory tract, consisting of a y-shaped bifurcation and two symmetrical latex bags, would only influence the performed measurements in case of high flows (i.e. flow > 120 L/min, airway resistance of 5 hPa/l/s causes a pressure drop of 10 hPa [94]). It is important to note, that the used latex bags are following Laplace's law for elastic spheres. However, the introduced primed porcine lung represents physiological structures and their characteristics. The behaviour is different as in the asymmetrical setup of the lung, smaller alveoli do not collapse into connected bigger ones, as stated by Prange [95] and in concordance with physiological lung mechanics. Because of this behaviour, latex bags are introduced into the xPULM™ system mainly for calibration purposes, rather than for actual lung simulation measurements.

1.4.3 Measurement with the porcine lungs

Breathing simulations conducted with the primed porcine lungs are influenced by the properties of the tissue and deviate from the typical sinusoidal curve, as shown in Fig. 1.6. Airflow during the inhalation period increases gradually until the 20 % of the breathing cycle is reached. Previously semi-collapsed alveolar regions expand at this point causing a steep increase of flow and prolonged inspiratory breathing phase. This phenomenon is particularly noticeable during simulations with higher tidal volumes. The expiratory breathing phase is shorter as the airflow expelled from the lung is reinforced by the elastic property of the porcine tissue. The influence of elastic recoil of the primed porcine lung to the breathing simulation is greater in comparison to latex bags. The I:E ration varies with increasing tidal volume reaching approximately the value of 2:1 at V_{T}= 600 mL. Such behaviour shows high compliance of the used porcine lung and could be compensated by the inclusion of a closed-loop feedback flow control algorithm. Such an algorithm could continuously adapt motor movement to reach the desired flow and pressure values. Additionally, the inclusion of a fresh porcine lung, with compliance comparable to the physiological range of the human lung, would further enhance sinusoidal respiratory curve approximation.

Focusing on the approach using a polymer bag as lung equivalent, it can be stated that the compliance of the latex bag is influenced by the properties of the material and does not introduce additional forces that would affect the breathing pattern simulations as can be seen in Fig. 1.5. The calculated compliance value for the used latex bags ($C_{\mathrm{Latex}} = 0.5\,\mathrm{L/hPa}$) is marginally above the physiological range of 0.1–0.4 L/hPa. This high compliance can be explained by the high elasticity of the used polymer material and the absence of any inner structure. In contrast, the included primed porcine lung is characterised by a considerably lower compliance value

($C_{\text{Porcine}} = 0.02\,\text{L/hPa}$), which is caused by the used preservatives influencing the tissue properties and adhering inner structures of the lung tissue. For these reasons, the measurements performed with the latex bags are characterised by high cycle-to-cycle reproducibility with low standard deviation and minor differences across all simulation parameters for both airflow and pressure. The positive expiratory pressure during the simulation was maintained to utilise the entire volume of the latex bags. Due to the missing inner structure of this lung equivalent, its full deflation can be neglected. Fluctuations over time identified during high volume and frequency simulations are caused by the pneumatic system not being completely airtight.

1.4.4 Challenges and further work

Future challenges include the introduction of vivid porcine tissue, which has not been compromised by the extraction process at the abattoir, or by preservatives. The possible fields of application of the xPULM™ would increase by the implementation of other, partially also pathological, breathing patterns. The advantages of integrating realistic tissue samples include the possibility of visualising model-machine interactions with ventilation devices to a greater extent. The simulator can then be used for training and testing including the simulation of the patient condition with a physical model where a result of an action is immediately visible, and misuse can result in e.g. tearing of the lung equivalent. The xPULM™ model can be further applied in simulations for teaching purposes of ventilation where the response and course of action dependent on the change of lung behaviour shall be demonstrated and practised. In medical research, the simulator can be used as an alternative to animal testing. In order to provide an overview of the characteristics of introduced lung equivalents, further measurements will focus on P-V loops at low flow rates within the physiological volume range. By these means, different lung conditions can be evaluated and characterised for further breathing simulation. These may include combinations of adult and children lung capacities with or without restrictive and/or obstructive pathologies. The adaptability of the breathing simulation parameters coupled with the use of different lung equivalents represents an important advancement towards anatomically realistic modelling of the respiratory system.

1.5 Conclusion

The xPULM™ simulator represents a new approach to the respiratory system behaviour modelling, combining the techniques of in silico, ex vivo and mechanical models. More specifically the in silico part is represented by the mathematical model, the ex vivo component is included by using the primed porcine lung, whereas

the mechanical model is the xPULM™ simulator setup itself. Construction of the simulator has been inspired by the functionality of the human respiratory system under physiological conditions and adapts a key concept of moving the air into and out of the lungs due to the pressure gradient between the atmosphere and the thoracic cavity. Measurements of the simulated sinusoidal breathing patterns demonstrate high reproducibility and stability of the system for all five tested tidal volumes at four breathing frequencies. The respiratory simulations were conducted with simplified lung equivalent and primed porcine lungs. Influence of a lung equivalents' mechanical properties on flow and pressure characteristic represents processes naturally occurring during the human respiration cycle. This is especially applicable for a primed porcine lung where the extraction process requires increased attention. The results show that the xPULM™ simulator is capable of reliably capturing the flow and pressure changes for a range of physiological tidal volumes and frequencies with multiple lung equivalents and during sinusoidal breathing simulations.

2 Patient-ventilator interaction testing

Abstract

During mechanical ventilation, a disparity between flow, pressure or volume demands of the patient and the assistance delivered by the mechanical ventilator often occurs. Asynchrony effect and ventilator performance are frequently studied from ICU datasets or using commercially available lung simulators and test lungs. This paper introduces an alternative approach of simulating and evaluating patient-ventilator interactions with high fidelity using the electro-mechanical lung simulator xPULM™ under selected conditions. The xPULM™ approximates respiratory activities of a patient during alternating phases of spontaneous breathing and apnoea intervals while connected to a mechanical ventilator. Focusing on different triggering events, volume assist-controlled (V/A-C) and pressure support ventilation (PSV) modes were chosen to test patient-ventilator interactions. In V/A-C mode a double-triggering was detected every third breathing cycle leading to an asynchrony index of 16.67%, being classified as severe. This asynchrony causes a major increase of Peak Inspiratory Pressure PIP = $12.80 \pm 1.39\,\mathrm{cmH_2O}$ and Peak Expiratory Flow PEF = $-18.33 \pm 1.13\,\mathrm{L/min}$ when compared to synchronous phases of the breathing simulation. Additionally, events of premature cycling were observed during PSV mode. In this mode, the peak delivered volume during simulated spontaneous breathing phases almost doubles compared to apnoea phases. The presented approach demonstrates the possibility of simulating and evaluating disparities in fundamental ventilation characteristics caused by double-triggering and premature cycling under V/A-C and PSV ventilation modes. Various dynamic clinical situations can be approximated and could help to identify undesired patient-ventilation interactions in the future. Rapidly manufactured ventilator systems could also be tested using this approach.

Keywords

biomedical engineering, breathing simulation, electro-mechanical lung simulator, patient-ventilator interactions, rapidly manufactured ventilator systems testing

This chapter is published as:

- R. Pasteka, J. P. Santos da Costa, N. Barros, R. Kolar, and M. Forjan, "Patient–Ventilator Interaction Testing Using the Electromechanical Lung Simulator xPULMTM during V/A-C and PSV Ventilation Mode," Appl. Sci., vol. 11, no. 9, p. 3745, Apr. 2021, doi: 10.3390/app11093745.

Author contributions statement:

- Conceptualization, R.P., M.F. and P.S.; methodology, R.P., M.F. and P.S.; formal analysis, R.P. and P.S; investigation, R.P.; data curation, R.P., P.S.; writing—original draft preparation, R.P.; writing—review and editing, P.S., M.F., N.B. and R.K.; visualization, R.P.; supervision, M.F., N.B. and R.K;. All authors have read and agreed to the published version of the manuscript.

2.1 Introduction

The functionality of the human respiratory system can be impaired mainly by respiratory pump failure or lung failure. These effects may occur based on a variety of causes like trauma, drug effects, neural damages and other pathologies such as oedema [14], [96], [97]. Furthermore, a combination of both respiratory failures may occur simultaneously, as is a case in patients with chronic obstructive pulmonary disease (COPD) and carbon dioxide retention [14], [98]. Respiratory pump failure ultimately leads to the need for controlled or assisted mechanical ventilation, which is meant to support or fully replace spontaneous breathing of a patient providing time for recovery [11], [12], [99]. In such scenarios, mechanical ventilators can be deployed to decrease the work of breathing and to deliver a high concentration of oxygen into the lungs. A mechanical ventilator is essentially a medical device combining actuators, sensors, digital electronic and software to fulfil a predefined ventilation strategy [100]–[102]. The basic structure and main functional building blocks of a typical mechanical ventilator are depicted in Fig. 2.1. Assisted mechanical ventilation should be ideally fully adaptive to a patient's respiratory behaviour by providing limited and fully synchronous respiratory support. Otherwise, asynchrony between the patient needs and the output of the ventilator arises [103], [104].

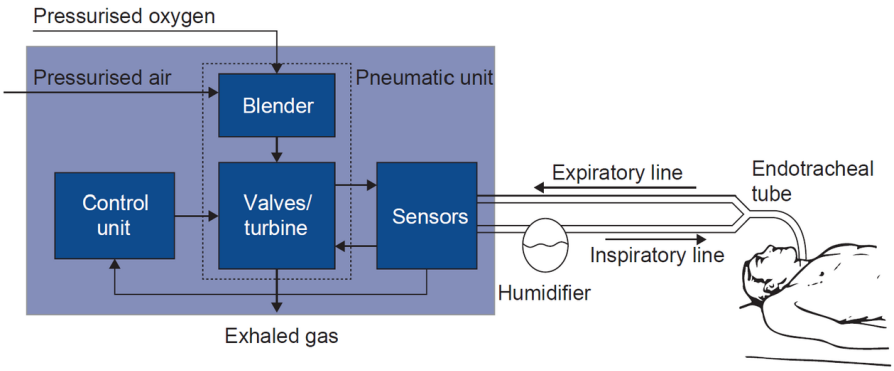

Fig. 2.1: Basic structure and main functional building blocks of a mechanical ventilator (taken and adapted from [100])

2.1.1 Patient-ventilator asynchrony

Patient-ventilator asynchrony (PVA) occurs when inspiratory and expiratory times of a ventilator do not match the neural control of patient's respiratory effort or when there is a disparity between flow, pressure or volume demands of the patient and the assistance delivered by the mechanical ventilator [15]. The neural inspiratory time can be estimated to describe the demands of a patient's respiratory system by measuring the electrical activity of the respiratory muscles. For this purpose, diaphragm electromyographic recordings and airflow signals of healthy subjects are evaluated according to respiratory protocols on respiratory rate increments and fractional inspiratory time decrements [105]. Modern synchronisation algorithms use new approaches such as deep learning [15], [106], [107] to estimate patients' respiratory mechanics and neural activity based on the measured pressure and flow waveforms, oesophageal pressure or transdiaphragmatic pressure readings, or diaphragm electromyography [108], [109]. However, errors of bias in the estimations can further contribute to an increased incidence of PVA [108].

2.1.2 Occurrence of PVA

The PVA occurs during both invasive and non-invasive ventilation and can be categorised into four general types: flow asynchrony; trigger asynchrony; cycle asynchrony; and mode asynchrony [15], [103]. Commonly manifestations are cases of auto-triggering, double-triggering, ineffective breaths, premature cycling and late cycling [17], [110]. Non-invasive ventilation techniques are prone to PVA due to leakages [110]. A framework for evaluating the clinical impact of PVA and attempts to better structure such efforts was presented by Gonzalez-Bermejo et al. [111].

Patient-ventilator asynchronies occur frequently and in the most common ventilation modes [17], [109], [112]. A severe PVA can be defined by proportion (PVA events in $\geq$10% of breathing cycles) or by clustering in 3 min period (PVA in 50% of breaths, assuming a breathing rate of 20 per minute) [17], [113]. Recently suggested method estimate PVA severity based on recurrence (PVA is observed twice a day for at least two minutes) [114]. However, the proposed concept requires further validation. Negative physical and mental outcomes such as excessive load on respiratory muscles, lung injury, prolonged ICU stay, discomfort and anxiety have been linked with severe PVA [15], [16], [112], [115], [116]. A higher frequency of asynchronies has been associated with higher mortality as well [15], [17]. Some studies report a lower incidence of severe asynchronies when modern ventilation modes such as neurally adjusted ventilation assist (NAVA) is used in comparison to conventional ones (PSV, V/A-C) [103], [109], [117]–[120]. However, conventional modes of mechanical ventilation stand a test of time and remain frequently used. This is in part due

to the increased complexity of new ventilation modes. Current emerging solutions focus on shortening the weaning process and increasing lung protective ventilation techniques [121], mainly supported by AI software solutions with advanced in vivo monitoring [122], [123]. In some cases, this can lead to the ventilation device becoming a "black-box" for an attending physician. Furthermore, there is no strict taxonomy in the naming of ventilation modes and manufacturers often introduce different names for similar modes which can lead to confusion. Further advances in the complex field of mechanical ventilation could benefit from a truly interdisciplinary approach combining the knowledge of medical professionals and biomedical engineers. [100], [124]

2.1.3 Simulation techniques utilised in PVA studies

Studies evaluating patient-ventilator interactions (e.g. triggering functions) often utilise simulation techniques to represent the patient. There are various approaches to test and calibrate a mechanical ventilator. On the one hand, several approaches target to simulate a passive lung with singular interchangeable properties, like resistance and compliance. On the other hand, some testing devices allow to also target patient ventilator interaction at specific boundary conditions (e.g. chosen ventilation modes, patient specific characteristics).[55]–[57]

Examples for the passive test systems are the IMT test lung (imtmedical, Switzerland), representing a single compartment solution as well as the TTL lung simulator (Michigan Instruments, USA), allowing a two compartment simulation. The ASL500 breathing simulator (IngMar Medical, USA) is an example of a more sophisticated test system, targeting also the comparison of ventilation modes, which has been shown in several studies [125]–[128]. The fundamental disadvantage of such methods are the unchangeable maximum volume of the test lung, restricted possibility of simulating lung behaviour and limited simulation of expiratory efforts [127].

2.1.4 Aim of the work

This work aims to introduce a novel approach of simulating and evaluating disparities in fundamental ventilation characteristics using electro-mechanical lung simulator xPULM™ [62] . This simulator can be used as a hybrid simulation device. It provides the basic, passive lung simulation with interchangeable resistance and compliance characteristics on one side. Additionally the xPULM™ is acting as a spontaneous actively breathing lung on the other side. For both modes the lung volumes and the breathing pattern can be tailored in accordance to the individual simulation conditions (e.g. varying inspiratory and expiratory efforts). Moreover, the simulator at hand provides the option to easily exchange lung equivalent as well.

This includes the use of latex bags of different sizes and properties, as well as the inclusion of artificial organoid structures or even the use of explanted lung tissue as the lung equivalent.

In this paper patient-ventilator interactions are evaluated for two, frequently used ventilation modes, (i) volume/assist-control ventilation mode and (ii) pressure support ventilation mode during spontaneous breathing simulation [129].

2.2 Materials & Methods

The measurement setup consists of the electro-mechanical lung simulator xPULM™ connected with a standard single-tube to a Bellavista™ 1000 mechanical ventilator (imtmedical, Switzerland) [130]. The simulator acts as a ventilated patient and replicates spontaneous sinusoidal breathing while supported by different modes of assisted ventilation. Frequently used volume/assist-control mode (V/A-C) ventilation mode and Pressure Support Ventilation (PSV) modes were chosen in this study as they account for 53% of ventilation modes used in mechanically ventilated and intubated patients [129].

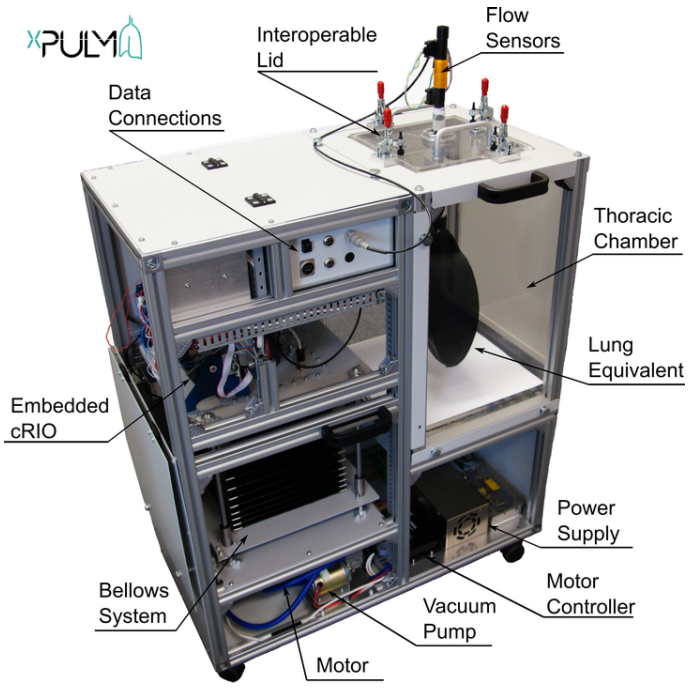

Fig. 2.2: Key functional elements of the xPULM™ electro-mechanical lung simulator [62].

2.2.1 Electro-mechanical lung simulator xPULM™

The electro-mechanical lung simulator xPULM™ has been developed to replicate anatomically as well as physiologically realistic breathing simulation. The basic mechanical setup of the xPULM™ consists of a thoracic chamber, housing a lung equivalent, and a connected bellows system acting as a respiratory pressure driving unit (Fig. 2.2).

The system, as described by Pasteka et al. in [62], allows the use of simplified lung equivalents like latex bags of different sizes, as well as the inclusion of a porcine lung. The breathing simulation is controlled by a real-time data acquisition and processing FPGA (field-programmable gate array) unit (National Instruments, USA). The opportunity to simulate active spontaneous breathing patterns of various parameters is the key for patient-ventilator interaction testing, presented in this work. In contrast to common ventilator testing setups and mechanical lung simulators, the xPULM™ simulator does not actively pump the gaseous volume into the lung equivalent. The driving power of the volume displacement during breathing simulation with xPULM™ is the pressure difference between the thoracic chamber and the surrounding atmosphere. Depending on the included lung equivalent, different lung capacities can be simulated. Furthermore, key parameters of the respiratory system such as airway resistance and lung compliance are adjustable. A resistance of the airways can be simulated by inclusion of an exchangeable resistive element. Both linear and parabolic resistances can be used in this setup. Additionally, lung equivalents from different materials can be included in the thoracic chamber representing various values of lung compliance. [62]

2.2.2 Volume/Assist-Control ventilation mode (V/A-C)

Under volume-controlled ventilation, a predefined tidal volume (V_T) is administered to the patient's lung at a set rate. Therefore, the airway pressure depends on the tidal volume as well as lung compliance and resistance. Advantages of having V_T as a control variable is a stable minute volume and lower initial flow rate than in pressure-controlled modes, depicted on Fig. 2.3a. However, insufficient flow may increase incidence of patient-ventilator asynchronies. In the measurement setup, the V_T is adapted to the currently measured tidal volume $V_{Tcurrent}$ according to the eq. 2.1. Frequently used version of the volume-controlled ventilation is the volume/assist-control mode (V/A-C) where spontaneous respiratory efforts of the patient trigger controlled breaths during the ventilation cycles. [130], [131]

$$V_{Tcurrent} = \frac{V_{Tinsp} + V_{Texp}}{2} \tag{2.1}$$

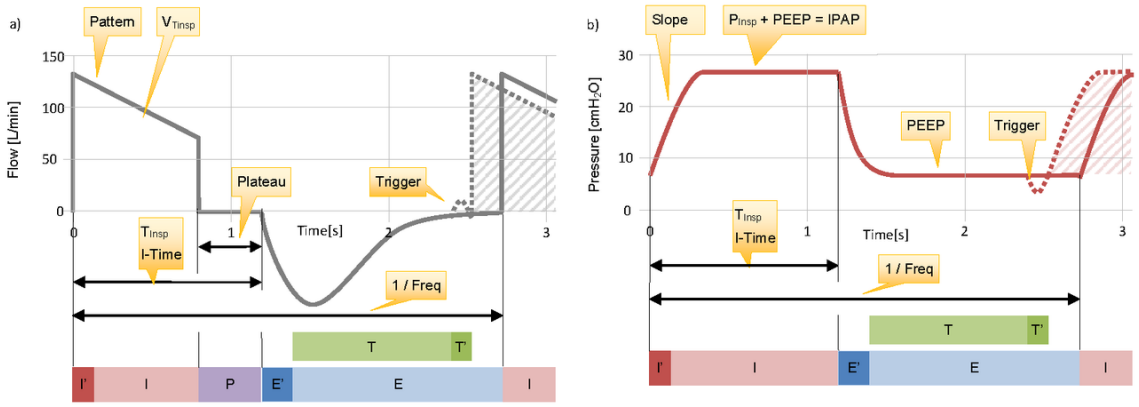

Fig. 2.3: Relationships between ventilation parameters in a) volume-controlled and b) pressure-controlled ventilation mode in relation to the ventilation phases of (I') minimal inspiration time, (I) inspiration, (E') minimal exhalation time, (E) exhalation, (T) waiting for a trigger (T') trigger action, (P) plateau phase. The main ventilation parameters are depicted as well,including slope, PEEP, T_{insp} and f as well as a schematic representation of a trigger event in the pressure and flow regime (taken and adapted from [130]

2.2.3 Pressure support ventilation mode (PSV)

In pressure-controlled ventilation Fig. 2.3b, a pressure applied to the airway is the controlled variable of the system. Therefore, tidal volume depends on the inspiratory pressure as well as lung compliance and resistance. This mode of ventilation has been advocated to reduce barotrauma and to reduce the work of breathing. However, the delivered V_T could be too high. For patients exhibiting spontaneous breathing activity a pressure support ventilation (PSV) has been the recommended option. The ventilation device delivers an inspiratory pressure-supported breaths P_{supp} triggered on a synchronised basis. [130], [131]

2.2.4 Measurement setup & protocol

The measurement setup includes two main components: The xPULM™ simulator and the IMT Bellavista™ ventilator. Two 3 L latex bags with measured compliance $C_{stat} =$ 49 mL/cmH_2O and $C_{dyn} =$ 47 mL/cmH_2O are used as a lungs equivalent. Additionally, parabolic airway resistance Rp20 (Michigan Instruments, USA) with characteristic similar to that of standard endotracheal tubes is included in the setup [132]. The pressure drop across the resistor ΔP can be expressed as:

$$\Delta P = \frac{k}{2}\rho\bar{\nu}^2 \tag{2.2}$$

Tab. 2.1: Calculated pressure drop ΔP and equivalent linear airway resistance (R) values for flow-rates in the measurement region for the used parabolic resistor Rp20.

Resistor	k	$\dot{V}$ [L/min]	ΔP [cmH_2O]	R [cmH_2O·s/L]
Rp20	21.5	15	1.09	4.39
		30	4.39	8.78
		45	9.88	13.17
		60	17.57	17.57

where ρ is the gas density, $\overline{\nu}$ is the average gas velocity over the cross-section of the resistor and k is a resistive loss coefficient as stated by Martin et al. [125]. Calculated pressure drop and equivalent airway resistance values for flow-rates in the measurement region are summarised in Tab. 2.1.

The xPULM™ simulator acts as a spontaneously breathing human with a breathing frequency of 12 bpm (breaths per minute) and a tidal volume (V_T) of 500 mL. The apnoea phase ($\dot{V} = 0$ L/min) is introduced after 60 s of sinusoidal spontaneous breathing simulation for a time interval of 60 s. After the apnoea, active spontaneous breathing is resumed, with the same settings, again for a duration of 60 s. The lung simulator and the mechanical ventilator are started consecutively. This manoeuvre represents patients suffering from severe cases of diseases accompanied by respiratory failure. Intervention with mechanical ventilation is required as the disease progresses. The scenario was inspired by the cases presented by Williams et al. [133].

The mechanical ventilator was operated in two ventilation modes Volume Assist-Control Mode and Pressure Support Ventilation mode. The measurement protocol with the apnoea interval was used in both cases. The measurements were repeated three times. The V-A/C mode is operated with the following settings: $V_T = 500$ mL, PEEP$= 0$ cmH_2O, $f = 12$ bpm, $T_{insp} = 1.7$ s, $Flow_{trigg} = 2.0$ L/min. The PSV mode is operated with the following settings: $P_{supp} = 10$ cmH_2O, PEEP$= 0$ cmH_2O, If apnoea occures the backup ventilation mode is switched on with $f = 12$ bpm, $T_{inspMax} = 1.7$ s, $Flow_{trigg} = 2.0$ L/min. Both measurements were performed under laboratory conditions ($T = 21.6$ °C, $RH = 52$ % $P_{atm} = 1030$ hPa) and with an ambient air gas mixture (21 % O_2, 78 % N and 1 % trace gasses).

2.2.5 Asynchrony index

The asynchrony index (AI) for each ventilation mode is calculated across all measurement trials as a number of asynchrony events (N_{AE}) / total respiratory rate (RR_{Total}) x 100 [112].

2.3 Results

The patient-ventilator interaction measurements are separated into two phases and are investigated under two different ventilator modes. The phases are divided into initial spontaneous breathing (SB) performed by the xPULM™ simulator (Phase 1), with simulated apnoea (SA) phase in between where the electro-mechanical simulator is not operating (Phase 2). The tracings of flow, volume and pressure at the airways showing the interactions between the xPULM™ simulator and the mechanical ventilator for both phases are depicted on Fig. 2.4 & 2.5. The transitions between phases are characterised by rapid changes of airway pressure and flow. For each phase, a total of 36 breathing cycles were analysed.

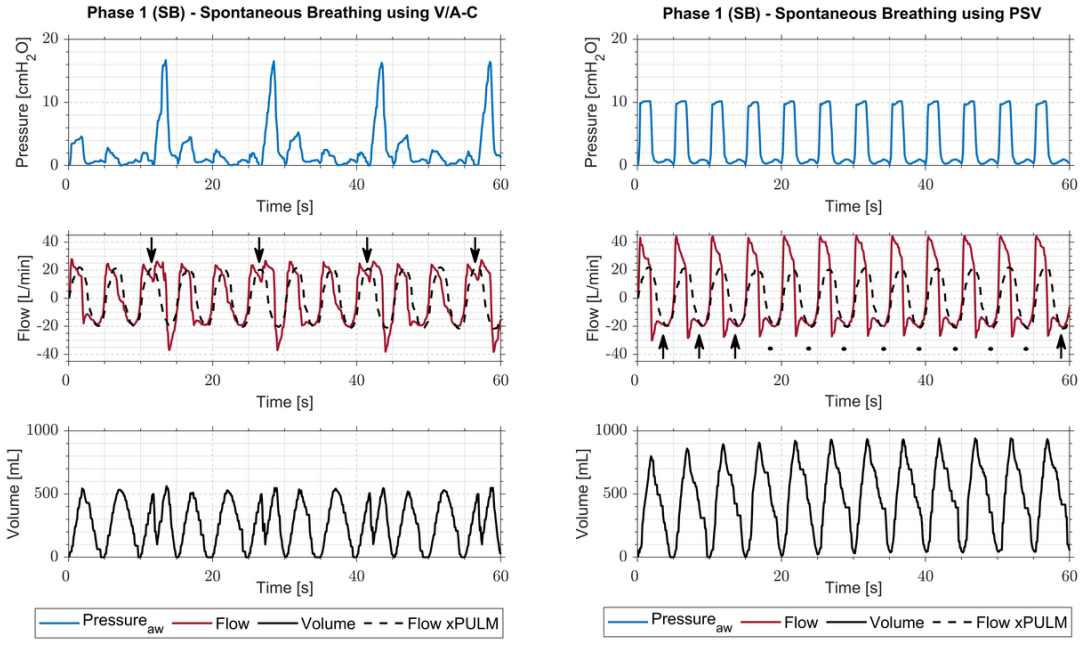

Fig. 2.4: Pressure, flow and volume tracings during spontaneous breathing simulation (SB) phases with the xPULM™ and mechanical ventilator BellaVista™ in the V/A-C mode (left) and in the PSV mode (right). Simulated patient's breathing frequency is not in phase with the ventilator's frequency representing realistic conditions. This leads to trigger asynchrony (double-triggering) in the V/A-C mode (arrows on the left) and trigger asynchrony (premature cycling) in the PSV mode (arrows on the right).

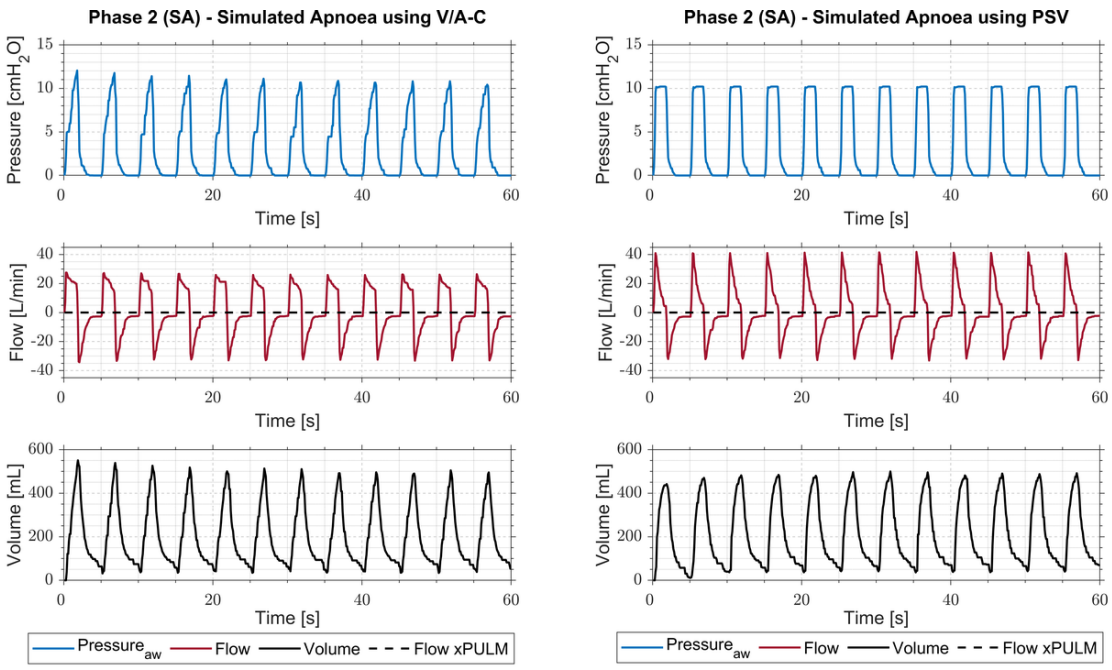

Fig. 2.5: Pressure, flow and volume tracings during simulated apnoea (SA) phase. The xPULM™ does not generate any airflow, in this phase, and the mechanical ventilator BellaVista™ is overtaking the entire ventilation process using the V/A-C mode (left) and the PSV mode (right).

2.3.1 Measurements with V/A-C ventilation mode

The measurements of the xPULM™ simulator and the mechanical ventilator operating in V/A-C mode are shown in Fig. 2.4. During Phase 1, the xPULM™ is actively breathing while the mechanical ventilator is operating for a period of 60 s. A forced second inhalation cycle is triggered (double triggering) by the mechanical ventilator every third breathing cycle, leading to an abrupt increase of pressure, which is followed by a higher exhalation flow in comparison to the other breathing cycles. With a total amount of 4 asynchronies during the observed time span, the asynchrony index for both phases in V/A-C mode is 16.67 %. In the Phase 2, the electro-mechanical simulator was paused to simulate apnoea with the mechanical ventilator taking over the entire breathing effort. Steady breathing cycles can be seen with maximum pressure peaks at the end of the inhalation cycle. To reach the same flow the necessary pressure exerted by the mechanical ventilator doubles in comparison to the Phase 1.

Tab. 2.2: Patient-ventilator interaction. Differentiation between phases (1: Spontaneous Breathing (SB) and 2: Simulated apnoea (SA)) for both V/A-C and PSV mode with a breathing frequency of 12 bpm.

Ventilator Mode	Phase	Peak Inspiratory Flow ($\pm\sigma_{\text{FLOW}}$) [L/min]	Peak Inspiratory Pressure ($\pm\sigma_{\text{PRESSURE}}$) [cm$H_2O$]	Peak Expiratory Flow ($\pm\sigma_{\text{FLOW}}$) [L/min]	Peak Expiratory Pressure ($\pm\sigma_{\text{PRESSURE}}$) [cm$H_2O$]
V/A-C	SB	25.56 (± 1.34)	7.96 (± 6.38)	-25.57 (± 8.93)	0.14 (± 0.20)
	SA	26.43 (± 0.57)	11.09 (± 0.49)	-32.9 (± 0.54)	0 (± 0.03)
PSV	SB	43.96 (± 0.01)	10.18 (± 0.04)	-27.5 (± 0.97)	0.24 (± 0.08)
	SA	41.19 (±0.31)	10 (± 0.02)	-32.16 (± 0.51)	0 (± 0.03)

2.3.2 Measurements with PSV ventilation mode

In Fig. 2.5, the measurement of interactions between simulated spontaneous breathing and the PSV mode of the mechanical ventilator are depicted. Similarly to the V/A-C mode the mechanical ventilator is not fully in phase with the lung simulator. The inspiratory time of the lung simulator does not surpass the set maximum inspiratory time threshold of the PSV mode, leading to an intended interaction for all phases during the measurement. However, the delivered peak volume during the active Phases 1 is nearly double than in the apnoea Phase 2. With a total amount of 12 asynchronies during the observed time span, the asynchrony index for both phases in PSV mode is 50 %. The effect of asynchronies can be seen in the increased inspiratory flow of both the lung simulator and mechanical ventilator.

2.3.3 Comparison of measurements with V/A-C and PSV

The comparison of simulation measurements showing patient-ventilator interactions using different modes of ventilation is summarised in Tab. 2.2. The results exhibit high standard deviations σ_{FLOW} for inhalation and exhalation peak flow and σ_{PRESSURE} for inhalation peak pressure in both spontaneous breathing phases during V/A-C mode. The standard deviation for exhalation peak pressure can be neglected for both modes as the PEEP was set to zero for both modes and minor oscillations around zero for dynamic systems are expected. The high standard deviation outcome for V/A-C mode during spontaneous breathing is linked to double triggering

which can be seen in Fig. 2.4 for every third breathing cycle. During simulated apnoea in V/A-C mode, the standard deviation σ_{FLOW} lies below 2.17% for inhalation and exhalation peak flow and $\sigma_{\mathrm{PRESSURE}}$ lies below 4.42% for inhalation peak pressure. For the PSV mode, σ_{FLOW} lies below 3.53% for inhalation and exhalation peak flow and $\sigma_{\mathrm{PRESSURE}}$ lies below 0.41% for inhalation peak pressure when considering both phases.

2.3.4 The V/A-C asynchronous events

The maximum inhalation and exhalation peaks for flow and pressure values were analysed for the breathing cycles where the lung simulator interacts with the mechanical ventilator in-phase (Synchronous) as shown in Tab. 2.3. Additionally, the values were calculated for breathing cycles where the lung simulator and the mechanical ventilator are out of phase (Asynchronous) which is characterised by the occurrence of double triggering. This caused a major increase of Peak Inspiratory Pressure PIP $= 12.80 \pm 1.39\,\mathrm{cmH_2O}$ and Peak Expiratory Flow PEF = -$18.33 \pm 1.13\,\mathrm{L/min}$ when comparing synchronous to an asynchronous phase of spontaneous breathing simulation. The differentiation resulted in a decrease of σ_{FLOW} and $\sigma_{\mathrm{PRESSURE}}$ during synchronous and asynchronous simulator-ventilator interaction in comparison to the non-differentiated event analysis (see Tab. 2.2 & Tab. 2.3).

2.3.5 The PSV asynchronous events

In Fig. 2.4 (PSV mode, Phase 1), the arrows depicted in the flow graph are pointing to the initiation of trigger asynchrony events. Rises in flow, being out of phase with simulator's flow pattern, can be observed during exhalation phase. The asynchronous events occur during every exhalation phase. In this specific case, the flow is set as trigger parameter for the PSV measurements. The simulator's expiratory time is delayed in comparison to the ventilator's calculated expiratory time. The resulting rise in flow, caused by the simulator-ventilator interaction, is not sufficient to start the inspiration phase, which ultimately leads to premature cycling.

2.3.6 Pressure changes in the thoracic chamber of the xPULM™

Recordings of pressure changes inside the thoracic chamber of the xPULM™ (hereafter referred to as a thoracic pressure), depicted in Fig. 2.6, present alternative opportunity to further explore the effect of PVA on patients and operation of mechanical ventilators. Automatic adjustments of ventilator's control algorithm in response to the asynchronous events are evident.

Tab. 2.3: Comparison of peak flow and pressure values for the recorded spontaneous breathing phase (SB) of the V/A-C mode. The mode introduced a forced inspiratory cycle (double triggering) based on the trigger event. The inspiratory and expiratory peaks are differentiated based on the trigger event (Synchronous: the lung simulator's spontaneous breathing is in phase with the mechanical ventilator during V/A-C mode; Asynchronous: the lung simulator and the mechanical ventilator are out of phase during V/A-C mode).

Phase (V/A-C)	Triggered Event	Peak Inspiratory Flow ($\pm\sigma_{\text{FLOW}}$) [L/min]	Peak Inspiratory Pressure ($\pm\sigma_{\text{PRESSURE}}$) [cm$H_2O$]	Peak Expiratory Flow ($\pm\sigma_{\text{FLOW}}$) [L/min]	Peak Expiratory Pressure ($\pm\sigma_{\text{PRESSURE}}$) [cm$H_2O$]
SB	Synchronous	25.06 (± 1.38)	3.68 (± 1.21)	-19.53 (± 0.45)	0.24 (± 0.15)
	Asynchronous	26.54 (± 0.49)	16.48 (± 0.17)	-37.66 (± 0.68)	-0.07 (± 0.07)

Changes in the driving pressure exerted by the ventilator to deliver the predefined tidal volume in V/A-C mode can be observed prior to the asynchronous event (double triggering). Thoracic pressure applied during first breath following the double triggering event is significantly lower to SA phase. This is partially compensated by the increase of driving pressure during the second breath. However, in the course of the third breath double-triggering occurs and the entire process repeats as shown in Fig. 2.6 (left).

The effect of premature cycling during PSV ventilation are equivalently reflected in the changes of the thoracic pressure. This trigger asynchrony causes an increase of the delivered tidal volume and manifests as a secondary peak in the thoracic pressure recordings Fig. 2.6 (right).

The changes in peak pressure (>4 cmH_2O, left) and occurrence of premature cycling at every breath (right) in Fig. 2.6 are complementary to the data-set recorded by the ventilator and shown in Fig. 2.4 & 2.5 and indicate the occurrence of asynchronous events during Phase 1 simulations.

2.4 Discussion

Thorough testing of patient-ventilator interactions is necessary to ensure that patient demands during all phases of mechanical ventilation are met. The occurrence of asynchronies have been linked to high load on ventilation muscles and cause overload, fatigue or even injury [15], [16], [115]. Modern approaches are needed to capture the

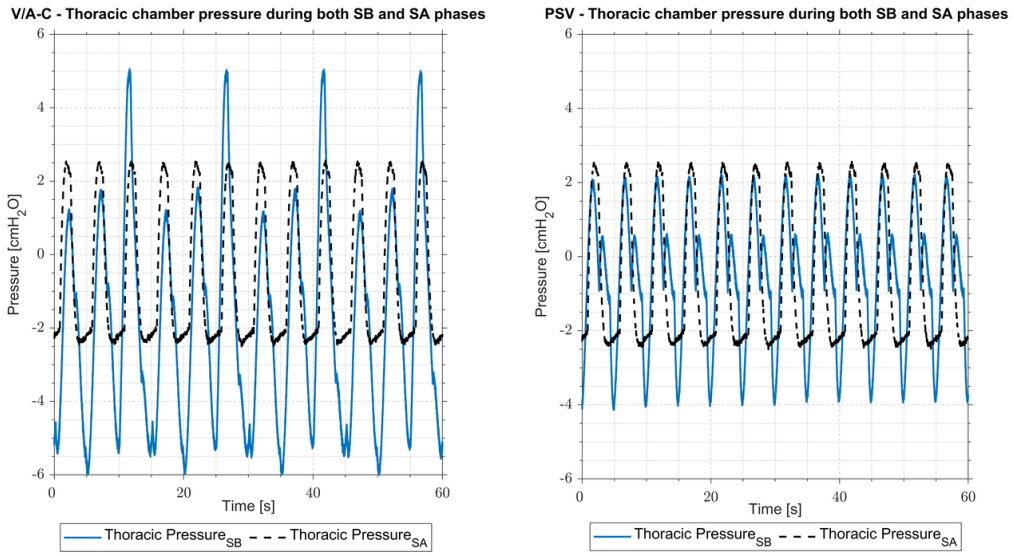

Fig. 2.6: Pressure changes in the thoracic chamber of the xPULM™ recorded during Phase 1 - spontaneous breathing (SB), blue solid line and Phase 2 - simulated apnoea (SA), black dashed line in the V/A-C mode (left) and in the PSV mode (right). The changes in peak pressure (>4 cmH_2O, left) and occurrence of premature cycling at every breath (right) indicate asynchrony events during mechanical ventilation and correspond to the data recorded by the ventilator.

clinical environment with higher fidelity. The xPULM™ simulator reliably replicates sinusoidal human breathing with adjustable waveform parameters (e.g. tidal volume, frequency) as shown in our previous work [62]. The lung simulator, therefore, seems like a suitable candidate to expand setups for patient-ventilator interaction testing and to aid the development of modern ventilation modes in the future. This especially applies for exploring patient-ventilation interactions under various dynamic conditions (changing breathing patterns and timing of respiration phases) and different pulmonary parameters (airway resistance and lung compliance). The focus of this paper is to introduce this simulation approach and to examine changes of ventilation during widely used V/A-C and PSV ventilation modes. The measurement setup simulates a physiological respiratory system situation. Airway resistance is represented by the inclusion of an interchangeable pneumatic resistor to further simulate realistic airway behaviour. The resistors used allow to reflect different physiological and pathological conditions of the airways. The same applies to the used lung equivalent. The results show occurrences of asynchronies during V/A-C and PSV ventilation modes with a simulated patient during spontaneous breathing and apnoea periods.

2.4.1 Influences of V/A-C and PSV ventilation mode

The first trial show the interaction with the simulated patient during the V/A-C mode, which is based on a continuous mandatory ventilation mode. In this case, simulated patient's breathing frequency is not in phase with the ventilator's frequency representing realistic conditions. Patient-ventilator asynchrony can be identified and manifests as a forced second inhalation every third breathing cycle (double-triggering). This event represents a force working against the effort of a spontaneous breathing patient. The mechanical ventilator intervenes despite the patient being sufficiently ventilated. However, this is in concordance with the principle of the V/A-C ventilation mode where the patient always receives at least the set tidal volume. The forced second inhalation, in general, occurs when the ventilator inspiratory time is shorter than the patient's inspiratory time. The results are corresponding with clinical findings reported by Thille et al. [112].

The second trial demonstrate the influence of PSV ventilation mode during simulations of spontaneous breathing and apnoea phases. Mechanical ventilation in PSV mode is supportive but leads to an excessively high peak pressure during spontaneous breathing phases caused by premature cycling. The volume supplied by the mechanical ventilator is compounded to the tidal volume delivered by spontaneous breathing. Consequently, the total volume during SB phases doubles in comparison to the apnoea phases. This leads to insufficient ventilation during the apnoea phases.

Furthermore, the pressure changes inside the thoracic chamber of the xPULM™ which are complementary to the data-set recorded by the ventilator have been presented. This provides additional information about how asynchronies influence the conditions in the thoracic chamber in comparison to synchronous mechanical ventilation. These pressure changes in the thoracic chamber partially reflect the interplay between changing compliance of the lung, the chest wall mechanics and the varying respiratory muscle effort (P_{MUS}), which is at the heart of most clinically relevant PVA.

2.4.2 Limitations of the approach

The primary limitation of the presented approach and other studies using test lungs or lung simulators is the principal inability of capturing the full complexity of patient-ventilator interactions [57], [128]. This raises the question of medical relevance. The ventilation parameters like flow, average peak pressure and plateau pressure, observed at bed-site, can be higher than has been simulated in this work. Nevertheless the presented results serve as proof of concept and set the basis for scaleable experiments.

Typically ASL500 breathing simulator (IngMar Medical, USA) or Michigan Instruments double compartment test lung (Michigan instruments, USA) are used to represent the behaviour of a patient [55]–[57], [125]–[128]. However, such models capture lung properties and expiratory efforts only to a limited extend [56], [57], [125]–[128]. The lung simulator xPULM™ used in this paper can represent various lung properties (compliance, volume, inner structure) by the inclusion of different lung equivalents. In this study two 3L latex bags have been used and have to be seen as limiting realistic measurements due to their missing inner structure and their specific elasticity characteristics. Moreover, this study is limited by strictly regular, sinusoidal simulation of the patient's breathing and the use of only one mechanical ventilator operated in two ventilation modes.

2.4.3 Further work

The modes and techniques used during mechanical ventilation are mature and cover a wide spectrum of cases encountered in the clinical environment. Despite this fact, there is a room for further improvements and innovations. One of the opportunities is to simulate patients behaviour with high fidelity of anatomical and physiological characteristics using lung simulators. Breathing simulations with a primed porcine lung was shown to be feasible and representative of anatomical and physiological situations in previous work [62]. Further research will, therefore, aim to include primed porcine lungs obtained from the slaughterhouse process to the xPULM™ ventilator testing setup.

Additionally, rapidly manufactured ventilator systems are being developed to cover potential shortages of mechanical ventilators during an emergency. Such solutions should be rigorously tested due to the cyclical occurrence of events triggering such demands (e.g. viral pandemic). Interactions of rapidly manufactured ventilators could be tested using the lung simulator xPULM™. Comprehensive evaluation could be conducted, helping to identify strengths and weaknesses of different approaches under realistic scenarios.

2.5 Conclusion

In this paper, an approach of testing patient-ventilator interactions using the electromechanical lung simulator xPULM™ is introduced. The simulator is used to replicate a spontaneously breathing patient under mechanical ventilation. Overall the presented approach demonstrates the possibility of simulating and evaluating disparities in fundamental ventilation characteristics under V/A-C and PSV ventilation

modes. Due to the versatility of the used lung simulator, dynamic changes in breathing patterns can be simulated. This method approximates the clinical situation and can help to identify, investigate and test undesired patient-ventilation interactions under laboratory conditions. Rapidly manufactured ventilator systems could also be tested using this approach.

3 Experimental evaluation of dry powder inhalers

Abstract

Dry powder inhalers are used by a large number of patients worldwide to treat respiratory diseases. The objective of this work is to experimentally investigate changes in aerosol particle diameter and particle number concentration of pharmaceutical aerosols generated by four dry powder inhalers under realistic inhalation and exhalation conditions. To simulate patients undergoing inhalation therapy, the active respiratory system model (xPULM™) was used. A mechanical upper airway model was developed, manufactured and introduced as a part of the xPULM™ to represent the human upper respiratory tract with high fidelity. Integration of optical aerosol spectrometry technique into the setup allowed for evaluation of pharmaceutical aerosols. The results show that there is a significant difference ($p < 0.05$) in mean particle diameter between inhaled and exhaled particles with the majority of the particles depositing in the lung, while particles with the size of (>0.5 µm) are least influenced by deposition mechanisms. The fraction of exhaled particles ranges from 2.13% (HandiHaler®) over 2.94% (BreezHaler®), 6.22% (Turbohaler®) to 10.24% (Ellipta®). These values are comparable to previously published studies. Furthermore, the mechanical upper airway model increases the resistance of the overall system and acts as a filter for larger particles (>3 µm). In conclusion, the xPULM™ active respiratory system model is a viable option for studying interactions of pharmaceutical aerosols and the respiratory tract regarding applicable deposition mechanisms. The model strives to support the reduction of animal experimentation in aerosol research and provides an alternative to experiments with human subjects.

Keywords

dry powder inhaler resistance, inspiratory flow rate, inspiratory pressure, aerosol particle deposition, mechanical upper airway model, optical aerosol spectrometry, biomedical engineering

This chapter is published as:

- R. Pasteka, L. Schöllbauer, J. P. Santos da Costa, R. Kolar, and M. Forjan, "Experimental Evaluation of Dry Powder Inhalers During In- and Exhalation Using a Model of the Human Respiratory System (xPULM™)," Pharm. 2022, Vol. 14, no. 3, p. 500, Feb. 2022, doi: 10.3390/PHARMACEUTICS14030500.

Author contributions statement:

- R.P.: Conceptualization, Methodology, Validation, Data curation, Writing-Original draft preparation, Visualization, Investigation L.S.: Investigation, Writing- Reviewing and Editing, P.S.C: Formal analysis, Writing- Reviewing R.K.: Writing- Reviewing and Editing, M.F.: Conceptualization, Investigation, Writing- Reviewing and Editing, Supervision.

3.1 Introduction

According to the report on the global impact of respiratory disease published by the Forum of International Respiratory Societies from 2017 [9] approximately 65 million people globally suffer from mild to severe chronic obstructive pulmonary disease (COPD) and 334 million people suffer from asthma. In conjunction with acute lower respiratory tract infections, these diseases are among the most prevalent severe illnesses and causes of death [9]. Based on Eurostat statistics [134] from 2016, diseases of the respiratory system accounted for approximately 7.5% of all deaths in the former EU-27. Targeted delivery of pharmaceuticals directly into the affected part of the respiratory region via inhalation drug therapy is crucial for managing cases of obstructive respiratory diseases [22].

Inhalation therapeutic devices can be categorised into four main types, including nebulisers, pressurised-metered dose inhalers (pMDI), soft mist inhalers (SMI) and dry powder inhalers (DPI) [22]. In terms of units sold in 2014, pMDIs and DPIs constitute the majority of devices for inhalation drug delivery [21]. For this reason, this article focuses purely on the evaluation of DPIs. In contrast to pMDIs, DPIs work with larger lactose particles carrying the active substance and are environmentally preferable due to the absence of hydrofluorcarbons [135]. Nevertheless, DPIs require a minimum peak flow during inhalation, created by the patient, to detach and propel the aerosol in direction of the lung regions. The lack of required synchronity between activation and inhalation of the DPI is reducing a potential source of misuse [136]. However, other errors such as loading and priming the DPI for use or exhalation into the DPI before the inhalation step are present and have a significant negative effect on the delivered dose [136], [137]. The optimum flow profile varies for the currently available DPIs and may lead to a suboptimal delivered dose for the patients [136]. Most recently developed DPIs only deliver a low dose of medication while the users have to be able to create a minimum inspiratory flow and have the cognitive ability to properly operate the DPI [138]. This is accompanied by the need for an adequate lung volume of the user, therefore excluding children below the age of 5 years [138]. Considering only a single peak inspiratory flow rate (PIFR) value as the main criterion for determining the capability of the patient to use an

inhaler efficiently may be an insufficient criterion as the DPIs vary in their design and resistance to airflow [61]. While several available studies evaluating DPIs focus mainly on inspiratory flow rate [139]–[143] a more suitable criteria has proven to be ensuring a sufficient pressure drop of $\geq$1 kPa across the device. Inhalation under these conditions leads to delivery of an adequate lung dose of the pharmaceutical [61]. Focusing on the pressure drop across the device could help prevent exclusion of patients from DPI usage due to insufficient or excessive peak inspiratory flow rate. Both have been shown to negatively impact pulmonary drug delivery [139], [144]. Therefore, the pressure drop over the DPI has been taken as the main evaluation criterion for successful inhalation processes for this work.

In vitro pharmaceutical aerosol test systems often include either sample collection tubes or cascade impactors, such as the Andersen non-viable impactor, or the Next Generation Impactor to collect the particles for classification [145]–[147]. The results using such systems provide insights about the properties of the inhaled aerosol, such as the sizes of the inhaled particles and the deposition fraction, which can be used for comparison with radio-nuclide imaging studies [59] or to validate in silico dosimetry models [148]–[150]. Cascade impactors consist of stages, each containing impaction plates which represent obstacles for an incoming airstream [151]. These plates create an abrupt bend in the airstream causing the particles, whose inertia exceeds a cut off size, to deposit [152]. Due to the operating principle of cascade impactors and sample collection tubes, evaluation of aerosol during consecutive inhalation and exhalation is not feasible [153]. The aerosol particles deposit on the impaction plates during inhalation and are consequently not present in the exhalatory airstream . For this reason, optical aerosol spectrometry was utilised in this work allowing for evaluation of particles within both inhalation and exhalation airstream.

Pulmonary drug delivery is based on the primary mechanisms of aerosol deposition, which are defined as inertial impaction, gravitational sedimentation, Brownian diffusion, turbulent deposition, electrostatic precipitation, and interception [154]. The effect of deposition mechanisms on aerosol particles depends on the particle characteristics such as particle size, overall size distribution, shape, composition, surface characteristics and charge [155]. Moreover, the processes resulting from molecular transfer between particles and their respective surrounding gas are nucleation, condensation, evaporation hygroscopicity and coagulation [156]. Inhalation drug therapy aims at targeted delivery of pharmaceuticals into the lung. The inhaled particles must overcome filtration mechanisms in the upper airways causing them to deposit within this region [157]. The deposition mechanism occurring mainly in the upper airways is inertial impaction affecting mostly large particles (>2-5 µm) with a strong dependency on the airflow rate. The deposition in this region of the respiratory tract results from direction changes of flow when the particles deviate from the

streamline and collide with the airway walls. The probability of such deviation can be described by the Stoke's number where particle diameter, carrier gas viscosity and airway diameter are used to calculate the probability of deposition [158]. In the respiratory tract, gravitational sedimentation of particles in the size range of (>1-8 µm), refers to the settling of particles under the influence of gravity. Brownian diffusion results from random motion and the collision of the particles with the carrier gas molecules. The effect of mutual repulsion due to electric charges concerning the inhaled particles is defined as electrostatic precipitation. The described mechanisms arise mostly in the upper and conducting airway region of the respiratory tract, whereas diffusion and electrostatic precipitation is also taking place in the acinus region of the pulmonary system for particles <3 µm. [154]

The objective of this work is to experimentally investigate changes in aerosol particle diameter and particle number concentration of pharmaceutical aerosols under realistic inhalation and exhalation conditions, resulting in a calculated lung deposition. The active respiratory system model (xPULM) used in this work includes two core elements; a computed tomography (CT) derived mechanical upper airway model (UAM), and a primed porcine lung serving as human lung equivalent. This setup is used to represent a patient undergoing inhalation therapy. In contrast to widely spread measurement setups, this work integrates an optical aerosol spectrometer for inhalation and exhalation measurements to eliminate the drawbacks introduced by cascade impactors [153], [159]. To cover a wide spectrum of devices used in clinical practice, four commonly used DPIs are investigated. Instead of focusing on PFIR, the focus was put on reaching a pressure drop of at least ($P_{DROP} \geq 1$ kPa) for all inhalers. This article aims to provide an alternative respiratory model suitable to reduce animal experimentation in aerosol research. Furthermore, the work aspires to mitigate the shortage of experimental data, viable to substitute demanding and constrictive experiments with human subjects. Moreover, the experimental setup including the xPULM™ model, can be seen as a basis for an alternative to animal testing, as the porcine lung, included in this trial, has been salvaged from an abattoir.

3.2 Materials and Methods

3.2.1 Measurement setup and procedure

The following two measurement trials were conducted during this study: A) Characterisation measurements and B) Respiration measurements. To assess the particles generated by the DPIs, Characterisation measurements were performed using a simple connection element to the respiratory model xPULM™. This connector

is characterised by a simplified version of the human laryngeal space, in form of a 90 degree bend and includes a sampling nozzle. This aerosol sampling point is in-line with the inhalatory airstream to ensure isoaxial aerosol sampling. Moreover, the control loop of the optical aerosol spectrometer maintains a constant sampling flow, regardless of the inhalation flow profile. The active model of the human respiratory system, xPULM™, was used with polymer breathing bags, to simulate the inhalation effort of a patient during particle characterisation measurements.

In the second step, Respiration measurements (see Fig. 3.1) were conducted to investigate changes in aerosol particle diameter and particle number concentration during inhalation and exhalation. For this purpose, a primed porcine lung was used as a anatomically realistic lung equivalent. The porcine lung has been proven to be a suitable model of the anatomy of the human lung [160] and has been used in previous studies to research the pathogenesis of diseases such as cystic fibrosis [161]. The lung equivalent was connected to a mechanical UAM which was rapidly manufactured

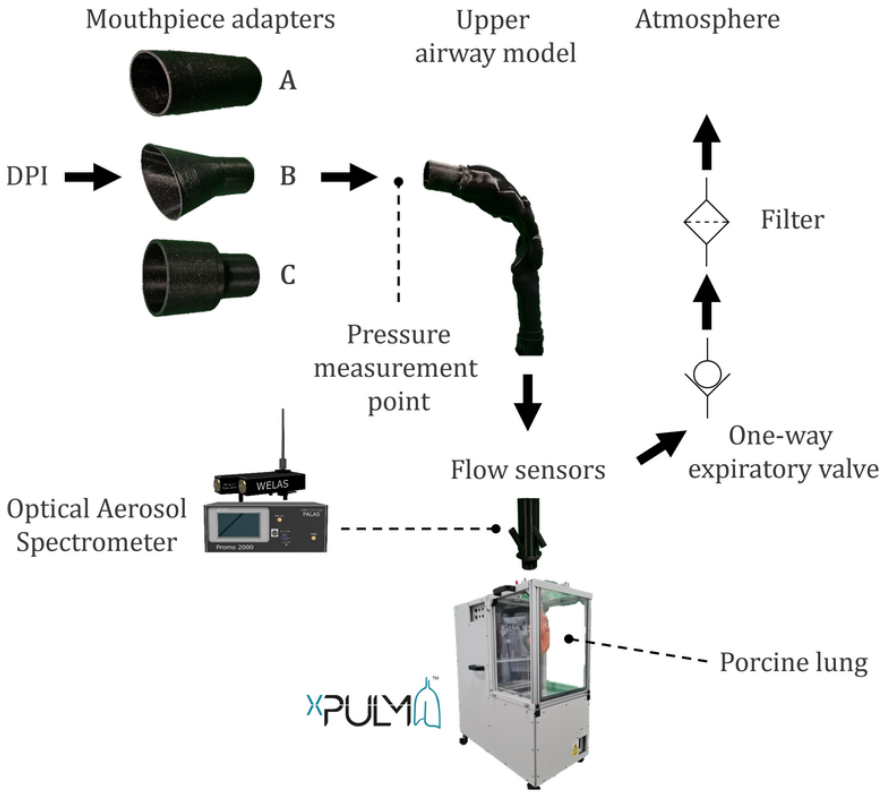

Fig. 3.1: The measurement setup for Respiration measurements consisting of mouthpiece adapters for A) BreezHaler® B) Ellipta®, HandiHaler® C) Turbohaler®, the mechanical UAM derived from CT examinations, optical aerosol spectrometer used to characterise the aerosol particles and the active model of the human respiratory system xPULM™ with the porcine lung.

using 3D-printing techniques. The UAM is based on a clinically annotated CT examination of a healthy subject. In contrast to the characterisation measurements, sampling took place at the lower end of the mechanical UAM to assess the influence of its geometry on the measured values. The DPIs were mounted to the UAM using custom mouthpiece adapters to ensure airtight connection.

The measurement procedure of the Respiration measurements consists of three phases (i) inhalation, (ii) breath-hold, (iii) exhalation. Inhalation with maximum effort was simulated until the pressure drop across the DPI, measured with the Flow-Analyser PF-300 (IMT Analytics, Switzerland), reached at least the recommended pressure drop of $\geq$1 kPa [61]. However, if achieveable, a pressure drop of 4 kPa, was targeted [162]. The driving force of the inhalation was terminated when the peak value of the pressure drop was reached. However, inhalation continued briefly, due to inertia and compliance of the lung equivalent. Inhaler-specific inhalation profiles were recorded using mass flow sensors SFM3300-AW (Sensirion, Switzerland).

All measurements have been performed under laboratory conditions and environmental parameters have been recorded. The results have been adjusted for the recorded background aerosol load. After each measurement trial, breathing simulation was run until the background load was reached.

The inhalation manoeuvre was followed by a 5 s breath-hold period prior to slow and steady exhalation at a flow of 30 L/min for the duration of 6 s. For each tested DPI, the measurements were repeated 12 times (n=12). The in-/exhalation airstream was sampled by the optical aerosol spectrometer Promo 2000 (PALAS, Germany) connected to a white light aerosol sensor Welas 2070 (PALAS, Germany) with a constant flow rate of 5 L/min. The sensor is capable of measuring particles in the range of 0.2 µm to 10 µm.

3.2.2 Model of the Human Respiratory System

The active model of the human respiratory system xPULM™ has been used in this study. The xPULM™ replicates human breathing efforts exerted during the use of DPIs. Fundamental respiratory characteristics (e.g., flow, pressure, and volume) of a rapidly inhaling human are captured during the simulation with high fidelity. Properties of the human respiratory system such as airway resistance and lung compliance are represented by using lung equivalents (porcine lungs) and mechanical UAMs (based on CT examinations). The displacement of gasses during spontaneous breathing occurs due to the pressure difference between the atmosphere and the human lung. This physiological process is recreated by the xPULM™. During the breathing simulation, pressure changes in the thoracic chamber are induced by the movement of a bellows system. For inhalation, a negative pressure is created in

the chamber by expanding the bellows, leading to air following the pressure gradient resulting in inflation of the lung equivalent. During exhalation the opposite process occurs. The bellows is moved back to its original position, increasing the pressure in the chamber and deflating the lung equivalent. The movement of the bellows system can be precisely adjusted in the control software of the xPULM™. This allows for the simulation of different breathing scenarios under various conditions as demonstrated in [163]. A detailed description of the xPULM™ functionality and components including validation measurements are presented in our previous work [62].

Representation of the Upper Respiratory Tract

The mechanical UAM includes the oral cavity, oropharynx, larynx, and trachea. A CT examination of a 28-year-old, healthy, non-smoking, male was used for the UAM reconstruction. The subject has been annotated as healthy by clinical staff and did not show any sign of abnormal restrictions or geometrical limitations. Therefore, this CT examination has been considered to serve as a valid representation of an exemplary upper airway similar to previous works [164], [165]. The selected dataset contained 280 images with a slice thickness of 0.75 mm and was exported in a Digital Imaging and Communications in Medicine (DICOM) format for further processing. The upper respiratory tract was segmented using a combination of thresholding and region growing techniques. The outcomes of the semi-automatic segmentation were inspected on a slide-by-slide basis and the segmentation parameters were adapted

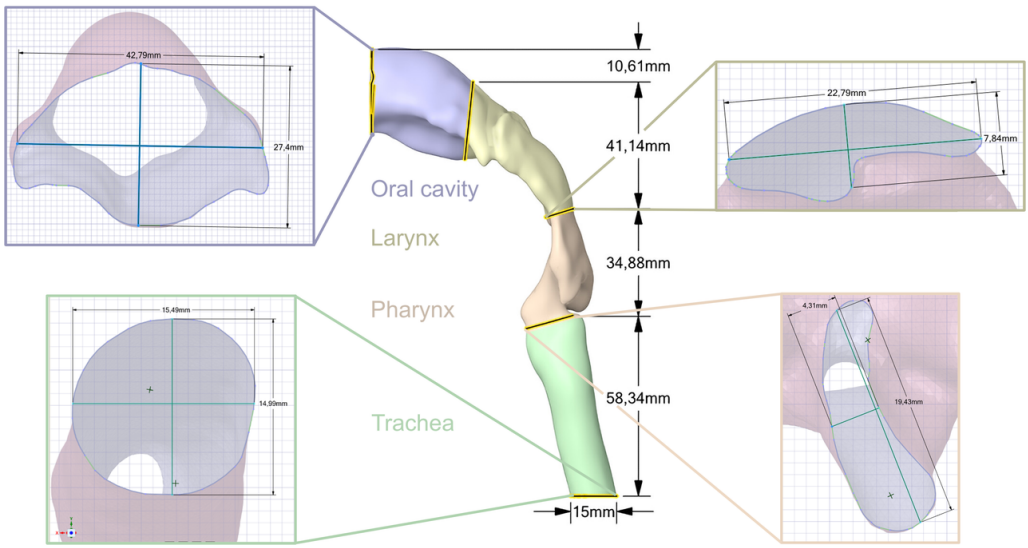

Fig. 3.2: The manufactured 3D model of an upper respiratory tract of a 28-year-old, healthy, non-smoking, male.

Tab. 3.1: Summary of the mechanical UAM dimensions of a 28-year-old, healthy, non-smoking, male. The sections correspond to the highlighted sections in Fig. 3.2. SA - surface area

Section	Volume [mm^3]	Lower SA [mm^2]	Diameter Y [mm]	Dimeter X [mm]	Upper SA [mm^2]	Diameter Y [mm]	Diameter X [mm]
Trachea (green)	10657.02	188.39	15.49	14.99	86.60	18	4.93
Pharynx (orange)	7311.52	119.06	19.43	4.31	86.60	4.86	24.51
Larynx (yellow)	15902.39	119.11	7.84	22.79	777.57	24.93	44.34
Oral cavity (blue)	22265.60	777.60	7.84	22.79	529.90	7.84	22.79

to obtain a precise segmentation of the upper airways. The resulting 3D model was exported as a Standard Triangle Language (STL) file and post-processed to be 3D-printable. The final 3D mechanical UAM was manufactured using rapid prototyping techniques and coated with resin. An emphasis was placed on positioning the model to minimise usage of support structure in the flow path. The dimensions for each section of the final model are summarised in Fig. 3.2 and Tab. 3.1. Custom connectors were designed based on the geometry of each DPI to ensure an airtight connection between the inhaler and the mechanical UAM.

All rapidly produced components were manufactured from Polylactic acid (PLA) with a wall thickness of 2 mm and a layer height of 0.2 mm.

Representation of the Lower Respiratory tract

The lower respiratory tract consists of the bronchi, bronchioles, and alveoli, which form the lung. During breathing simulations, these structures have been represented by a primed porcine lung. The lung was salvaged from a slaughterhouse process and is therefore compliant with the 3R principles [27] which denote responsible use of animal or animal organs during experiments. The Nasco-guard® (Nasco, Wisconsin, USA) preservation process keeps the porcine lung inflatable, elastic and covered with the parietal pleura. These properties are necessary for physiologically and anatomically realistic simulations of human breathing.

3.2.3 Dry powder inhalers

In total, four DPIs were evaluated in this study, grouped into single-dose and multiple dose inhalers. The single-dose devices (BreezHaler® and HandiHaler®) are loaded with a capsule containing the dose which is punctured prior to use. The remaining three were multi-dose DPIs (Ellipta®, Turbuhaler®) which store multiple doses within the devices. Outlets of all DPIs were modified with custom rapidly

Tab. 3.2: Summary of the relevant parameter values of the used DPIs taken from literature [61], [166].

Device	Active substance	Resistance [$kPa^{1/2}$/L/min]	Metered Dose [µg]	Lactose [mg]	Dose type
Seebri® Breezhaler®	Glycopyrronium	0.0216	44	23.6	multi-dose, pre-dispensed
Anoro® Ellipta®	Fluticasone furoate and vilanterol	0.0286	55/22	25	multi-dose, pre-dispensed
Spiriva® HandiHaler®	Tiotropium bromide	0.0504	18	5.5	single-dose, hard capsules
Symbicort® Turbohaler®	Budesonide and formoterol	0.0313	200/6	0.73	multi-dose, pre-dispensed

manufactured adapters to enable well-fitted, airtight, connection to the oral cavity of the mechanical UAM.

3.2.4 Data Processing and Statistics

The optical aerosol spectrometry measurements were conducted with 128 intervals per decade. The arithmetic centre of the intervals (x_i) is then:

$$x_i = x_{i,lower} + \frac{x_{i,upper} - x_{i,lower}}{2} = x_{i,lower} + \frac{\Delta x_i}{2} \; [\mu m] \tag{3.1}$$

For further calculations, the differential particle number distribution $q_0(x_i)$ is defined as:

$$q_0(x_i) = \frac{1}{\sum n_i} \frac{n_i}{\Delta x_i} \; [\mu m^{-1}] \tag{3.2}$$

where n_i is the measured particle number within the interval limits $x_{i,lower}$ and $x_{i,upper}$. Leading to the mean particle diameter M_1 calculation:

$$M_1 = \sum (x_i \; q_0(x_i) \; \Delta x_i) = \bar{x} \; [\mu m] \tag{3.3}$$

Further information about the inhaled aerosol is obtained by calculating the particle number concentration:

$$dCn = n_i \frac{1}{V_m} \; [P/cm^3] \tag{3.4}$$

where the measured volume V_m is defined as:

$$V_m = u \; Iw \; t_{measurement} \; [cm^3] \tag{3.5}$$

where u is particle velocity and Iw is the cross-section of the optical sensor.

For the chosen measurement setup equation 3.5 can be simplified to

$$V_m = Qt_{measurement} \; [cm^3] \tag{3.6}$$

where Q is the volumetric airflow (5 L/min). The measurement data is evaluated with non-parametric methods as the requirements for normal distribution and hence

parametric test methods are not fulfilled. The data groups are compared pairwise using the Kruskal-Wallis test by ranks (or one-way ANOVA on ranks) with a significance level of $\alpha = 0.05$, H values and p values are calculated and compared to a critical $\chi^2 = 3.841$ for a degree of freedom $df = 1$.

3.3 Results and Discussion

3.3.1 Inspiratory flow rate and pressure drop measurements

Flow profiles measured during Characterisation and Respiration measurements for the evaluated DPIs are presented in Fig. 3.3. During Characterisation measurements, the resistance of the system is primarily resulting from the inner resistance of the DPIs. The peak inspiratory flow, measured at the pressure drop values, provided in Tab. 3.3, ranges from 45 to 120 L/min. The shape of the inhalation profile, shown in Fig. 3.3A is characteristic for each used DPIs and reflects the individual constructional solution of the devices included in this evaluation. Vibrations of the capsule, for example, are distinctive for HandiHaler® and manifest in rapid oscillations of the inspiratory flow. Inhalation time required to reach the necessary pressure drop is influenced by the inner resistance of the DPIs. The shape of the measured flow profiles with xPULM™are comparable to full flow-rate profiles of

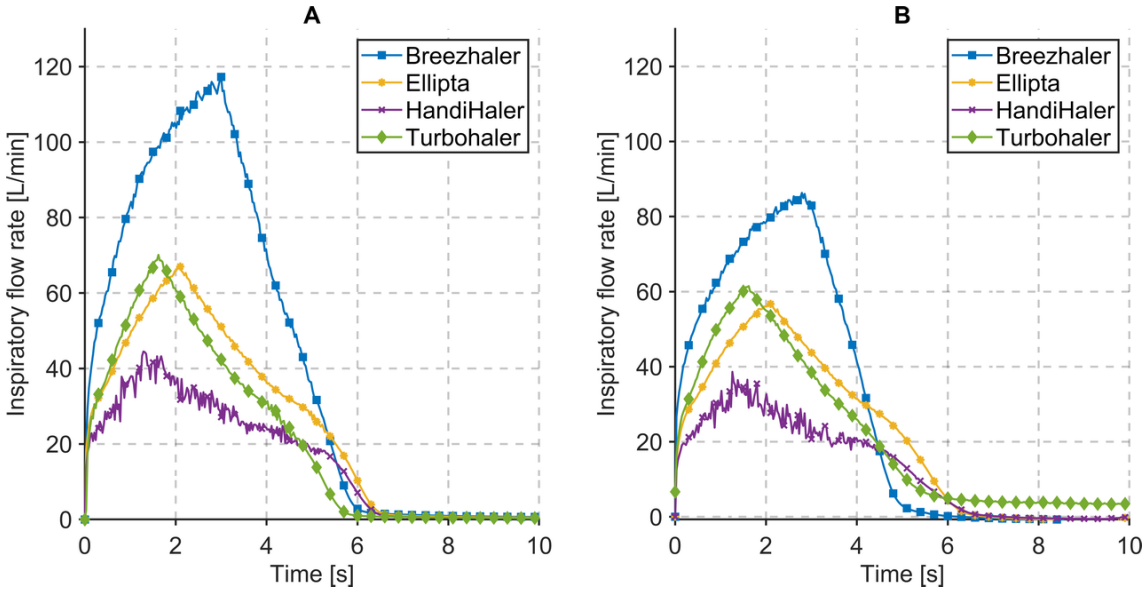

Fig. 3.3: Flow profiles during A) Characterisation measurements B) Respiration measurements while inhaling through Breezhaler®, Ellipta®, HandiHaler® and Turbohaler® at a pressure drop given in Tab. 3.3.

patients [166].

The inspiratory flow rate during Respiration measurements is, in contrast to Characterisation measurements, influenced by resistance and compliance of the included mechanical UAM and the primed porcine lung, respectively. This is evident for DPIs with low inner resistance (e.g., Breezhaler®) where the inspiratory flow rate drops by 30 L/min. In case of DPIs with higher inner resistance (e.g., HandiHaler®) the flow rate is influenced moderately as the increase of the overall system resistance is lower. The peak inspiratory flow, measured at the pressure drop values, provided in Tab. 3.3, ranges from 39 to 86 L/min. The system resistance refers to a combination of DPI inner resistance (constant) and the resistance of attached pneumatic components.

The flow results of the different DPIs, as shown in Fig. 3.3, allow conclusions on the handling of the inhaler and its characteristics during use. The HandiHaler® for example shows a wider range of flow values as well as higher volatility in pressure drop values (see Fig. 3.4), than most of the other inhalers. This is mainly caused by the propelling mechanism, which is based on the mechanical movement of the aerosol loaded capsule. Based on the user guide, the capsule has to move (also acoustically noticeable) within the inhaler, in order to disperse the powder. This oscillating movement leads to a volatile flow and oscillating pressure drop measurements, therefore, characterisation of this inhaler is influenced by the handling of the

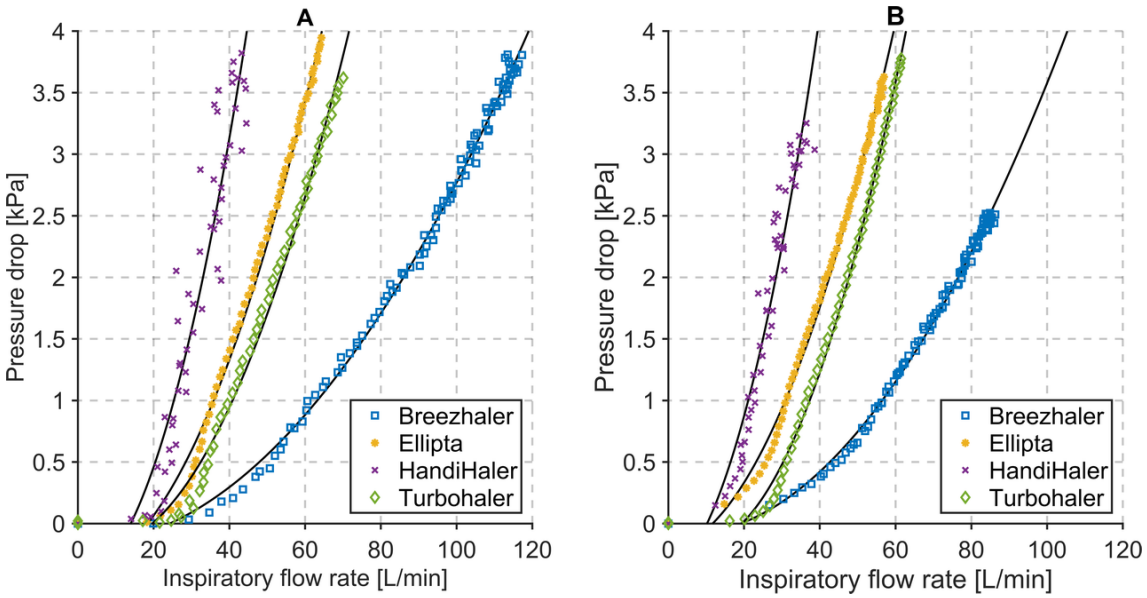

Fig. 3.4: Relationships between inspiratory flow rate and pressure drop of four commercial DPIs during A) Characterisation measurements B) Respiration measurements.

capsule and inhaler.

A comparable observation can be made for the use of the second capsule-based DPI, the Breezhaler®. This product is also based on the oscillation of the capsule in order to propel the aerosol properly. These oscillations are moreover influenced by the holding position and angle of the device during inhalation. In contrast to the HandiHaler®, the capsule within the Breezhaler® is not limited in movement mechanically, but mainly by gravitation. When the Breezhaler® is moved to a horizontal position the likelihood of the capsule dropping out of the holding cavity increases, impacting the aerosol production mechanism.

The correspondingly changed flow profiles caused by different lung equivalents can be observed in Fig. 3.3. The compliance of the introduced lung tissue (depicted by the flow curves in Fig. 3.3B influences the peak flow as well as the flow profile. The anatomic components of the used porcine lung and its geometric properties lead to a prolonged inhalation time and flattened flow profile when using identical inhalation settings as with the polymer-based breathing bags as lung equivalent.

3.3.2 Influence of the mechanical UAM and the primed porcine lung

Effects of the mechanical UAM and the primed porcine lung during Respiration measurements are evident from the relationship between inspiratory flow rate and pressure drop across the inhalers, see Fig. 3.4B. The resistance of the measurement system increases significantly ($p < 0.05$) with all inhalers (see Tab. 3.3) and a pressure drop of 4 kPa is reached for lower inspiratory flow rates.

The measurements revealed limitations in reaching the pressure drop of 4 kPa consistently for Breezhaler®. Based on the recorded observations, the position of the capsule within the DPI, as well as the angle of the device are critical. Even a slight movement of the capsule changes the behaviour of the device. The pressure drop set prior to measurements could not be reached despite high inspiratory flow and prolonged inhalation time. A pressure drop $\geq$1 kPa with any DPI is sufficient for the patient to receive an adequate lung dose [61]. This criterion (defined as a minimum requirement) was met over all conducted measurements.

Relevant parameter values for the used DPIs, Characterisation measurements and Respiration measurements are summarised in Tab. 3.3. These parameter values complement the graphical result shown in Fig. 3.3 and Fig. 3.4. Additionally, they provide further inside about the relationship between the inner resistance of the DPIs, inhaled volume, inhalation time and peak inspiratory flow at particular pressure drop values.

Tab. 3.3: Summary of the relevant parameter values for the used DPIs, during Characterisation and Respiration measurements. Where: V_{INH} - inhaled volume, P_{DROP} - pressured drop across the inhaler during inhalation, PIF - peak inspiratory flow, and t_{INH} - inhalation time.

Dry powder inhalers	Characterisation parameters					Respiration parameters				
Device	Vinh [L]	P_{DROP} [kPa]	PIF [L/min]	tinh [s]	System Resistance [$kPa^{1/2}$/L/min]	Vinh [L]	P_{DROP} [kPa]	PIF [L/min]	tinh [s]	System Resistance [$kPa^{1/2}$/L/min]
Seebri® Breezhaler®	6.98	3.81	117.28	3.00	0.0166	4.55	2.52	86.31	3.00	0.0184*
Anoro® Ellipta®	4.06	4.27	67.01	2.10	0.0308	3.38	3.63	56.94	2.10	0.0335*
Spiriva® HandiHaler®	2.60	3.82	44.50	1.40	0.0439	2.05	3.25	38.62	1.40	0.0467*
Symbicort® Turbohaler®	3.52	3.83	70.11	1.60	0.0279	3.40	3.89	61.48	1.60	0.0320*

* $p < 0.05$ for difference between resistances measured with and without the mechanical UAM

The difference between the inner resistances of DPI measured during characterisation and the values extracted from the literature is in an acceptable tolerance range of $\pm 0.01\,kPa^{1/2}$/L/min.

3.3.3 Changes in mean particle diameter

Changes in mean particle diameter (M_1) during DPI Characterisation and Respiration measurements using the mechanical UAM and primed porcine lung are depicted in Fig. 3.5. During characterisation measurements the mean particle diameter ranges from 0.95 µm (TurboHaler®) to 2.90 µm (HandiHaler®). These results are comparable to literature values reporting particles ranging from 2.20 µm (Ellipta®) to 3.90 µm (HandiHaler®) [166]. Differences in the absolute values of mean particle diameter are to be expected, based on the different components of the used measurement setup. As reported by several authors [61], [139], [166], [167] the aerodynamic properties of the generated drug particles vary based on quantities such as peak inspiratory flow rate, flow acceleration, inhalation time and inhaled volume. These quantities are patient-specific and vary from the presented measurements. Filtration properties of the mechanical UAM cause the mean particle diameter to shift towards lower values during inhalation. This can be observed for all tested DPI, as Fig. 3.5 depicts. It has been shown, that the upper respiratory tract indeed acts as a particulate filter. Larger particles (>3 µm) deposit more easily in the upper respiratory tract. While the smaller particles (<3 µm) pass into the lower respiratory tract as the filtration function decreases with particle size. [168], [169]

Exhaled particles during our measurements are characterised by a mean particle diameter in a narrow range from 0.31 µm (HandiHaler®) to 0.56 µm (BreezHaler®). These results were expected as the deposition of aerosol particles in the lung reaches

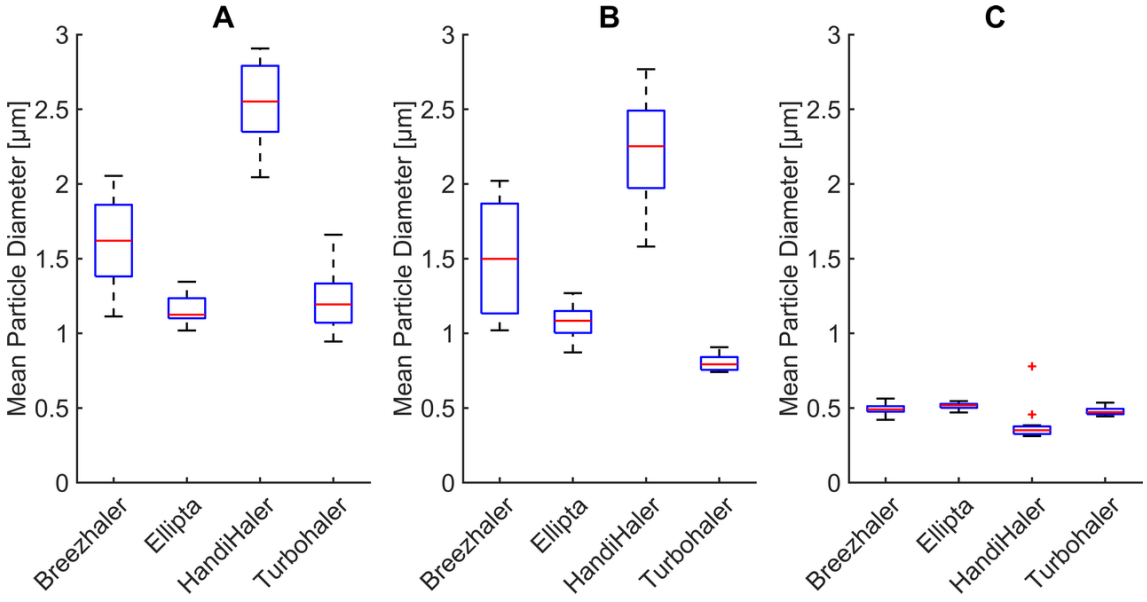

Fig. 3.5: Changes in mean particle diameter during A) Characterisation measurements B) Inhalation measurements C) Exhalation measurements for four commercial DPIs

its minimum at 0.5 µm [170], [171]. Furthermore, there is a significant difference ($p < 0.05$) in mean particle diameter between inhaled and exhaled particles Fig. 3.5B & C for all tested DPIs (K-W test, $H = 17.29$, $p = 0.00003$). This change is caused by the interaction of the aerosol particles with the primed porcine lung tissue. The interaction is caused by a highly complex and constantly changing inner geometry of the lung tissue, which influences the mean particle diameter. Additionally, the high relative humidity within the lung tissue may lead to hygroscopic growth and therefore also to adhesion of particles.

3.3.4 Deposition of particles in the porcine lung

The difference between the particle number concentration in inhaled and exhaled air can be considered as number concentration of particles depositing in the porcine lung. The deposition is expressed as a percentage of particle number concentration averaged over the individual inhalation or exhalation cycles and depicted in Fig. 3.6. The deposition of particles in the respiratory tract reaches its minimum in the range of 0.40 µm–0.60 µm [171]. The measured particle size distribution for Ellipta and Turbohaler during inhalation is characterised by lower mean particle diameters (1.08 µm and 0.79 µm respectively). This corresponds to the deposition effects and measured number concentration represented in Figures 3.6 & 3.7. However, all

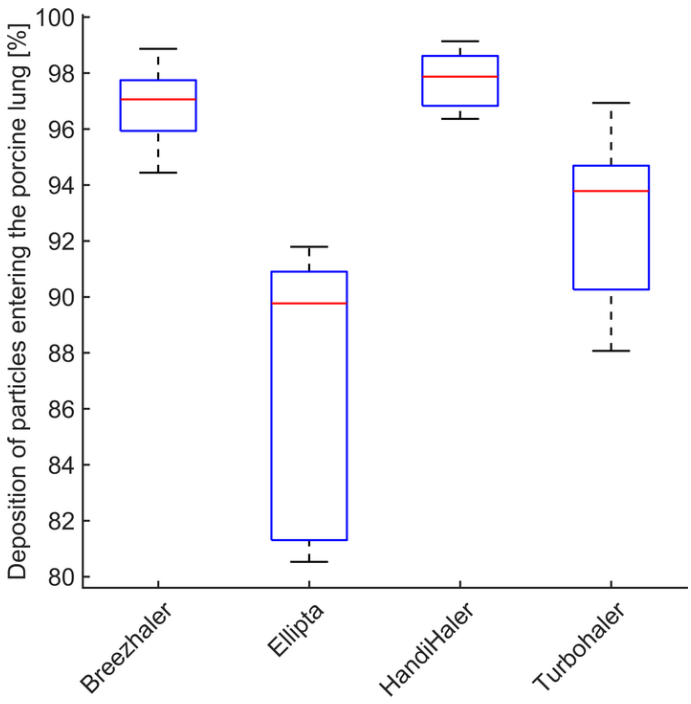

Fig. 3.6: Deposition of aerosol particles in the porcine lung (expressed as a percentage of particle number concentration measured posterior of the mechanical UAM) for four commercial DPIs inhalers.

measured DPIs show deposition above 80% achieving the intended drug delivery.

Differences between aerosol particle number concentration sampled from the air stream during A) Inhalation and B) Exhalation for all inhalers are depicted in Fig. 3.7. There is a statistically significant difference ($p < 0.05$) between particle number concentration in inhaled and exhaled airstream for all tested inhalers (K-W test, $H = 17.29$, $p = 0.00003$). This is caused by particles depositing in the primed porcine lung.

The generated drug particles from the DPIs are inhaled through the mechanical UAM which represents the naso-oro-pharyngo-laryngeal region (extrathoracic region). Larger particles (>3 µm) deposit in this region mainly due to effects of inertial impaction [171]. The rest of the drug particles penetrates the deeper regions of the respiratory tract model and reach the primed porcine lung. The complex geometry and high relative humidity of the lung present an ideal environment for most of the particles to deposit due to sedimentation and Brownian diffusion [150], [171].

Regional lung deposition and bronchodilator response of pharmaceutical aerosols was studied extensively in previous works [172], [173]. Their results confirm that small particles are exhaled with exhalation fractions for particle diameters 1.5 µm, 3 µm and 6 µm being 22%, 8%, and 2% respectively [173]. A lung deposition study

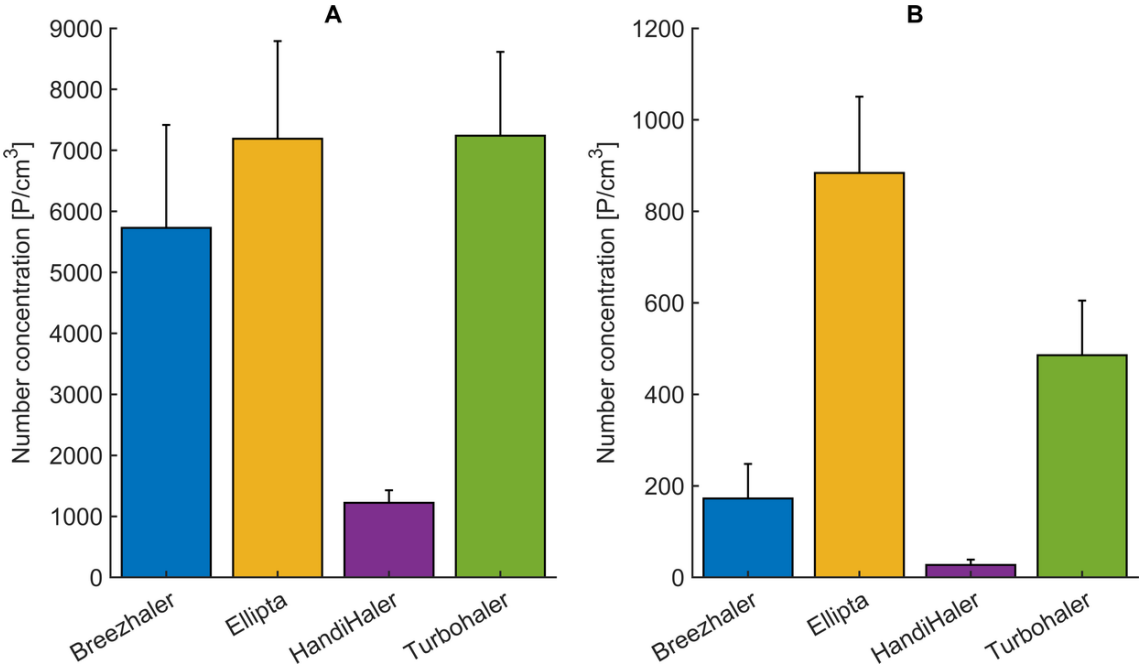

Fig. 3.7: Differences between aerosol particle number concentration sampled from the air stream during A) Inhalation and B) Exhalation for four commercial DPIs. Respiration parameters are provided in Tab. 3.3.

in healthy human subjects showed a exhalation fraction of exhaled dose of 1.2% [174]. In this study, however, a MAGhaler DPI was used to aerosolise the powder.

Research conducted with healthy individuals, asthmatic and COPD patients show no significant difference in drug deposition of aerosols generated with DPIs [175]. The reported fraction of exhaled particles ranges between 1.6% and 3.3%. These findings are consistent with our measurements where the fraction of exhaled particles ranges from 2.13% (HandiHaler®), 2.94% (BreezHaler®), 6.22% (Turbohaler®) to 10.24% (Ellipta®).

3.4 Summary and Conclusion

For a large number of patients, DPIs are the device of choice for the delivery of pharmaceuticals to manage asthma and COPD [139], [176]. The number of commercially available DPIs is growing [61] with inhalers varying in their design, operating mechanisms, and resistance to inhaled airflow [61], [177]. Accounting for these properties and the patient's ability to use the specific device is essential for efficient drug delivery. Testing setups provide an option to evaluate aerosolised dry powders generated by DPIs and allow for further insights into DPI performance under various condi-

tions [59], [178]–[180].

In this work, aerosol particle diameter and particle number concentration of pharmaceutical aerosols generated by four commercially available DPIs were investigated. The measurement setup consists of the active respiratory system model xPULM™ in combination with optical aerosol spectrometry and a mechanical UAM. This allows for the evaluation of pharmaceutical aerosols in the range of 0.2 µm to 10 µm and the calculation of deposition of particles in the porcine lung under realistic inhalation and exhalation simulations. Experimental data measured during exhalation are scarce when in vitro pharmaceutical aerosol test systems are employed due to the operating principle of impactors.

To represent the human upper respiratory tract with high fidelity a mechanical UAM was developed, manufactured, and introduced as a part of the xPULM™. The model was derived from CT examinations of a 28-year-old healthy male, which has been clinically annotated. A primed porcine lung was used to simulate the complex inner structures of the human lower respiratory tract. The integration of the mechanical UAM and primed porcine into the xPULM™ model represents an important step forward towards the realistic simulation of a breathing human. Additionally, the combination of xPULM™ with an optical aerosol spectrometer presents an alternative approach to animal experimentation suitable for applications in aerosol research.

Our results can be summarised as follows:

- Integration of a mechanical UAM, as a part of the xPULM™, increases the resistance of the overall system. This affects inhalatory flow and pressure characteristics of DPIs with lower inner resistance more than DPIs with high inner resistance, where the change is negligible.
- Inclusion of a porcine lung as a representation of the human lower respiratory tract (compliant with the 3R principles) allows comparable particle deposition to reported findings [173]–[175].
- Handling and placement of a capsule into single-dose DPIs influences aerosol production during inhalation drug therapy. Slight changes in capsule placement may influence the amount of delivered drug. Correct handling of the inhaler should be emphasised alongside acceptable inhalation manoeuvres (as defined by the device manufacturer) to ensure the desired result.
- Mean particle diameter is reduced by the filtration properties of the mechanical UAM, affecting mostly larger particles (>3 µm). Such models, when based on CT examinations, are reliably representing the function of the human upper respiratory tract.
- The majority of particles entering the porcine lung deposit within, minimum deposition is reached for the particle size of (0.5 µm). The primed porcine lung

is therefore a suitable lung equivalent and representation of the human lung.

- Sampling of the airstream during inhalation and exhalation and its subsequent evaluation using optical aerosol spectrometry techniques is a viable alternative to impactors for evaluating pharmaceutical aerosols.

In conclusion, the xPULM™ active respiratory system model in combination with the introduced mechanical UAM and the optical aerosol spectrometer is a viable option for investigating particle diameter and particle number concentration of pharmaceutical aerosol depositing in the porcine lung under realistic breathing conditions. Further research will focus on the inclusion of additional components and techniques (e.g., nano-dots, tissue sampling, histopathology) to quantify the regional deposition of pharmaceutical aerosols in lung tissue obtained by 3R compliant processes. Additionally, coating of the inner surface of the mechanical UAM will be considered, to ensure the least possible artifacts and interference of the 3D printing materials on the particle transportation effects. Besides regional deposition, also mass-based approaches will be included, to further increase comparability with established deposition measurement techniques.

Further directions & future work

Due to the rapid advancements in the underlying technology (e.g. CFD and microfluidics), in silico and in vitro organ-on-a-chip models of the human respiratory system are the most prominent in the research landscape. These models facilitate developments in applications such as drug development and toxicity testing. Nevertheless, in silico models are limited by challenges of simulating turbulent and transitional flows, static boundary conditions (airway expands during inhalation) and require simplifications of respiratory system geometry. Furthermore, there is a need to validate such models experimentally. In vitro models lack a systemic response, have difficulties to capturing interactions between different cell types and the impact of long term exposure and must cope with a limited lifespan of the used cells. Other, complementary modelling approaches fill the gaps resulting from these limitations. Every modelling approach has advantages and disadvantages. It is the combination of findings from each of them that allows for continuous advancements in respiratory research.

Further directions include:

- Implementation of new technologies to the existing models and creation of new models to allow for high-fidelity simulation representing in realistic manner anatomy, physiology, and pathophysiology of the human respiratory system.
- Personalised approaches in medicine where patient-specific respiratory patterns, airway geometry and lung condition are being simulated to achieve the best possible result for the individual.
- Research of novel methods in guided pulmonary drug delivery, drug formulation, and inhalation of antibiotics, biopharmaceuticals or anti-cancer treatment.
- Compliance and the advancements of the 3R principles (Replace, Reduce, Refine) of humane animal research being at the forefront of all modern research endeavours.

This thesis can be seen as one of the major steps on the path to further research of clinically relevant applications of the xPULM™. The results of the thesis enable advances in research focusing on breathing simulations with other animal lungs (e.g. rabbit, sheep), development of different UAM with various manufacturing mechanisms and materials, testing of additional medical aerosol generators such as nebulisers, and implementation of new aerosol measurement techniques. Building on the presented work, new research projects are currently underway and focus on the development of novel treatment options in neonatal care, methods to minimise patient-ventilator asynchronies, comparison of different upper airway geometries, and determination of local aerosol particle deposition in the lungs.

Conclusion

This thesis aims to establish a physical model of the human respiratory system (xPULM™) that represents an innovative approach to respiratory system behaviour modelling. To reach this aim, three applications were researched, namely (i) breathing simulation, (ii) patient-ventilator interaction testing and (iii) aerosolised drug delivery. These applications reflect state-of-the-art directions in which respiratory system models are being used.

First, the reproducibility of sinusoidal breathing simulation has been verified for a range of physiological tidal volumes and frequencies. The xPULM™ simulator represents an innovative approach to the respiratory system behaviour modelling and is capable of simulating different breathing patterns with high fidelity. The possibility of using lung equivalents such as polymer-based breathing bags or animal lungs is unique and allows for the representation of processes naturally occurring during the human respiration cycle. The breathing simulation reliably captures flow and pressure changes representative of those occurring during human breathing.

Second, a new approach of testing patient-ventilator interactions using the xPULM™ simulator has been introduced. The results show that different asynchronies can be triggered when the simulator is used to represent a patient undergoing assisted mechanical ventilation. This approach can support identification, investigation and testing of undesired patient-ventilation interactions and contribute to efforts minimising their occurrences, increasing the well-being of patients.

Third, the number concentration and size distribution of aerosol particles generated by commonly used dry powder inhalers have been experimentally evaluated. Investigation of the characteristics of the particles under realistic inhalation and exhalation is possible due to the inclusion of an optical aerosol spectrometer. This technique is not routinely used for such purposes and provides insights into the interactions of aerosol particles in the porcine lungs during breathing. Additionally, a mechanical upper airway model was developed, manufactured, and introduced as a part of the xPULM™. The model was derived from CT examinations and is representative of realistic airway geometry. This approach proposes an alternative to animal experimentation suitable for applications in aerosol research.

The results of this thesis are embedded in teaching and research activities at the University of Applied Sciences Technikum Wien. Additionally, this thesis contributes to the continuous collaboration between the University of Applied Sciences Technikum Wien, Brno University of Technology and other institutions.

In conclusion, the set objectives of the dissertation have been met. The thesis contains original research that has been presented at international conferences and published in three impact factor journals.

Bibliography

[1] K. Harper and G. Armelagos, "The changing disease-scape in the third epidemiological transition", *International Journal of Environmental Research and Public Health 2010, Vol. 7, Pages 675-697*, vol. 7, pp. 675–697, 2 Feb. 2010, ISSN: 16604601. DOI: 10.3390/IJERPH7020675.

[2] M. Wahdan, "The epidemiological transition", *Eastern Mediterranean Health Journal*, pp. 8–20, 1996, ISSN: 1687-1634. DOI: https://doi.org/10.26719/1996.2.1.8.

[3] W. H. Organisation, *World health statistics 2021: monitoring health for the SDGs, sustainable development goals*, 12. World Health Organisation, 2021, vol. 58, ISBN: 9789240027053.

[4] OECD, *Health at a Glance 2021*, ser. Health at a Glance. OECD, Nov. 2021, ISBN: 9789264961012. DOI: 10.1787/ae3016b9-en.

[5] A. P. Roth, C. F. Lange, and W. H. Finlay, "The effect of breathing pattern on nebulizer drug delivery.", *Journal of aerosol medicine : the official journal of the International Society for Aerosols in Medicine*, vol. 16, no. 3, pp. 325–339, 2003. DOI: 10.1089/089426803769017677.

[6] W. H. Organization, "Towards the end of the epidemics: First progress report", en, World Health Organization, Geneva, Tech. Rep., 2017.

[7] OECD, *Health at a Glance 2019: OECD Indicators*, ser. Health at a Glance. OECD, Nov. 7, 2019, ISBN: 9789264382084. DOI: 10.1787/4dd50c09-en.

[8] G. A. Network, *The Global Asthma Report 2018*. Auckland, New Zealand, ISBN: 9780473465230.

[9] F. of International Respiratory Societies, *The Global Impact of Respiratory Disease*. European Respiratory Society, 2017.

[10] W. H. Organization, *Assessing national capacity for the prevention and control of noncommunicable diseases: report of the 2019 global survey*. Geneva: World Health Organization, 2020, Section: ix, 101 p., ISBN: 9789240002319.

[11] T. Pham, L. J. Brochard, and A. S. Slutsky, *Mechanical ventilation: State of the art*, Sep. 2017. DOI: 10.1016/j.mayocp.2017.05.004.

[12] E. C. Goligher, N. D. Ferguson, and L. J. Brochard, *Clinical challenges in mechanical ventilation*, Apr. 2016. DOI: 10.1016/S0140-6736(16)30176-3.

[13] P. M. Lepper and R. M. Muellenbach, "Mechanical ventilation in early covid-19 ards", *EClinicalMedicine*, vol. 28, p. 100 616, Nov. 2020, ISSN: 2589-5370. DOI: 10.1016/J.ECLINM.2020.100616.

[14] C. Roussos and A. Koutsoukou, "Respiratory failure", *Eur Respir J*, vol. 22, pp. 3–14, 2003. DOI: 10.1183/09031936.03.00038503.

[15] C. de Haro, L. Sarlabous, J. Esperanza, R. Magrans, and L. Blanch, in *ERS practical Handbook of Invasive Mechanical Ventilation*, M. J. S. Leo Heunks, Ed. The European Respiratory Society, 2019, ch. Monitoring patient-ventilator interaction. DOI: 10.1183/9781849841221.eph01.

[16] C. de Haro, A. Ochagavia, J. López-Aguilar, S. Fernandez-Gonzalo, G. Navarra-Ventura, R. Magrans, J. Montanyà, and L. Blanch, "Patient-ventilator asynchronies during mechanical ventilation: Current knowledge and research priorities", *Intensive Care Medicine Experimental*, vol. 7, no. S1, 2019, ISSN: 2197-425X. DOI: 10.1186/s40635-019-0234-5.

[17] L. Blanch, A. Villagra, B. Sales, *et al.*, "Asynchronies during mechanical ventilation are associated with mortality", *Intensive Care Medicine*, vol. 41, no. 4, pp. 633–641, Apr. 2015, ISSN: 14321238. DOI: 10.1007/s00134-015-3692-6.

[18] J. Bousquet and N. Kaltaev, "Global surveillance, prevention and control of chronic respiratory diseases : A comprehensive approach / edited by Jean Bousquet and Nikolai Khaltaev", en, *A word where all people breathe freely*, 2007, Place: Geneva Publisher: World Health Organization Section: vii, 146 p., ISSN: 9789241563468.

[19] J. Bousquet, R. Dahl, and N. Khaltaev, "Global alliance against chronic respiratory diseases", *European Respiratory Journal*, vol. 29, pp. 233–239, 2 Sep. 2006, ISSN: 0903-1936. DOI: 10.1183/09031936.00138606.

[20] M. B. Dolovich and R. Dhand, "Aerosol drug delivery: Developments in device design and clinical use", *The Lancet*, vol. 377, pp. 1032–1045, 9770 Mar. 2011, ISSN: 0140-6736. DOI: 10.1016/S0140-6736(10)60926-9.

[21] S. W. Stein and C. G. Thiel, "The History of Therapeutic Aerosols: A Chronological Review", en, *Journal of Aerosol Medicine and Pulmonary Drug Delivery*, vol. 30, no. 1, pp. 20–41, Feb. 2017, ISSN: 1941-2711, 1941-2703. DOI: 10.1089/jamp.2016.1297.

[22] C. Sorino, S. Negri, A. Spanevello, D. Visca, and N. Scichilone, "Inhalation therapy devices for the treatment of obstructive lung diseases: The history of inhalers towards the ideal inhaler", *European Journal of Internal Medicine*, vol. 75, pp. 15–18, May 2020, ISSN: 0953-6205. DOI: 10.1016/J.EJIM.2020.02.023.

[23] M. Sakagami, "In vivo, in vitro and ex vivo models to assess pulmonary absorption and disposition of inhaled therapeutics for systemic delivery", *Advanced drug delivery reviews*, vol. 58, pp. 1030–1060, 9-10 Oct. 2006, ISSN: 0169-409X. DOI: 10.1016/J.ADDR.2006.07.012.

[24] J. D. Harding, "Nonhuman Primates and Translational Research: Progress, Opportunities, and Challenges", *ILAR Journal*, vol. 58, no. 2, pp. 141–150, 2017, ISSN: 1084-2020. DOI: 10.1093/ilar/ilx033.

[25] S. Festing and R. Wilkinson, "The ethics of animal research. talking point on the use of animals in scientific research", *EMBO reports*, vol. 8, no. 6, pp. 526–530, Jun. 2007, 17545991[pmid], ISSN: 1469-221X. DOI: 10.1038/sj.embor.7400993.

[26] M. Liebsch, B. Grune, A. Seiler, D. Butzke, M. Oelgeschläger, R. Pirow, S. Adler, C. Riebeling, and A. Luch, "Alternatives to animal testing: Current status and future perspectives", *Archives of Toxicology*, vol. 85, pp. 841–858, 8 Aug. 2011, ISSN: 03405761. DOI: 10.1007/S00204-011-0718-X.

[27] W. M. S. Russell and R. L. Burch, *The principles of humane experimental technique*, English. Methuen London, 1959, 238 p. DOI: https://doi.org/10.5694/j.1326-5377.1960.tb73127.x.

[28] V. Monamy, *Animal Experimentation*. Cambridge University Press, 2017, ISBN: 9781316678329. DOI: 10.1017/9781316678329.

[29] E. Council and E. Parliament, "Caring for animals aiming for better science", *Official Journal of the European Union*, pp. 1–162, 2010.

[30] F. Gruber and T. Hartung, "Alternatives to animal experimentation in basic research", *Altex*, vol. 21, no. Suppl 1/04, pp. 3–31, Oct. 2004.

[31] N. T. Nguyen, S. A. M. Shaegh, N. Kashaninejad, and D. T. Phan, "Design, fabrication and characterization of drug delivery systems based on lab-on-a-chip technology", *Advanced Drug Delivery Reviews*, vol. 65, no. 11-12, pp. 1403–1419, 2013, ISSN: 0169409X. DOI: 10.1016/j.addr.2013.05.008.

[32] J. Shrestha, S. R. Bazaz, H. A. Es, D. Y. Azari, B. Thierry, M. E. Warkiani, and M. Ghadiri, "Lung-on-a-chip: The future of respiratory disease models and pharmacological studies", *https://doi.org/10.1080/07388551.2019.1710458*, vol. 40, pp. 213–230, 2 Feb. 2020, ISSN: 15497801. DOI: 10.1080/07388551.2019.1710458.

[33] J. Wu, M. Dong, C. Rigatto, Y. Liu, and F. Lin, "Lab-on-chip technology for chronic disease diagnosis", *npj Digital Medicine 2018 1:1*, vol. 1, pp. 1–11, 1 Apr. 2018, ISSN: 2398-6352. DOI: 10.1038/s41746-017-0014-0.

[34] D. Wang, Y. Cong, Q. Deng, X. Han, S. Zhang, L. Zhao, Y. Luo, and X. Zhang, "Physiological and disease models of respiratory system based on organ-on-a-chip technology", *Micromachines 2021, Vol. 12, Page 1106*, vol. 12, p. 1106, 9 Sep. 2021, ISSN: 2072666X. DOI: 10.3390/MI12091106.

[35] G. Lacroix, W. Koch, D. Ritter, *et al.*, "Air-liquid interface in vitro models for respiratory toxicology research: Consensus workshop and recommendations", *Applied In Vitro Toxicology*, vol. 4, pp. 91–106, 2 Jun. 2018, ISSN: 23321539. DOI: 10.1089/AIVT.2017.0034/ASSET/IMAGES/LARGE/FIGURE4.JPEG.

[36] J. W. Yang, Y. C. Shen, K. C. Lin, *et al.*, "Organ-on-a-chip: Opportunities for assessing the toxicity of particulate matter", *Frontiers in Bioengineering and Biotechnology*, vol. 8, p. 519, May 2020, ISSN: 22964185. DOI: 10.3389/FBIOE.2020.00519/BIBTEX.

[37] N. Khalid, I. Kobayashi, and M. Nakajima, "Recent lab-on-chip developments for novel drug discovery", *Wiley Interdisciplinary Reviews: Systems Biology and Medicine*, vol. 9, e1381, 4 Jul. 2017, ISSN: 1939-005X. DOI: 10.1002/WSBM.1381.

[38] B. Palsson, "The challenges of in silico biology", *Nature Biotechnology*, vol. 18, pp. 1147–1150, 11 Nov. 2000, ISSN: 1087-0156. DOI: 10.1038/81125.

[39] ICRP, "Human respiratory tract model for radiological protection", *Radiation Protection Dosimetry*, vol. 60, no. 4, pp. 307–310, Jul. 1995, ISSN: 1742-3406. DOI: 10.1093/oxfordjournals.rpd.a082732.

[40] ICRP, "Limits for intakes of radionuclides by workers", *Radiation Protection Dosimetry*, vol. 3, p. 562, 1979. DOI: 10.1097/00004032-198104000-00005.

[41] N. C. on Radiation Protection and M. (U.S.), *Mammography: recommendations of the National Council on Radiation Protection and Measurements*, 66. The Council, 1980, p. 85, ISBN: 0913392510.

[42] V. K. H. Bui, J. Y. Moon, M. Chae, D. Park, and Y. C. Lee, "Prediction of aerosol deposition in the human respiratory tract via computational models: A review with recent updates", *Atmosphere*, vol. 11, no. 2, 2020, ISSN: 20734433. DOI: 10.3390/atmos11020137.

[43] S. Ehrmann, O. Schmid, C. Darquenne, *et al.*, "Innovative preclinical models for pulmonary drug delivery research", *Expert Opinion on Drug Delivery*, vol. 17, no. 4, pp. 463–478, 2020. DOI: 10.1080/17425247.2020.1730807.

[44] R. U. Agu and M. I. Ugwoke, "In situ and ex vivo nasal models for preclinical drug development studies", *Drug Absorption Studies*, pp. 112–134, Dec. 2008. DOI: 10.1007/978-0-387-74901-3_5.

[45] "Efficacy of milk-derived bioactive peptides on health by cellular and animal models", *Nutrients in Dairy and Their Implications for Health and Disease*, pp. 303–311, Jan. 2017. DOI: 10.1016/B978-0-12-809762-5.00023-1.

[46] M. Dusinska, E. Rundén-Pran, J. Schnekenburger, and J. Kanno, "Toxicity tests: In vitro and in vivo", *Adverse Effects of Engineered Nanomaterials: Exposure, Toxicology, and Impact on Human Health: Second Edition*, pp. 51–82, Jan. 2017. DOI: 10.1016/B978-0-12-809199-9.00003-3.

[47] J. T. Ross, N. Nesseler, J. W. Lee, L. B. Ware, and M. A. Matthay, "The ex vivo human lung: Research value for translational science", *JCI insight*, vol. 4, 11 Jun. 2019, ISSN: 2379-3708. DOI: 10.1172/JCI.INSIGHT.128833.

[48] V. V. Meka and J. H. van Oostrom, "Bellows-less lung system for the human patient simulator", *Medical and Biological Engineering and Computing*, vol. 42, no. 3, pp. 413–418, 2004, ISSN: 01400118. DOI: 10.1007/BF02344718.

[49] E. Essoukaki, M. Rattal, L. B. Taleb, M. Harmouchi, A. Assir, A. Mouhsen, and A. Lyazidi, "Design of a new artificial breathing system for simulating the human respiratory activities", *Journal of medical engineering & technology*, vol. 42, pp. 52–58, 1 Jan. 2018, ISSN: 1464-522X. DOI: 10.1080/03091902.2018.1430185.

[50] J. Azarnoosh, K. Sreenivas, and A. Arabshahi, "Numerical simulation of tidal breathing through the human respiratory tract", *Journal of biomechanical engineering*, vol. 142, 6 Jun. 2020, ISSN: 1528-8951. DOI: 10.1115/1.4046005.

[51] R. Nossa, J. Costa, L. Cacopardo, and A. Ahluwalia, "Breathing in vitro: Designs and applications of engineered lung models.", *Journal of tissue engineering*, vol. 12, p. 20 417 314 211 008 696, Apr. 2021, ISSN: 2041-7314. DOI: 10.1177/20417314211008696.

[52] J. G. Chase, T. Yuta, K. J. Mulligan, G. M. Shaw, and B. Horn, "A novel mechanical lung model of pulmonary diseases to assist with teaching and training", *BMC Pulmonary Medicine*, vol. 6, pp. 1–11, 2006. DOI: 10.1186/1471-2466-6-21.

[53] W. M. Kuebler, M. Mertens, and A. R. Pries, "A two-component simulation model to teach respiratory mechanics", *American Journal of Physiology - Advances in Physiology Education*, vol. 31, no. 2, pp. 218–222, 2007, ISSN: 15221229. DOI: 10.1152/advan.00001.2007.

[54] S. Heili-Frades, G. Peces-Barba, and M. J. Rodriguez-Nieto, "Design of a lung simulator for teaching lung mechanics in mechanical ventilation", *Arch Bronconeumol.*, vol. 43, no. 12, pp. 674–679, Dec. 2007. DOI: 10.1157/13112966.

[55] N. S. Marjanovic, A. De Simone, G. Jegou, and E. L'her, "A new global and comprehensive model for icu ventilator performances evaluation", *Annals of Intensive Care*, vol. 7, p. 68, 2017. DOI: 10.1186/s13613-017-0285-2.

[56] M. Garnier, C. Quesnel, J. P. Fulgencio, M. Degrain, G. Carteaux, F. Bonnet, T. Similowski, and A. Demoule, "Multifaceted bench comparative evaluation of latest intensive care unit ventilators", *British Journal of Anaesthesia*, vol. 115, no. 1, pp. 89–98, 2015, ISSN: 14716771. DOI: 10.1093/bja/aev028.

[57] E. L'Her, A. Roy, and N. Marjanovic, "Bench-test comparison of 26 emergency and transport ventilators", *Critical Care*, vol. 18, no. 5, pp. 1–14, 2014, ISSN: 1466609X. DOI: 10.1186/s13054-014-0506-0.

[58] R. R. Delvadia, X. Wei, P. W. Longest, J. Venitz, and P. R. Byron, "In vitro tests for aerosol deposition. iv: Simulating variations in human breath profiles for realistic dpi testing", *Journal of Aerosol Medicine and Pulmonary Drug Delivery*, vol. 29, p. 196, 2 Apr. 2016, ISSN: 19412703. DOI: 10.1089/JAMP.2015.1215.

[59] X. Wei, M. Hindle, A. Kaviratna, B. K. Huynh, R. R. Delvadia, D. Sandell, and P. R. Byron, "In vitro tests for aerosol deposition. vi: Realistic testing with different mouth-throat models and in vitro - in vivo correlations for a dry powder inhaler, metered dose inhaler, and soft mist inhaler", *Journal of Aerosol Medicine and Pulmonary Drug Delivery*, vol. 31, no. 6, pp. 358–371, 2018, ISSN: 19412703. DOI: 10.1089/jamp.2018.1454.

[60] P. W. Longest, K. Bass, R. Dutta, V. Rani, M. L. Thomas, A. El-Achwah, and M. Hindle, "Use of computational fluid dynamics deposition modeling in respiratory drug delivery", *Expert Opinion on Drug Delivery*, vol. 16, pp. 7–26, 1 Jan. 2018, ISSN: 17447593. DOI: 10.1080/17425247.2019.1551875.

[61] A. R. Clark, J. G. Weers, and R. Dhand, "The confusing world of dry powder inhalers: It is all about inspiratory pressures, not inspiratory flow rates", *Journal of Aerosol Medicine and Pulmonary Drug Delivery*, vol. 33, no. 1, pp. 1–11, 2020, ISSN: 19412703. DOI: 10.1089/jamp.2019.1556.

[62] R. Pasteka, M. Forjan, S. Sauermann, and A. Drauschke, "Electro-mechanical lung simulator using polymer and organic human lung equivalents for realistic breathing simulation", *Scientific Reports*, vol. 9, no. 1, pp. 1–12, 2019. DOI: 10.1038/s41598-019-56176-6.

[63] R. Pasteka, J. P. S. da Costa, N. Barros, R. Kolar, and M. Forjan, "Patient–ventilator interaction testing using the electromechanical lung simulator xpulm during v/a-c and psv ventilation mode", *Applied Sciences*, vol. 11, p. 3745, 9 Apr. 2021, ISSN: 2076-3417. DOI: 10.3390/app11093745.

[64] R. Pasteka, L. Schöllbauer, J. P. Santos da Costa, R. Kolar, and M. Forjan, "Experimental Evaluation of Dry Powder Inhalers During In- and Exhalation Using a Model of the Human Respiratory System (xPULM™)", *Pharmaceutics 2022, Vol. 14, Page 500*, vol. 14, no. 3, p. 500, Feb. 2022, ISSN: 1999-4923. DOI: 10.3390/PHARMACEUTICS14030500.

[65] R. Pasteka and M. Forjan, "Actively breathing mechanical lung simulator development and preliminary measurements", *IFMBE Proceedings*, vol. 65, pp. 751–754, 2017. DOI: 10.1007/978-981-10-5122-7_188.

[66] R. Pasteka, M. Forjan, and A. Drauschke, "Comparison of mathematical and controlled mechanical lung simulation in active breathing and ventilated state", vol. 51, no. 6, pp. 42–47, 2018, ISSN: 24058963. DOI: 10.1016/j.ifacol.2018.07.127.

[67] R. Pasteka, J. P. Santos da Costa, and M. Forjan, "Characteristic waveforms for testing of medical aerosol inhalers", *8th European Medical and Biological Engineering Conference*, pp. 240–246, Nov. 2021. DOI: 10.1007/978-3-030-64610-3_28.

[68] R. Pasteka and M. Forjan. "Evaluation of an active lung simulator for aerosol inhalation test replacement". (2017), [Online]. Available: https://proceedings.altex.org/?2017-01 (visited on 10/02/2022).

[69] R. Pasteka, M. Forjan, and A. Drauschke. "Comparison of breathing patterns for aerosol inhalation using an electro-mechanical lung simulator". (2018), [Online]. Available: https://proceedings.altex.org/?2018-02 (visited on 10/02/2022).

[70] R. Pasteka and M. Forjan, "Changes of particle deposition caused by different breathing patterns during active lung simulation", *2019 41st Annual International Conference of the IEEE Engineering in Medicine and Biology Society (EMBC)*, pp. 4969–4972, Jul. 2019. DOI: 10.1109/EMBC.2019.8857407.

[71] L. Harper, K. W. Herbst, and N. Kalfa, "Ethical issues in research: Human and animal experimentation", *Journal of Pediatric Urology*, vol. 14, no. 3, pp. 287–288, 2018, ISSN: 14775131. DOI: 10.1016/j.jpurol.2017.12.012.

[72] E. Parliament, "Directive 2010/63/eu - on the protection of animals used for scientific purposes", *Official Journal of the European Union*, pp. 33–79, 2010. DOI: data.europa.eu/eli/dir/2010/63/oj.

[73] E. Parliament, "Regulation 2019/1010 - on the alignment of reporting obligations in the field of legislation related to the environment, and amending regulations (ec) no 166/2006 and (eu) no 995/2010 of the european parliament and of the council, directives 2002/49/ec, 2", *Official Journal of the European Union*, vol. 2019, no. 5, pp. 115–127, 2019.

[74] V. Zuang, J. Barroso, S. Belz, E. Berggren, and C. Bernasconi, *Eurl ecvam status report on the development, validation and regulatory acceptance of alternative methods and approaches*, Oct. 2018. DOI: 10.2760/25602.

[75] I. Motola, L. A. Devine, H. S. Chung, J. E. Sullivan, and S. B. Issenberg, "Simulation in healthcare education: A best evidence practical guide. amee guide no. 82.", *Medical teacher*, vol. 35, no. 10, e1511–30, 2013, ISSN: 1466-187X. DOI: 10.3109/0142159X.2013.818632.

[76] A. Yokoyama, *Advances in Asthma: Pathophysiology, Diagnosis and Treatment*. Springer Singapore, 2019, ISBN: 9789811327896. DOI: 10.1007/978-981-13-2790-2.

[77] OECD and E. Union, *Health at a Glance: Europe 2016: State of Health in the EU Cycle*, ser. Health at a Glance: Europe. Paris: OECD Publishing, Nov. 2016. DOI: https://doi.org/10.1787/9789264265592-en.

[78] A. Chary, J. Hennen, S. G. Klein, T. Serchi, A. C. Gutleb, and B. Blömeke, "Respiratory sensitization: Toxicological point of view on the available assays", *Archives of Toxicology*, vol. 92, no. 2, pp. 803–822, Feb. 2018, ISSN: 14320738. DOI: 10.1007/s00204-017-2088-5.

[79] C. Zheng and G. Bennett, *Applied Contaminant Transport Modeling*. Wiley-Interscience New York, Feb. 2002, vol. 34, ISBN: 0471384771.

[80] P. W. Longest and L. T. Holbrook, *In silico models of aerosol delivery to the respiratory tract - development and applications*, Mar. 2012. DOI: 10.1016/j.addr.2011.05.009.

[81] P. Koullapis, S. Kassinos, J. Muela, *et al.*, "Regional aerosol deposition in the human airways: The siminhale benchmark case and a critical assessment of in silico methods", *European Journal of Pharmaceutical Sciences*, vol. 113, pp. 77–94, Feb. 2018, ISSN: 0928-0987. DOI: 10.1016/J.EJPS.2017.09.003.

[82] A. Verbraak, J. E. Beneken, J. M. Bogaard, and A. Versprille, "Computer-controlled mechanical lung model for application in pulmonary function studies", *Med Biol Eng Comput*, vol. 33, no. 6, pp. 776–783, 1995, ISSN: 0140-0118.

[83] S. Krueger-Ziolek, C. Knoebel, C. Schranz, and K. Moeller, "Combination of engineering and medical education using an active mechanical lung simulator", in *Proceedings of the 26th IEEE International Symposium on Computer-Based Medical Systems*, Jun. 2013, pp. 542–543. DOI: 10.1109/CBMS.2013.6627868.

[84] S. Perinel, J. Pourchez, L. Leclerc, J. Avet, M. Durand, N. Prévôt, M. Cottier, and J. M. Vergnon, "Development of an ex vivo human-porcine respiratory model for preclinical studies", *Scientific Reports*, vol. 7, p. 43 121, Feb. 2017, ISSN: 20452322. DOI: 10.1038/srep43121.

[85] A. Verbraak, P. Rijnbeek, J. Beneken, J. Bogaard, and A. Versprille, "A new approach to mechanical simulation of lung behaviour: Piston movement", *Medical & Biological Engineering & Computing*, vol. 39, pp. 82–89, 2001, ISSN: 0140-0118. DOI: 10.1007/BF02345270.

[86] S. Mesic, R. Babuska, H. C. Hoogsteden, and A. F. M. Verbraak, "Computer-controlled mechanical simulation of the artificially ventilated human respiratory system", *IEEE Transactions on Biomedical Engineering*, vol. 50, no. 6, pp. 731–743, Jun. 2003, ISSN: 0018-9294. DOI: 10.1007/BF02523009.

[87] W. Hofmann, "Modelling inhaled particle deposition in the human lung—a review", *Journal of Aerosol Science*, vol. 42, no. 10, pp. 693–724, Oct. 2011, ISSN: 0021-8502. DOI: 10.1016/J.JAEROSCI.2011.05.007.

[88] R. K. Calay, J. Kurujareon, and A. E. Holdo, "Numerical simulation of respiratory flow patterns within human lung", *Respiratory Physiology & Neurobiology*, vol. 130, no. 2, pp. 201–221, 2002, ISSN: 1569-9048. DOI: https://doi.org/10.1016/S0034-5687(01)00337-1.

[89] M. Forjan, K. Stiglbrunner, T. Steiner, Z. Bureš, and A. Drauschke, "Sensor system development for the novel spontaneous active breathing lung simulator, i-lung", *IFAC Proceedings Volumes*, vol. 45, no. 7, pp. 113–118, 2012, 11th IFAC,IEEE International Conference on Programmable Devices and Embedded Systems, ISSN: 1474-6670. DOI: https://doi.org/10.3182/20120523-3-CZ-3015.00024.

[90] V. David, M. Forjan, T. Steiner, Z. Bureš, and A. Drauschke, "Mechanical and electrical specifications of the active lung simulator i-lung - development of i-lung 1.0 to i-lung 2.0", in *IFAC Proceedings Volumes (IFAC-PapersOnline)*, vol. 12, 2013, pp. 13–23, ISBN: 9783902823533. DOI: 10.3182/20130925-3-CZ-3023.00075.

[91] F. Solc, F. Zezulka, I. Vesely, J. Sekora, M. Mezl, A. Eschli, and I. Provaznik, "The mathematical model of a lung simulator", *MEFANET Journal 2014*, vol. 2, no. 2, pp. 71–78, 2014.

[92] S. R. Braun, "Respiratory rate and pattern", in *Clinical Methods: The History, Physical, and Laboratory Examinations. 3rd edition*, Butterworths, 1990, ISBN: 0-409-90077-X.

[93] R. Carroll, "Elsevier's integrated physiology", in *Pulmonary System*, Mosby Elsevier, 2007, pp. 99–115, ISBN: 9780323043182.

[94] M. I. INC., *Model 1600 dual adult ttl training/test lung*, 2018.

[95] H. D. Prange, "Laplace's law and the alveolus: A misconception of anatomy and a misapplication of physics", *American Journal of Physiology - Advances in Physiology Education*, vol. 27, no. 1-4, pp. 34–40, 2003, ISSN: 10434046. DOI: 10.1152/advan.00024.2002.

[96] R. Scala and L. Heunks, "Highlights in acute respiratory failure", *European Respiratory Review*, vol. 27, no. 147, Mar. 2018, ISSN: 16000617. DOI: 10.1183/16000617.0008-2018.

[97] G. A. Schmidt, "Mechanical ventilation", in *Acute Respiratory Distress Syndrome: A Comprehensive Clinical Approach*, J. A. Russell and K. R. Walley, Eds. Cambridge University Press, 1999, pp. 139–162. DOI: 10.1017/CBO9780511575112.009.

[98] J. J. Marini, "Mechanical ventilation: Past lessons and the near future", *Critical Care*, vol. 17, no. S1, S1, Feb. 2013, ISSN: 1466609X. DOI: 10.1186/cc11499.

[99] J. J. Haitsma, *Physiology of mechanical ventilation*, Apr. 2007. DOI: 10.1016/j.ccc.2006.11.016.

[100] R. L. Dellaca, C. Veneroni, and R. Farre, "Trends in mechanical ventilation: Are we ventilating our patients in the best possible way?", *Breathe*, vol. 13, no. 2, pp. 84–98, 2017, ISSN: 20734735. DOI: 10.1183/20734735.007817.

[101] R. L. Chatburn, "Understanding mechanical ventilators", *Expert Review of Respiratory Medicine*, vol. 4, no. 6, pp. 809–819, Dec. 2010, ISSN: 17476348. DOI: 10.1586/ers.10.66.

[102] R. M. Kacmarek, J. K. Stoller, and A. Heuer, *Egan's Fundamentals of Respiratory Care*. Elsevier, 2013, ISBN: 9780323082037.

[103] R. M. Kacmarek, M. Pirrone, and L. Berra, *Assisted mechanical ventilation: The future is now!*, Jul. 2015. DOI: 10.1186/s12871-015-0092-y.

[104] E. Kondili, G. Prinianakis, and D. Georgopoulos, "Patient-ventilator interaction", *British Journal of Anaesthesia*, vol. 91, no. 1, pp. 106–119, 2003. DOI: 10.1093/bja/aeg129.

[105] L. Estrada, A. Torres, L. Sarlabous, and R. Jane, "Onset and offset estimation of the neural inspiratory time in surface diaphragm electromyography: A pilot study in healthy subjects", *IEEE Journal of Biomedical and Health Informatics*, vol. 22, no. 1, pp. 67–76, 2018. DOI: 10.1109/JBHI.2017.2672800.

[106] L. Zhang, K. Mao, K. Duan, *et al.*, "Detection of patient-ventilator asynchrony from mechanical ventilation waveforms using a two-layer long short-term memory neural network", *Computers in Biology and Medicine*, vol. 120, p. 103 721, May 2020, ISSN: 18790534. DOI: 10.1016/j.compbiomed.2020.103721.

[107] G. Perchiazzi, M. Högman, C. Rylander, R. Giuliani, T. Fiore, and G. Hedenstierna, "Assessment of respiratory system mechanics by artificial neural networks: An exploratory study", *Journal of Applied Physiology*, vol. 90, pp. 1817–1824, 5 May 2001, ISSN: 8750-7587. DOI: 10.1152/jappl.2001.90.5.1817.

[108] S. Parthasarathy, A. Jubran, and M. J. Tobin, "Assessment of neural inspiratory time in ventilator-supported patients", *American Journal of Respiratory and Critical Care Medicine*, vol. 162, no. 2 I, pp. 546–552, 2000, ISSN: 1073449X. DOI: 10.1164/ajrccm.162.2.9901024.

[109] C. Subirà, C. de Haro, R. Magrans, R. Fernández, and L. Blanch, "Minimizing asynchronies in mechanical ventilation: Current and future trends", *Respiratory Care*, vol. 63, no. 4, pp. 464–478, Apr. 2018, ISSN: 19433654. DOI: 10.4187/respcare.05949.

[110] L. Vignaux, F. Vargas, J. Roeseler, D. Tassaux, A. W. Thille, M. P. Kossowsky, L. Brochard, and P. Jolliet, "Patient-ventilator asynchrony during non-invasive ventilation for acute respiratory failure: A multicenter study", *Intensive Care Medicine*, vol. 35, no. 5, pp. 840–846, 2009, ISSN: 03424642. DOI: 10.1007/s00134-009-1416-5.

[111] J. Gonzalez-Bermejo, J. P. Janssens, C. Rabec, C. Perrin, F. Lofaso, B. Langevin, A. Carlucci, and M. Lujan, "Framework for patient-ventilator asynchrony during long-term non-invasive ventilation", *Thorax*, vol. 74, no. 7, pp. 715–717, Jul. 2019, ISSN: 14683296. DOI: 10.1136/thoraxjnl-2018-213022.

[112] A. W. Thille, P. Rodriguez, B. Cabello, F. Lellouche, and L. Brochard, "Patient-ventilator asynchrony during assisted mechanical ventilation", *Intensive Care Medicine*, vol. 32, no. 10, pp. 1515–1522, Oct. 2006, ISSN: 03424642. DOI: 10.1007/s00134-006-0301-8.

[113] K. Vaporidi, D. Babalis, A. Chytas, E. Lilitsis, E. Kondili, V. Amargianitakis, I. Chouvarda, N. Maglaveras, and D. Georgopoulos, "Clusters of ineffective efforts during mechanical ventilation: Impact on outcome", *Intensive Care Medicine*, vol. 43, no. 2, pp. 184–191, Feb. 2017, ISSN: 14321238. DOI: 10.1007/s00134-016-4593-z.

[114] K. C. See, J. Sahagun, and J. Taculod, "Defining patient–ventilator asynchrony severity according to recurrence", *Intensive Care Medicine*, vol. 10, 2020. DOI: 10.1007/s00134-020-05974-y.

[115] L. Gattinoni, J. J. Marini, F. Collino, G. Maiolo, F. Rapetti, T. Tonetti, F. Vasques, and M. Quintel, *The future of mechanical ventilation: Lessons from the present and the past*, Jul. 2017. DOI: 10.1186/s13054-017-1750-x.

[116] J. R. Beitler, S. A. Sands, S. H. Loring, R. L. Owens, A. Malhotra, R. G. Spragg, M. A. Matthay, B. T. Thompson, and D. Talmor, "Quantifying unintended exposure to high tidal volumes from breath stacking dyssynchrony in ards: The breathe criteria", *Intensive Care Medicine*, vol. 42, no. 9, pp. 1427–1436, Sep. 2016, ISSN: 14321238. DOI: 10.1007/s00134-016-4423-3.

[117] O. Lamouret, L. Crognier, F. V. Bounes, *et al.*, "Neurally adjusted ventilatory assist (nava) versus pressure support ventilation: Patient-ventilator interaction during invasive ventilation delivered by tracheostomy", *Critical Care*, vol. 23, no. 1, p. 2, Jan. 2019, ISSN: 1466609X. DOI: 10.1186/s13054-018-2288-2.

[118] C. Chen, T. Wen, and W. Liao, "Neurally adjusted ventilatory assist versus pressure support ventilation in patient-ventilator interaction and clinical outcomes: A meta-analysis of clinical trials", *Annals of Translational Medicine*, vol. 7, no. 16, pp. 382–382, Aug. 2019, ISSN: 23055839. DOI: 10.21037/atm.2019.07.60.

[119] H. Yonis, L. Crognier, J. M. Conil, *et al.*, "Patient-ventilator synchrony in neurally adjusted ventilatory assist (nava) and pressure support ventilation (psv): A prospective observational study", *BMC Anesthesiology*, vol. 15, no. 1, Aug. 2015, ISSN: 14712253. DOI: 10.1186/s12871-015-0091-z.

[120] P. M. Bertrand, E. Futier, Y. Coisel, S. Matecki, S. Jaber, and J. M. Constantin, "Neurally adjusted ventilatory assist vs pressure support ventilation for noninvasive ventilation during acute respiratory failure: A crossover physiologic study", *Chest*, vol. 143, no. 1, pp. 30–36, 2013, ISSN: 19313543. DOI: 10.1378/chest.12-0424.

[121] C. S. Calfee and M. A. Matthay, "Recent advances in mechanical ventilation", *American Journal of Medicine*, vol. 118, no. 6, pp. 584–591, 2005, ISSN: 00029343. DOI: 10.1016/j.amjmed.2004.12.005.

[122] D. L. Grieco, M. M. Bitondo, H. Aguirre-Bermeo, *et al.*, "Patient-ventilator interaction with conventional and automated management of pressure support during difficult weaning from mechanical ventilation", *Journal of Critical Care*, vol. 48, pp. 203–210, Dec. 2018, ISSN: 15578615. DOI: 10.1016/j.jcrc.2018.08.043.

[123] G. Gutierrez, "Artificial intelligence in the intensive care unit", *Critical Care*, DOI: 10.1186/s13054-020-2785-y.

[124] R. L. Chatburn and E. Mireles-Cabodevila, "Closed-loop control of mechanical ventilation: Description and classification of targeting schemes", *Respiratory Care*, vol. 56, no. 1, pp. 85–98, Jan. 2011, ISSN: 00201324. DOI: 10.4187/respcare.00967.

[125] A. R. Martin, I. M. Katz, K. Jenöfi, G. Caillibotte, L. Brochard, and J. Texereau, "Bench experiments comparing simulated inspiratory effort when breathing helium-oxygen mixtures to that during positive pressure support with air", *BMC Pulmonary Medicine*, vol. 12, no. 1, p. 62, Oct. 2012, ISSN: 14712466. DOI: 10.1186/1471-2466-12-62.

[126] A. W. Thille, A. Lyazidi, J. C. M. Richard, F. Galia, and L. Brochard, "A bench study of intensive-care-unit ventilators: New versus old and turbine-based versus compressed gas-based ventilators", *Intensive Care Medicine*, vol. 35, no. 8, pp. 1368–1376, Aug. 2009, ISSN: 03424642. DOI: 10.1007/s00134-009-1467-7.

[127] J. C. Ferreira, D. W. Chipman, and R. M. Kacmarek, "Trigger performance of mid-level icu mechanical ventilators during assisted ventilation: A bench study", *Intensive Care Medicine*, vol. 34, no. 9, pp. 1669–1675, 2008, ISSN: 03424642. DOI: 10.1007/s00134-008-1125-5.

[128] J. C. Richard, A. Carlucci, L. Breton, N. Langlais, S. Jaber, S. Maggiore, S. Fougère, A. Harf, and L. Brochard, "Bench testing of pressure support ventilation with three different generations of ventilators", *Intensive Care*

Medicine, vol. 28, no. 8, pp. 1049–1057, Aug. 2002, ISSN: 03424642. DOI: 10.1007/s00134-002-1311-9.

[129] P. G. Metnitz, B. Metnitz, R. P. Moreno, P. Bauer, L. D. Sorbo, C. Hoermann, S. A. De Carvalho, and V. M. Ranieri, "Epidemiology of mechanical ventilation: Analysis of the saps 3 database", *Intensive Care Medicine*, vol. 35, no. 5, pp. 816–825, Mar. 2009, ISSN: 14321238. DOI: 10.1007/s00134-009-1449-9.

[130] Imtmedical, *Service manual bellavista 1000/1000e*, 2017.

[131] R. Larsen, T. Ziegenfuß, and A. Mathes, *Beatmung : Indikationen - Techniken - Krankheitsbilder*. Springer Berlin Heidelberg, 2018, p. 516, ISBN: 3662548526.

[132] M. Instruments, *Dual adult ttl training/testing lung: User's manual*, Grand Rapids, 2016.

[133] K. Williams, M. Hinojosa-Kurtzberg, and S. Parthasarathy, "Control of breathing during mechanical ventilation: Who is the boss?", *Respiratory Care*, vol. 56, no. 2, pp. 127–139, Feb. 2011, ISSN: 00201324. DOI: 10.4187/respcare.01173.

[134] Eurostat, *Respiratory diseases statistics - Statistics Explained*. 2020, Available at https://ec.europa.eu/eurostat/statistics-explained/index.php?title=Respiratory_diseases_statistics&oldid=497079.

[135] K. Wintemute and F. Miller, "Dry powder inhalers are environmentally preferable to metered-dose inhalers", *CMAJ*, vol. 192, no. 29, E846–E846, Jul. 2020, ISSN: 0820-3946. DOI: 10.1503/CMAJ.75949.

[136] J. L. Rau, "Practical problems with aerosol therapy in copd", *Respiratory Care*, vol. 51, no. 2, pp. 158–172, 2006, ISSN: 0020-1324.

[137] M. S. Holmes, J. N. Seheult, P. O'Connell, S. D'Arcy, C. Ehrhardt, A. M. Healy, R. W. Costello, and R. B. Reilly, "An acoustic-based method to detect and quantify the effect of exhalation into a dry powder inhaler", *Journal of Aerosol Medicine and Pulmonary Drug Delivery*, vol. 28, no. 4, pp. 247–253, 2015. DOI: 10.1089/jamp.2014.1169.

[138] D. E. Geller, "Comparing clinical features of the nebulizer, metered-dose inhaler, and dry powder inhaler", *Respiratory Care*, vol. 50, no. 10, pp. 1313–1322, 2005, ISSN: 0020-1324. eprint: http://rc.rcjournal.com/content/50/10/1313.full.pdf.

[139] Atkins, Smaldone, MacIntyre, Hickey, and M. T. Amato, "Dry powder inhalers: An overview", *Respiratory Care*, vol. 50, no. 10, pp. 1304–1312, 2005, ISSN: 0020-1324.

[140] D. A. Mahler, L. A. Waterman, and A. H. Gifford, "Prevalence and COPD phenotype for a suboptimal peak inspiratory flow rate against the simulated resistance of the diskus® dry powder inhaler", *Journal of Aerosol Medicine and Pulmonary Drug Delivery*, vol. 26, no. 3, pp. 174–179, 2013, ISSN: 19412711. DOI: 10.1089/jamp.2012.0987.

[141] A. C. Grant, R. Walker, M. Hamilton, and K. Garrill, "The ELLIPTA® dry powder inhaler: Design, functionality, in vitro dosing performance and critical task compliance by patients and caregivers", *Journal of Aerosol Medicine and Pulmonary Drug Delivery*, vol. 28, no. 6, pp. 474–485, 2015, ISSN: 19412703. DOI: 10.1089/jamp.2015.1223.

[142] D. A. Mahler, "Peak inspiratory flow rate as a criterion for dry powder inhaler use in chronic obstructive pulmonary disease", *Annals of the American Thoracic Society*, vol. 14, no. 7, pp. 1103–1107, 2017, ISSN: 23256621. DOI: 10.1513/AnnalsATS.201702-156PS.

[143] A. G. Duarte, L. Tung, W. Zhang, E. S. Hsu, Y. F. Kuo, and G. Sharma, "Spirometry measurement of peak inspiratory flow identifies suboptimal use of dry powder inhalers in ambulatory patients with copd", *Chronic Obstructive Pulmonary Diseases*, vol. 6, no. 3, pp. 246–255, 2019, ISSN: 2372952X. DOI: 10.15326/jcopdf.6.3.2018.0163.

[144] S. Y. Chen, C. K. Huang, H. C. Peng, C. J. Yu, and J. Y. Chien, "Inappropriate peak inspiratory flow rate with dry powder inhaler in chronic obstructive pulmonary disease", *Scientific Reports*, vol. 10, no. 1, pp. 1–9, 2020, ISSN: 20452322. DOI: 10.1038/s41598-020-64235-6.

[145] M. Taki, C. Marriott, X. M. Zeng, and G. P. Martin, "Aerodynamic deposition of combination dry powder inhaler formulations in vitro: A comparison of three impactors", *International Journal of Pharmaceutics*, vol. 388, no. 1-2, pp. 40–51, 2010, ISSN: 03785173. DOI: 10.1016/j.ijpharm.2009.12.031.

[146] H. K. Versteeg, D. L. Roberts, F. Chambers, A. Cooper, M. Copley, J. P. Mitchell, and H. Mohammed, "A cross-industry assessment of the flow rate-elapsed time profiles of test equipment typically used for dry-powder inhaler (dpi) testing: Part 2– analysis of transient air flow in the testing of dpis with compendial cascade impactors", *Aerosol Science and Technology*, vol. 54, no. 12, pp. 1448–1470, 2020, ISSN: 15217388. DOI: 10.1080/02786826.2020.1792825.

[147] R. Greguletz, P. U. Andersson, A. Cooper, *et al.*, "A cross-industry assessment of the flow rate-time profiles of test equipment typically used for dry-powder inhaler (dpi) testing: Part 1–compendial apparatuses", *Aerosol Sci-*

ence and Technology, vol. 54, no. 12, pp. 1424–1447, 2020, ISSN: 15217388. DOI: 10.1080/02786826.2020.1792824.

[148] R. Ravi Kannan, A. J. Przekwas, N. Singh, R. Delvadia, G. Tian, and R. Walenga, "Pharmaceutical aerosols deposition patterns from a dry powder inhaler: Euler lagrangian prediction and validation", *Medical Engineering and Physics*, vol. 42, pp. 35–47, 2017, ISSN: 18734030. DOI: 10.1016/j.medengphy.2016.11.007.

[149] T. Kopsch, D. Murnane, and D. Symons, "Computational modelling and experimental validation of drug entrainment in a dry powder inhaler", *International Journal of Pharmaceutics*, vol. 553, no. 1-2, pp. 37–46, 2018, ISSN: 18733476. DOI: 10.1016/j.ijpharm.2018.10.021.

[150] E. Chalvatzaki, S. E. Chatoutsidou, and M. Lazaridis, "Simulations of the deposition of pharmaceutical aerosols in the human respiratory tract by dry powder inhalers (dpis)", *Journal of Drug Delivery Science and Technology*, vol. 59, p. 101 915, Oct. 2020, ISSN: 1773-2247. DOI: 10.1016/J.JDDST.2020.101915.

[151] B. J. Finlayson-Pitts and J. N. Pitts, "Analytical methods and typical atmospheric concentrations for gases and particles", *Chemistry of the Upper and Lower Atmosphere*, pp. 547–656, Jan. 2000. DOI: 10.1016/B978-012257060-5/50013-7.

[152] V. Kulkarni, *Handbook of non-invasive drug delivery systems : science and technology*. 2009, ISBN: 9780815520269.

[153] M. Bonam, D. Christopher, D. Cipolla, *et al.*, "Minimizing variability of cascade impaction measurements in inhalers and nebulizers", *AAPS PharmSciTech*, vol. 9, pp. 404–413, 2 Jun. 2008, ISSN: 15309932. DOI: 10.1208/S12249-008-9045-9.

[154] C. Darquenne, "Deposition mechanisms", *Journal of Aerosol Medicine and Pulmonary Drug Delivery*, vol. 33, no. 4, pp. 181–185, 2020. DOI: 10.1089/jamp.2020.29029.cd.

[155] A. Tsuda, F. S. Henry, and J. P. Butler, "Particle transport and deposition: Basic physics of particle kinetics", *Comprehensive Physiology*, pp. 1437–1471, 2013. DOI: 10.1002/cphy.c100085.

[156] C. Tomasi, S. Fuzzi, and A. A. Kochanovskij, Eds., *Atmospheric aerosols: life cycles and effects on air quality and climate*, eng, ser. Wiley series in atmospheric physics and remote sensing. Weinheim: Wiley-VCH Verlag GmbH & Co. KGaA, 2017, ISBN: 9783527336456.

[157] J. M. Borghardt, C. Kloft, and A. Sharma, "Inhaled therapy in respiratory disease: The complex interplay of pulmonary kinetic processes", 2018. DOI: 10.1155/2018/2732017.

[158] A. H. L. Chow, H. H. Y. Tong, P. Chattopadhyay, and B. Y. Shekunov, "Particle engineering for pulmonary drug delivery", *Pharmaceutical Research*, vol. 24, no. 3, pp. 411–437, 2007. DOI: 10.1007/s11095-006-9174-3.

[159] A. H. D. Boer, D. Gjaltema, P. Hagedoorn, and H. W. Frijlink, "Characterization of inhalation aerosols: A critical evaluation of cascade impactor analysis and laser diffraction technique", *International Journal of Pharmaceutics*, vol. 249, pp. 219–231, 1-2 Dec. 2002, ISSN: 0378-5173. DOI: 10.1016/S0378-5173(02)00526-4.

[160] E. P. Judge, J. M. L. Hughes, J. J. Egan, M. Maguire, E. L. Molloy, and S. O'Dea, "Anatomy and Bronchoscopy of the Porcine Lung. A Model for Translational Respiratory Medicine", en, *American Journal of Respiratory Cell and Molecular Biology*, vol. 51, no. 3, pp. 334–343, Sep. 2014, ISSN: 1044-1549, 1535-4989. DOI: 10.1165/rcmb.2013-0453TR.

[161] C. S. Rogers, W. M. Abraham, K. A. Brogden, *et al.*, "The porcine lung as a potential model for cystic fibrosis", en, *American Journal of Physiology-Lung Cellular and Molecular Physiology*, vol. 295, no. 2, pp. L240–L263, Aug. 2008, ISSN: 1040-0605, 1522-1504. DOI: 10.1152/ajplung.90203.2008.

[162] U. S. P. Convention, *USP35 NF30, 2012: <601> Aerosols, Nasal Sprays, Metered-Dose Inhalers, and Dry Powder Inhalers*, ser. The United States pharmacopeia. United States Pharmacopeial, 2011, ISBN: 9781936424009.

[163] R. Pasteka, J. P. Santos da Costa, N. Barros, R. Kolar, and M. Forjan, "Patient–ventilator interaction testing using the electromechanical lung simulator xpulm™ during v/a-c and psv ventilation mode", *Applied Sciences*, vol. 11, no. 9, p. 3745, Apr. 2021, ISSN: 2076-3417. DOI: 10.3390/app11093745.

[164] K. Ahookhosh, O. Pourmehran, H. Aminfar, M. Mohammadpourfard, M. M. Sarafraz, and H. Hamishehkar, "Development of human respiratory airway models: A review", *European Journal of Pharmaceutical Sciences*, vol. 145, p. 105 233, Mar. 2020, ISSN: 0928-0987. DOI: 10.1016/J.EJPS.2020.105233.

[165] F. Lizal, J. Jedelsky, K. Morgan, *et al.*, "Experimental methods for flow and aerosol measurements in human airways and their replicas", *European Journal of Pharmaceutical Sciences*, vol. 113, pp. 95–131, Feb. 2018, ISSN: 0928-0987. DOI: 10.1016/J.EJPS.2017.08.021.

[166] A. Horváth, I. Balásházy, G. Tomisa, and Á. Farkas, "Significance of breath-hold time in dry powder aerosol drug therapy of copd patients", *European Journal of Pharmaceutical Sciences*, vol. 104, no. April, pp. 145–149, 2017, ISSN: 18790720. DOI: 10.1016/j.ejps.2017.03.047.

[167] F. Buttini, G. Brambilla, D. Copelli, V. Sisti, A. G. Balducci, R. Bettini, and I. Pasquali, "Effect of Flow Rate on In Vitro Aerodynamic Performance of NEXThaler® in Comparison with Diskus® and Turbohaler® Dry Powder Inhalers", *Journal of Aerosol Medicine and Pulmonary Drug Delivery*, vol. 29, no. 2, pp. 167–178, 2016, ISSN: 19412703. DOI: 10.1089/jamp.2015.1220.

[168] A. Sahin-Yilmaz and R. M. Naclerio, "Anatomy and physiology of the upper airway", *Proceedings of the American Thoracic Society*, vol. 8, no. 1, pp. 31–39, 2011, ISSN: 15463222. DOI: 10.1513/pats.201007-050RN.

[169] R. J. Thomas, "Particle size and pathogenicity in the respiratory tract", *Virulence*, vol. 4, no. 8, pp. 847–858, Nov. 2013, ISSN: 21505594. DOI: 10.4161/viru.27172.

[170] M. Lippmann, D. B. Yeates, and R. E. Albert, "Deposition, retention, and clearance of inhaled particles", *British Journal of Industrial Medicine*, vol. 37, no. 4, pp. 337–362, 1980, ISSN: 00071072. DOI: 10.1136/oem.37.4.337.

[171] C. Darquenne, "Aerosol deposition in health and disease", *Journal of Aerosol Medicine and Pulmonary Drug Delivery*, vol. 25, no. 3, pp. 140–147, 2012, ISSN: 19412711. DOI: 10.1089/jamp.2011.0916.

[172] O. S. Usmani, M. F. Biddiscombe, J. A. Nightingale, S. R. Underwood, and P. J. Barnes, "Effects of bronchodilator particle size in asthmatic patients using monodisperse aerosols", *Journal of applied physiology (Bethesda, Md. : 1985)*, vol. 95, pp. 2106–2112, 5 2003, ISSN: 8750-7587. DOI: 10.1152/JAPPLPHYSIOL.00525.2003.

[173] O. S. Usmani, M. F. Biddiscombe, and P. J. Barnes, "Regional lung deposition and bronchodilator response as a function of β2-agonist particle size", *American Journal of Respiratory and Critical Care Medicine*, vol. 172, no. 12, pp. 1497–1504, 2005, ISSN: 1073449X. DOI: 10.1164/rccm.200410-1414OC.

[174] S. Newman, S. Malik, P. Hirst, G. Pitcairn, A. Heide, J. Pabst, A. Dinkelaker, and W. Fleischer, "Lung deposition of salbutamol in healthy human subjects from the maghaler dry powder inhaler", *Respiratory Medicine*, vol. 96, no. 12, pp. 1026–1032, 2002, ISSN: 09546111. DOI: 10.1053/rmed.2002.1387.

[175] J. C. Virchow, G. Poli, C. Herpich, C. Kietzig, H. Ehlich, D. Braeutigam, K. Sommerer, S. Häussermann, and F. Mariotti, "Lung Deposition of the Dry Powder Fixed Combination Beclometasone Dipropionate Plus Formoterol Fumarate Using NEXThaler® Device in Healthy Subjects, Asthmatic Patients, and COPD Patients", *Journal of Aerosol Medicine and Pulmonary Drug Delivery*, vol. 31, no. 5, pp. 269–280, 2018, ISSN: 19412703. DOI: 10.1089/jamp.2016.1359.

[176] M. L. Levy, W. Carroll, J. L. Izquierdo Alonso, C. Keller, F. Lavorini, and L. Lehtimäki, "Understanding dry powder inhalers: Key technical and patient preference attributes", *Advances in Therapy*, vol. 36, no. 10, pp. 2547–2557, 2019, ISSN: 18658652. DOI: 10.1007/s12325-019-01066-6.

[177] S. P. Newman and W. W. Busse, "Review: Evolution of dry powder inhaler design, formulation, and performance", *Respiratory Medicine*, 2002. DOI: 10.1053/rmed.2001.1276.

[178] M. Abadelah, G. Abdalla, H. Chrystyn, and H. Larhrib, "Gaining an insight into the importance of each inhalation manoeuvre parameter using altered patients' inhalation profiles", *Journal of Drug Delivery Science and Technology*, vol. 61, no. October, p. 102 181, 2021, ISSN: 17732247. DOI: 10.1016/j.jddst.2020.102181.

[179] D. Hira, T. Okuda, A. Mizutani, N. Tomida, and H. Okamoto, "In vitro evaluation of optimal inhalation flow patterns for commercial dry powder inhalers and pressurized metered dose inhalers with human inhalation flow pattern simulator", *Journal of Pharmaceutical Sciences*, vol. 107, no. 6, pp. 1731–1735, 2018, ISSN: 15206017. DOI: 10.1016/j.xphs.2018.02.002.

[180] M. Hamilton, R. Leggett, C. Pang, S. Charles, B. Gillett, and D. Prime, "In vitro dosing performance of the ELLIPTA® dry powder inhaler using asthma and COPD patient inhalation profiles replicated with the electronic lung (eLung™)", *Journal of Aerosol Medicine and Pulmonary Drug Delivery*, vol. 28, no. 6, pp. 498–506, 2015, ISSN: 19412703. DOI: 10.1089/jamp.2015.1225.

[181] Z. He and Y. Zhao, *Modeling in Respiratory Movement Using LabVIEW and Simulink, Modeling, Programming and Simulations Using LabVIEW Software*, A. R. De, Ed. InTech, 2011, ISBN: 9789533075211.

[182] P. W. Longest, G. Tian, R. L. Walenga, and M. Hindle, "Comparing mdi and dpi aerosol deposition using in vitro experiments and a new stochastic individual path (sip) model of the conducting airways", *Pharmaceutical Research*,

vol. 29, no. 6, pp. 1670–1688, 2012, ISSN: 07248741. DOI: 10.1007/s11095-012-0691-y.

[183] M. Gottschalk, G. Franzl, M. Frohner, R. Pasteka, and M. Uslar, "From integration profiles to interoperability testing for smart energy systems at connectathon energy", *Energies*, vol. 11, p. 3375, 12 Dec. 2018, ISSN: 19961073. DOI: 10.3390/en11123375.

[184] M. Forjan, R. Pasteka, and A. Drasuchke. "Lung simulation – an alternative approach to animal testing for applications in aerosol and respiratory research". (2018), [Online]. Available: https://proceedings.altex.org/?2018-02 (visited on 10/02/2022).

[185] R. Pasteka, M. Forjan, and S. Sauermann, "Development of a multidisciplinary and telemedicine focused system database", *Studies in Health Technology and Informatics*, vol. 236, pp. 144–151, 2017. DOI: 10.3233/978-1-61499-759-7-144.

[186] R. Pasteka, M. Forjan, and V. David, "A single point of contact data platform for rehabilitative exercises and equipment: Development of the rehabitation database", *ACM International Conference Proceeding Series*, pp. 317–322, 2018. DOI: https://doi.org/10.1145/3218585.3218676.

[187] V. David, M. Forjan, R. Paštěka, M. Scherer, and O. Hofstätter, "Development of a multi-purpose easy-to-use set of tools for home based rehabilitation: Use cases and applications developed during the rehabitation project", *ACM International Conference Proceeding Series*, pp. 323–330, 2018. DOI: 10.1145/3218585.3218677.

[188] M. Frohner, M. Gottschalk, G. Franzl, R. Pasteka, M. Uslar, and S. Sauermann, "Smart grid interoperability profiles development", *2017 IEEE International Conference on Smart Grid Communications (SmartGridComm)*, pp. 189–194, October Oct. 2017. DOI: 10.1109/SmartGridComm.2017.8340674.

[189] M. Gottschalk, G. Franzl, M. Frohner, R. Pasteka, and M. Uslar, "Structured workflow achieving interoperable smart energy systems", *Energy Informatics*, vol. 1, p. 25, S1 Oct. 2018, ISSN: 2520-8942. DOI: 10.1186/s42162-018-0039-x.

[190] J. Hrušková, J. Jakubík, M. Hendrych, R. Paštěka, J. Svačinová, K. Budinskaya, V. Kujalová, V. Vejtasová, and Z. Nováková, "Fyziologie – teorie k praktickým cvičením", 2021, Electronic book.

[191] J. Hrušková, J. Jakubík, M. Hendrych, R. Paštěka, J. Svačinová, K. Budinskaya, K. Veronika, V. Veronika, and Z. Nováková, *Workbook fyziologie protokoly - biomedicínská technika a nelékařské obory*. Masarykova univerzita, 2021, ISBN: 9788021098978.

A Appendix - Breathing simulation

The findings provided in this chapter were presented at the European Medical and Biological Engineering Conference & Nordic-Baltic Conference on Biomedical Engineering and Medical Physics the 8th European Medical and Biological Engineering Conference and published as:

- R. Pasteka and M. Forjan, "Actively breathing mechanical lung simulator development and preliminary measurements", *IFMBE Proceedings*, vol. 65, pp. 751–754, 2017. DOI: 10.1007/978-981-10-5122-7_188
- R. Pasteka, M. Forjan, and A. Drauschke, "Comparison of mathematical and controlled mechanical lung simulation in active breathing and ventilated state", vol. 51, no. 6, pp. 42–47, 2018, ISSN: 24058963. DOI: 10.1016/j.ifacol.2018.07.127
- R. Pasteka, J. P. Santos da Costa, and M. Forjan, "Characteristic waveforms for testing of medical aerosol inhalers", *8th European Medical and Biological Engineering Conference*, pp. 240–246, Nov. 2021. DOI: 10.1007/978-3-030-64610-3_28

This appendix summarises work focusing on simulation and evaluation of various breathing patterns. Reliable breathing simulation is fundamental for any application of the xPULM™ and spans from a comparison of the simulation to spirometry measurements to an evaluation of waveforms suitable for testing of inhalation devices.

A.1 Comparison of Sinusoidal Breathing Simulation with Spirometry

The spirometry measurements for this preliminary testing were recorded by 16 volunteers, age 24±0.9, 9 males, 7 females. All volunteers were non-smokers without a history of pulmonary diseases. The summary of relevant parameter values is given in Tab. A.1 and depicted in Fig. A.1.

Tab. A.1: Summary of the relevant parameter values for Spirometry (recorded with healthy volunteers) and breathing simulation with the xPULM™

Breathing pattern	Analysed breathing cycles [-]	Tidal volume [L]	Breathing frequency [bpm]	Maximum of inspiration* [%]	Lung equivalent [-]
Spirometry	148	0.78±0.38	13±3.3	45	Not applicable
PI mode	37	1.34±0.04	12**	46	2.3 L latex bags
Sin mode	46	0.98±0.09	12**	49	Porcine lungs

* given as a percentage of a breathing cycle after time normalisation; ** STD < 1 bpm

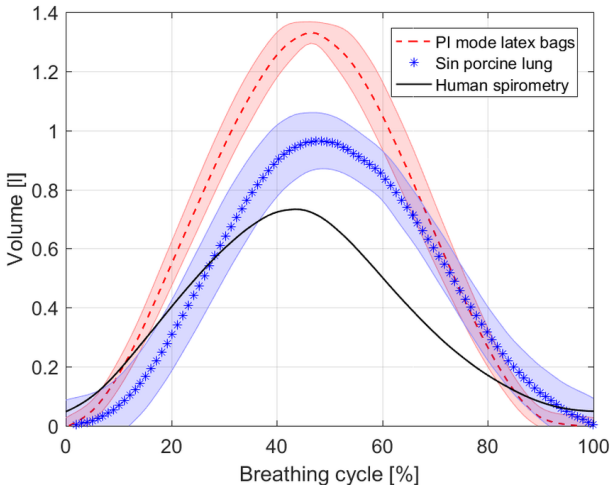

Fig. A.1: Comparison of average breathing cycle for: A) Spirometry - Healthy volunteers (solid line) B) xPULM™ set in PI sin mode (dashed line) C) xPULM™ set in Sin mode (stars).

A.2 Simulation of Breathing at Rest

A simplified model of a human respiratory system capable of describing flow dependencies at rest is a simple linear model, depicted in Fig. A.2. The airway resistance (R) over the whole length of a respiratory tract together with lung compliance (C) is assumed to be constant and also unchangeable in the course of the entire time of the simulation. This well-known single-compartment model is described with the following equation:

$$P_{mus}(t) = \frac{1}{C}V(t) + R\dot{V}(t) \tag{A.1}$$

Where: P_{mus} is a respiratory pressure generated by respiratory muscles, C is a lung's compliance R is an airway resistance, $V(t)$ is an air volume breathed in lungs and $\dot{V}(t)$ is a respiration air flow, model adapted from [181]. The performed simulation was run with following physiological values $R = 0.18\ Pa \cdot s/L$ and $C = 1.84\ L/kPa$ which were taken from [181].

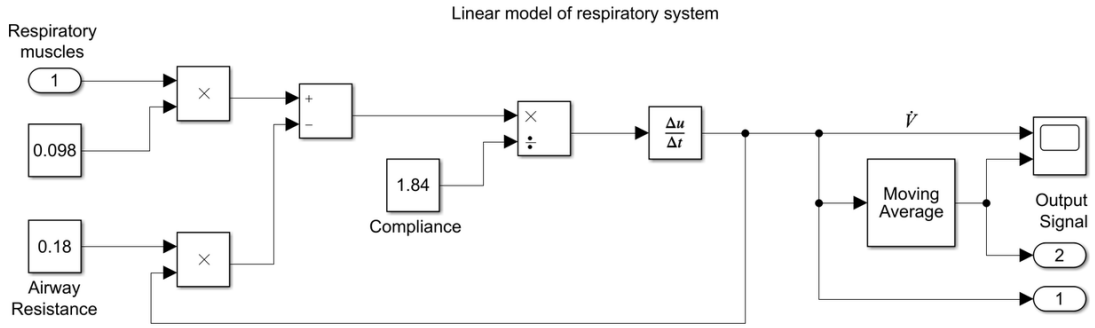

Fig. A.2: Linear single compartment model of the respiratory system (based on [181])

Comparison of the output of the linear single compartment model (required breathing pattern) with breathing simulation using xPULM™ is depicted in Fig. A.3.

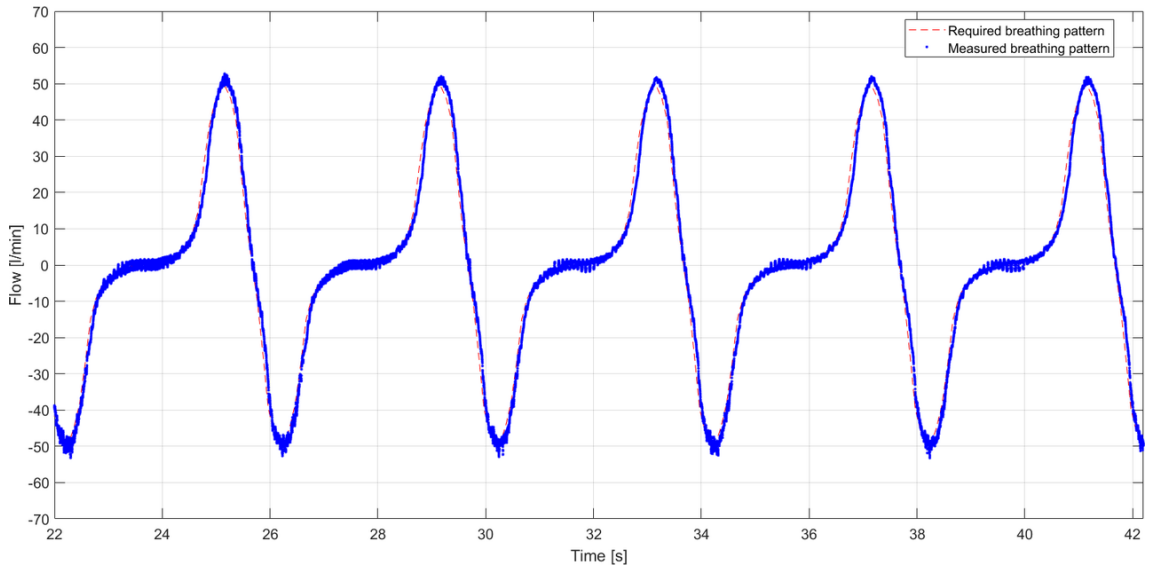

Fig. A.3: Breathing at rest - linear single compartment model: A) Red dashed line - required curved defined as an output of a mathematical model B) Blue dotted line - xPULM™ flow measurements

A.3 Simulation of Artificially Ventilated Patient

A simulation of an artificially ventilated patient suffering from cystic fibrosis is based on the non-linear single compartment mathematical model of the human respiratory system developed by [86]. The presented model further expands the simple linear single-compartment model by taking into account the dynamic, nonlinear and nonstationary character of the human respiratory system. The properties of the respiratory system are described by non-linear static and dynamic compliance and nonlinear flow-resistance. Resulting transfer functions describing two components of the lung compliance are:

$$G_{V1}(s) = \frac{1}{\tau_1 s + 1} \qquad G_{V2}(s) = \frac{1}{\tau_2 s + 1}. \tag{A.2}$$

Where: time constants represent the fast change in the lung volume due to lung elasticity $\tau_1 s$ or slow change due to viscosity $\tau_2 s$.

Furthermore, the upper-airways resistance is considered to be flow-dependent, the lower-airways resistance is modelled as volume-dependent and the resistance of small airways is taken as a constant.

These considerations result in equation (A.3) describing the airways resistance:

$$R = R_0 + K_V V + K_F |V|. \tag{A.3}$$

Where: R_0 is the resistance of small airways, K_V is the resistances of upper airways and K_F is the resistance of lower airways [86].

The adapted model used for simulating artificially ventilated patient can be seen in Fig. A.4. The final values of parameters estimated by Mesic were used during simulations and verified before using the model parameter estimation tool of Simulink. The model's input signal is a pressure at the mouth recorded from a ventilated patient suffering from cystic fibrosis by [86].

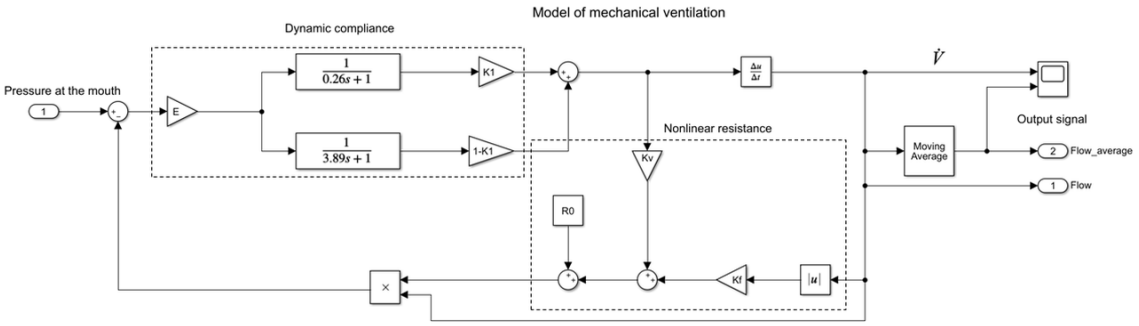

Fig. A.4: Complete non-linear single compartment mathematical model of the respiratory system (based on [86])

Comparison of the output of the non-linear single-compartment model (required breathing pattern) with breathing simulation using xPULM™ is depicted in Fig. A.5. The feedback control algorithm was also incorporated during this measurement. The fast changes of the signal during artificial ventilation lead to high demands on the mechanical system. Especially the rotational speed of the motor and the inertia of the system components lead to small fluctuations of the system's response. Nevertheless, these fluctuations are within an acceptable range and do not significantly influence the main flow output of the simulator.

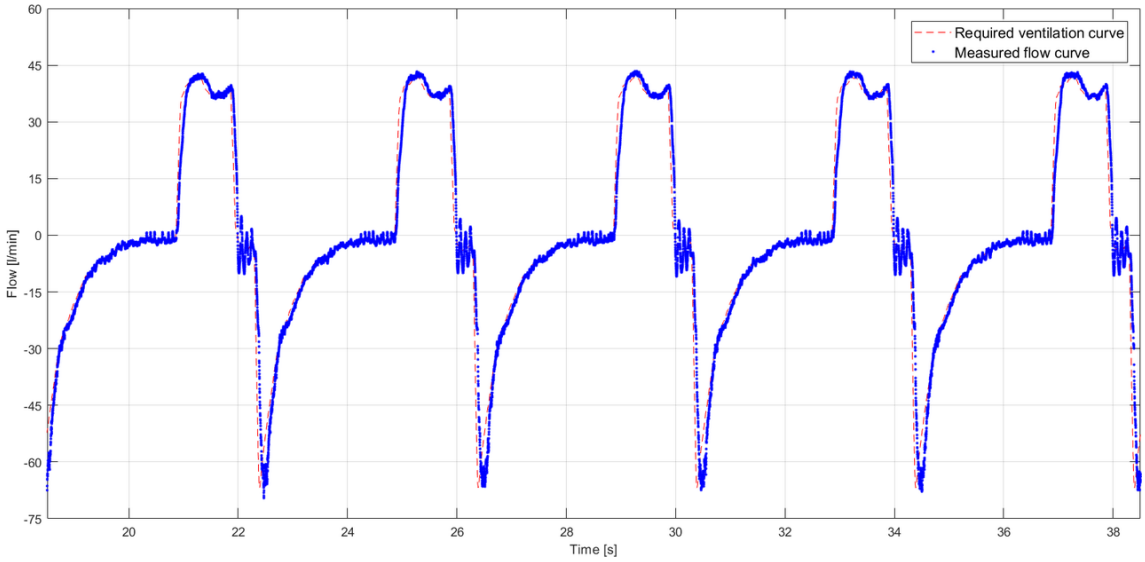

Fig. A.5: Artificially ventilated patient - non-linear single compartment model : A) Red dashed line - required curved defined as an output of a mathematical model B) Blue dotted line - xPULM™ flow measurements

A.4 Waveforms for Testing of Medical Inhalers

Four inhalatory waveforms, each covering a different inhalation scenario, are used for this comparison. The inhalatory waveforms are based on the work of [182] and are derived following the recommended instructions of use supplied by manufacturers with the medical inhalers. Typically the peak inhalatory flow rate (PIF) is reached at the time (t_{PIF}) occurring within the first 1/6 to 1/3 of the inhalatory period. All inhalatory waveforms used in this work were scaled to deliver the same total volume (V) of 2.5 L. The first two inhalatory waveforms represent a quick and deep (QD) inhalation (PIF = 83.32 L/min, t_{PIF} = 0.49 s) and a slow and deep (SD) inhalation (PIF = 34.59 L/min, t_{PIF} = 1.80 s). The equations describing inhalatory flowrate in

time for QD and SD waveform are [182]:

$$Q(t) = \frac{PIF}{t_{\mathrm{PIF}}} t \qquad \text{for} \quad 0 \leq t \leq t_{\mathrm{PIF}} \tag{A.4}$$

$$Q(t) = PIF \cos\left(\frac{2\pi(t - t_{\mathrm{PIF}})}{4(1 - tf_{\mathrm{PIF}} T}\right) \qquad \text{for} \quad t_{\mathrm{PIF}} \leq t \leq T \tag{A.5}$$

Where: tf_{PIF} is the time fraction of peak inhalatory flow rate and T is the period of inhalation.

The positive part of the sinus function (SIN) inhalation (PIF = 94.26 L/min, t_{PIF} = 1.24 s) represents an inhalatory waveform with the identical shape before and after reaching the PIF.

Additionally, the set of commonly used waveforms is extended by clinically recorded (CR) inhalation (PIF = 126.8 L/min, t_{PIF} = 0.42 s). The CR was obtained from spirometry measurement of 47 years old male suffering from mild COPD (Chronic Obstruction Pulmonary Disease) and represents a typical example of a focus group that utilises medical inhalers in everyday life. The spirometry was extracted throughout a retrospective study of respiratory signals recorded at the Department of Pulmonology of Centro Hospitalar De Trás-Os-Montes E Alto Douro hospital with the approval of the ethics committee.

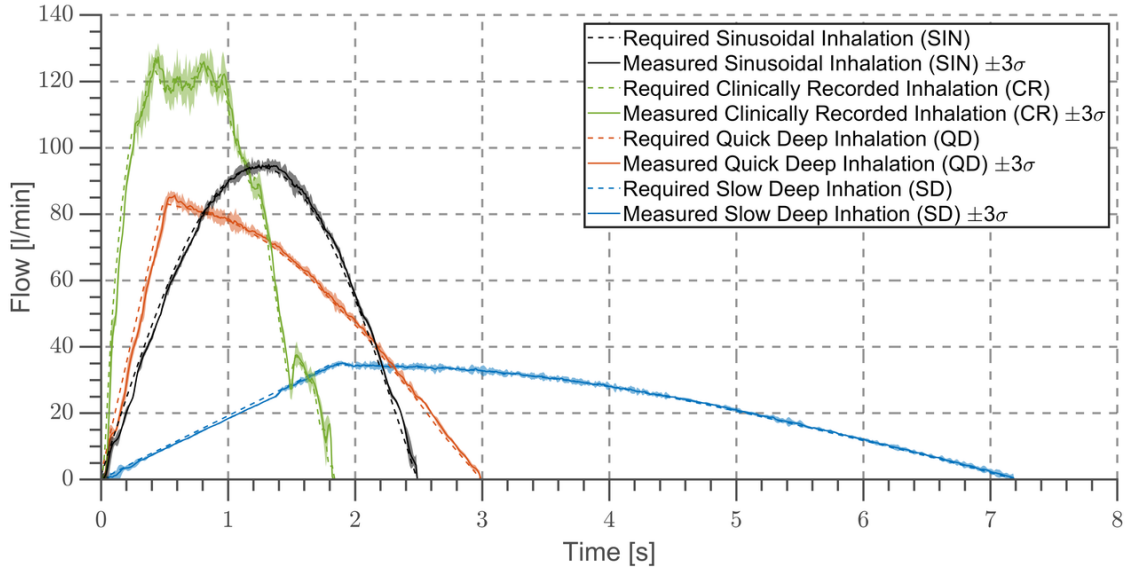

Fig. A.6: Comparison of simulation measurements with Sinusoidal (SIN), Clinically recorded (CR), Quick deep (QD) and Slow deep (SD) inhalatory waveforms. The required airflow output is indicated by dashed lines. The solid lines represent the mean measured airflow and the surrounding shaded bars the standard deviation 3σ, both calculated from 5 measurement trials.

B Appendix - Influence of breathing patterns on aerosol delivery

The findings provided in this chapter were presented at the 10th World Congress on Alternatives and Animal Use in the Life Sciences, 21st European Congress on Alternatives to Animal Testing, and the 41st Engineering in Medicine and Biology Conference. The contributions are published as:

- R. Pasteka and M. Forjan, "Changes of particle deposition caused by different breathing patterns during active lung simulation", *2019 41st Annual International Conference of the IEEE Engineering in Medicine and Biology Society (EMBC)*, pp. 4969–4972, Jul. 2019. DOI: 10.1109/EMBC.2019.8857407
- R. Pasteka, M. Forjan, and A. Drauschke. "Comparison of breathing patterns for aerosol inhalation using an electro-mechanical lung simulator". (2018), [Online]. Available: https://proceedings.altex.org/?2018-02 (visited on 10/02/2022)
- R. Pasteka and M. Forjan. "Evaluation of an active lung simulator for aerosol inhalation test replacement". (2017), [Online]. Available: https://proceedings.altex.org/?2017-01 (visited on 10/02/2022)

This appendix summarises work that has been done to evaluate the influences of breathing patterns on aerosol particle deposition. The changes in the number of in- and exhaled particles during several different breathing pattern situations are presented here. Representing natural conditions, polydisperse particles have been produced, leading to an aerosol covering a broad spectrum of particle sizes. The main particle diameter of the produced particles, 0.25 µm, was chosen to represent the subfraction of particulate matter.

Breathing was simulated using three breathing patterns (Fig. B.1), where the first one represents simplified breathing using a sinusoidal function as a basis. The second pattern represents more realistic breathing flows building upon a one-compartment model. The third breathing pattern is derived from human spirometry measurements and therefore includes natural fluctuations in frequency and breathing depth.

The decay of particle number during simulation is depicted in Fig. B.2. The differences between the number of inhaled and exhaled aerosol particles are visualised in Fig. B.3.

B.1 Breathing simulation for Aerosol Measurements

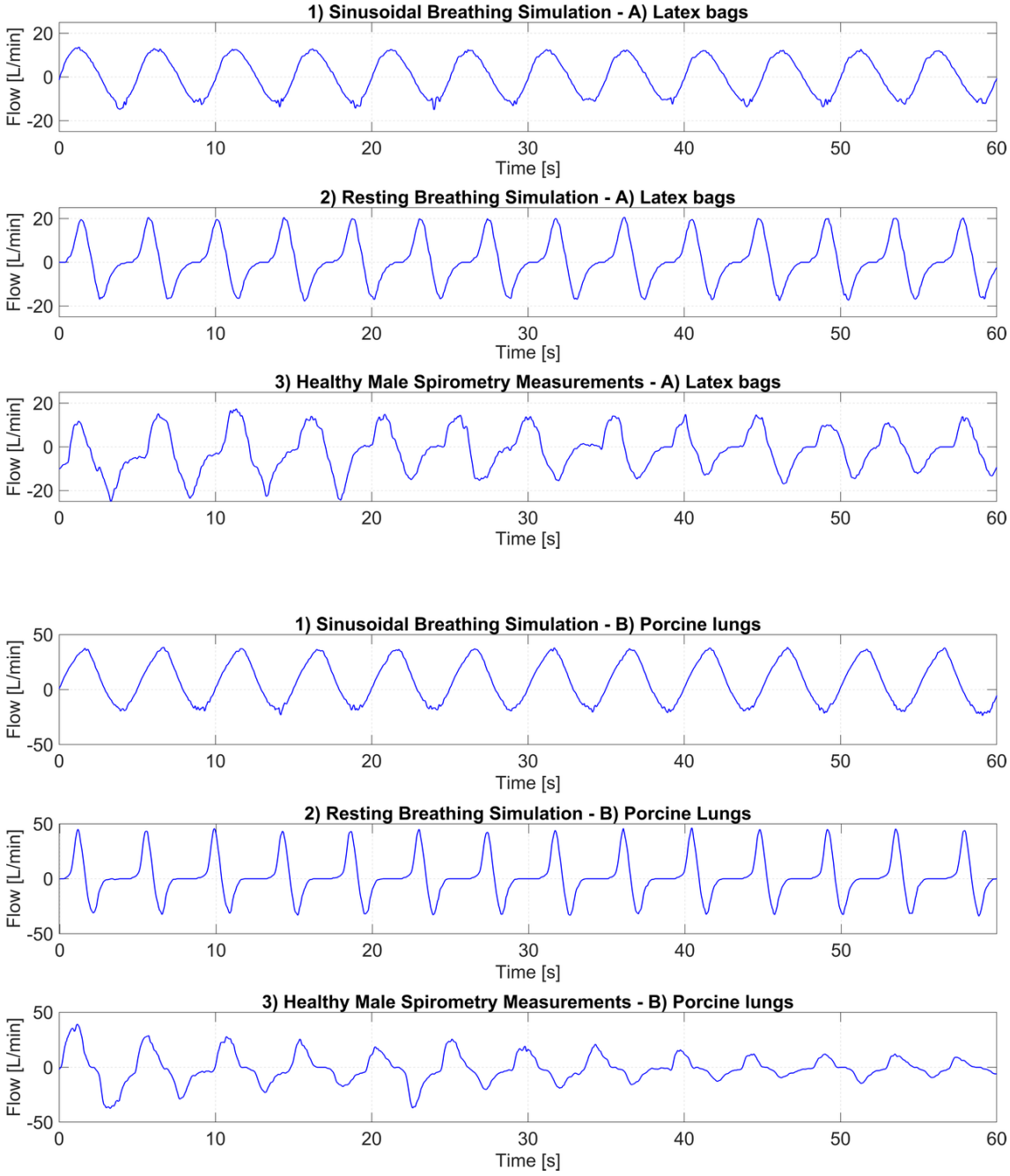

Fig. B.1: Airflow measurements recorded during simulation with xPULM™ for: 1) Sinusoidal Breathing Simulation, 2) Resting breathing Simulation, 3) Spirometry based breathing simulation. All breathing simulations were conducted with A) 2.3 L Latex bags and B) Porcine lungs

B.2 Decay of Particle Number During Breathing Simulations

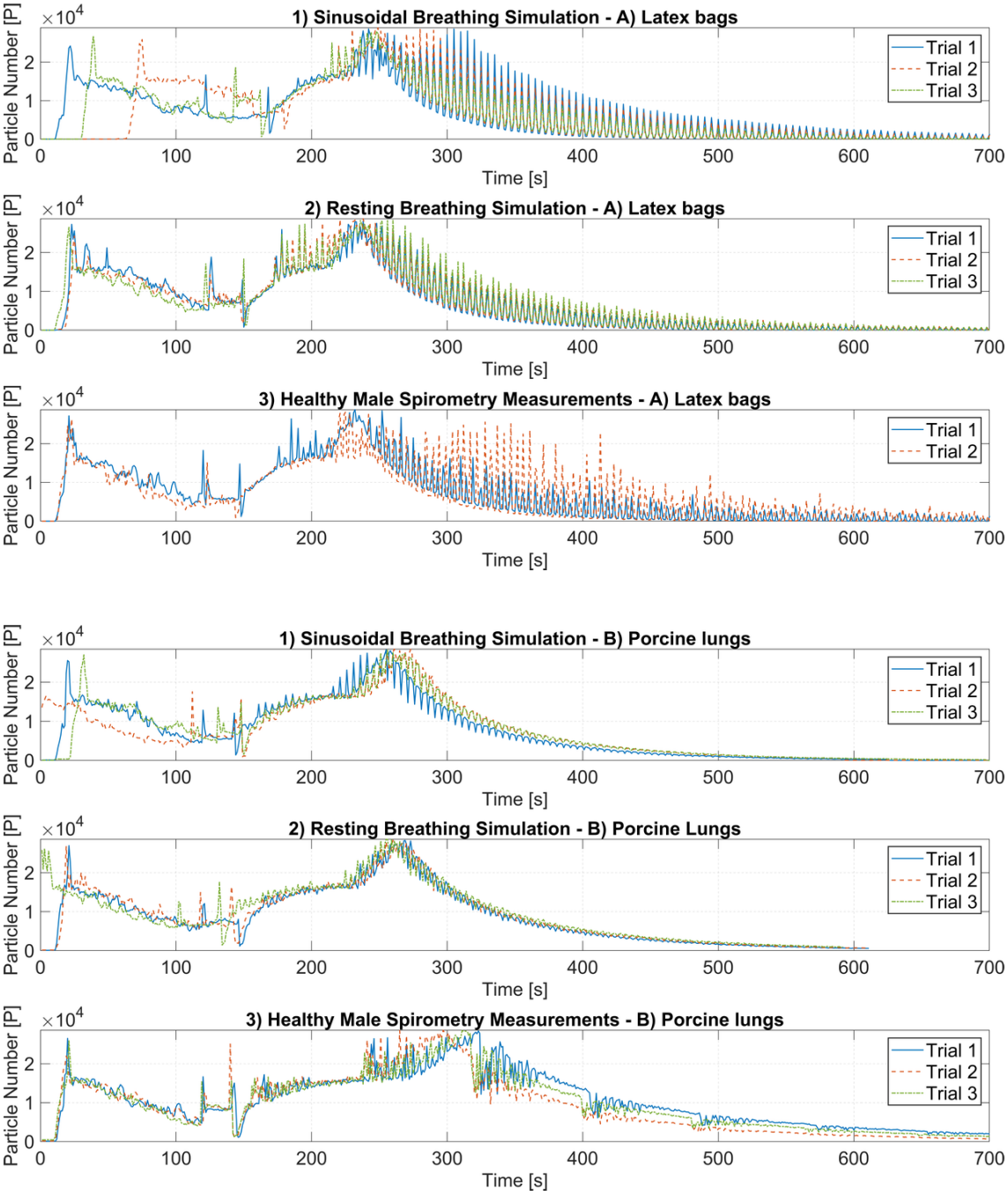

Fig. B.2: Decay of particle number during simulation with xPULM™ for: 1) Sinusoidal Breathing Simulation, 2) Resting breathing Simulation, 3) Spirometry based breathing simulation. Measurements were conducted with A) 2.3 L Latex bags and B) Porcine lungs

B.3 Differences between the number of inhaled and exhaled aerosol particles

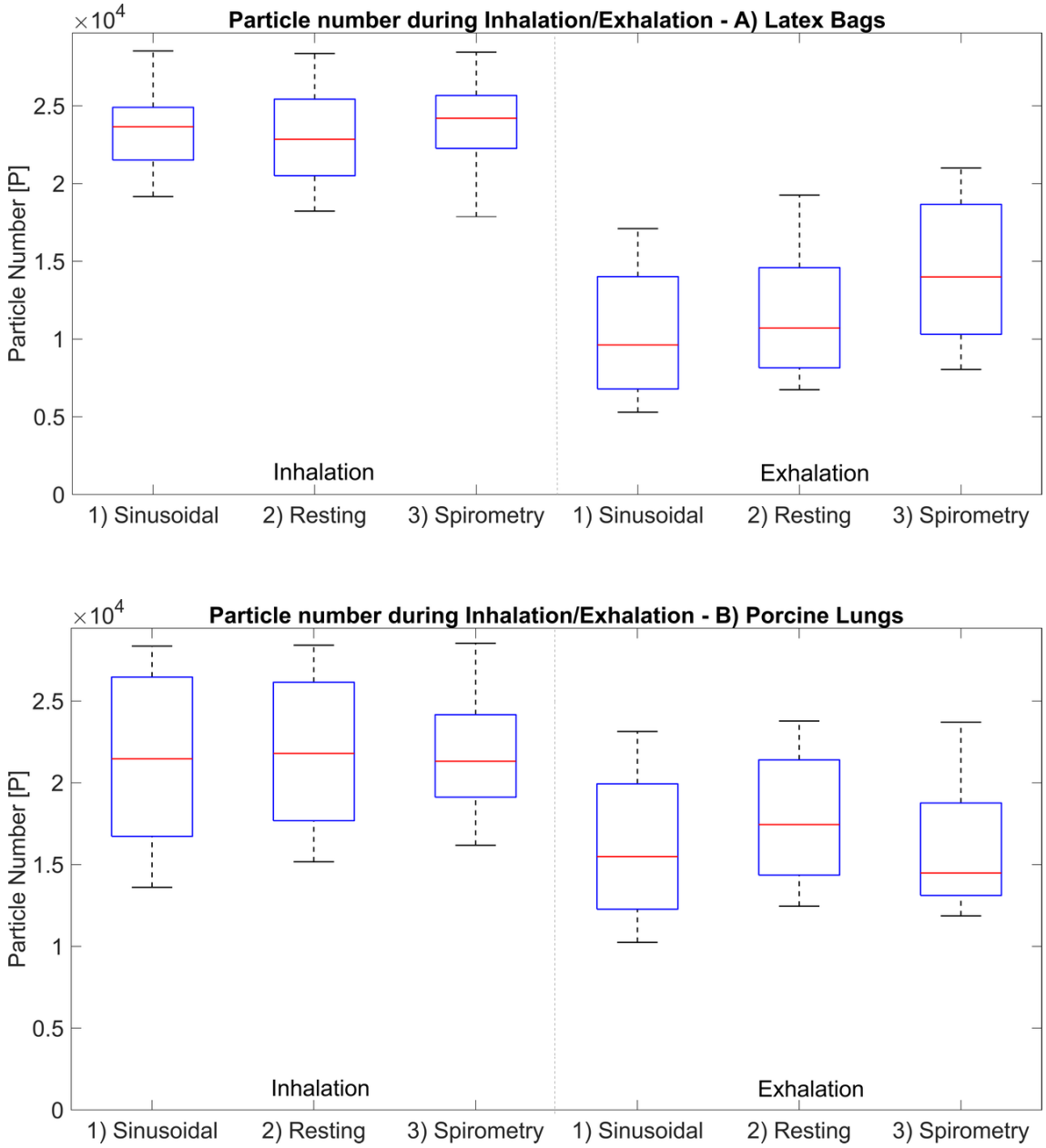

Fig. B.3: Differences between the number of inhaled and exhaled aerosol particles for: 1) Sinusoidal Breathing Simulation, 2) Resting breathing Simulation, 3) Spirometry based breathing simulation. Measurements were conducted with A) 2.3 L Latex bags and B) Porcine lungs

List of publications & scientific activities

Articles in journals with impact factor

- R. Pasteka, M. Forjan, S. Sauermann, and A. Drauschke, "Electro-mechanical lung simulator using polymer and organic human lung equivalents for realistic breathing simulation", *Scientific Reports*, vol. 9, no. 1, pp. 1–12, 2019. DOI: 10.1038/s41598-019-56176-6
- R. Pasteka *et al.*, "Patient–ventilator interaction testing using the electromechanical lung simulator xpulm during v/a-c and psv ventilation mode", *Applied Sciences*, vol. 11, p. 3745, 9 Apr. 2021, ISSN: 2076-3417. DOI: 10.3390/app11093745
- R. Pasteka *et al.*, "Experimental Evaluation of Dry Powder Inhalers During In- and Exhalation Using a Model of the Human Respiratory System (xPULM™)", *Pharmaceutics 2022, Vol. 14, Page 500*, vol. 14, no. 3, p. 500, Feb. 2022, ISSN: 1999-4923. DOI: 10.3390/PHARMACEUTICS14030500
- M. Gottschalk *et al.*, "From integration profiles to interoperability testing for smart energy systems at connectathon energy", *Energies*, vol. 11, p. 3375, 12 Dec. 2018, ISSN: 19961073. DOI: 10.3390/en11123375

Articles in international conference proceedings (indexed in WoS or Scopus)

- R. Pasteka, J. P. Santos da Costa, and M. Forjan, "Characteristic waveforms for testing of medical aerosol inhalers", *8th European Medical and Biological Engineering Conference*, pp. 240–246, Nov. 2021. DOI: 10.1007/978-3-030-64610-3_28
- R. Pasteka and M. Forjan, "Changes of particle deposition caused by different breathing patterns during active lung simulation", *2019 41st Annual International Conference of the IEEE Engineering in Medicine and Biology Society (EMBC)*, pp. 4969–4972, Jul. 2019. DOI: 10.1109/EMBC.2019.8857407
- R. Pasteka, M. Forjan, and A. Drauschke. "Comparison of breathing patterns for aerosol inhalation using an electro-mechanical lung simulator". (2018), [Online]. Available: https://proceedings.altex.org/?2018-02 (visited on 10/02/2022)
- R. Pasteka, M. Forjan, and A. Drauschke, "Comparison of mathematical and controlled mechanical lung simulation in active breathing and ventilated state", vol. 51, no. 6, pp. 42–47, 2018, ISSN: 24058963. DOI: 10.1016/j.

ifacol.2018.07.127

- M. Forjan, R. Pasteka, and A. Drasuchke. "Lung simulation – an alternative approach to animal testing for applications in aerosol and respiratory research". (2018), [Online]. Available: https://proceedings.altex.org/?2018-02 (visited on 10/02/2022)
- R. Pasteka and M. Forjan, "Actively breathing mechanical lung simulator development and preliminary measurements", *IFMBE Proceedings*, vol. 65, pp. 751–754, 2017. DOI: 10.1007/978-981-10-5122-7_188
- R. Pasteka and M. Forjan. "Evaluation of an active lung simulator for aerosol inhalation test replacement". (2017), [Online]. Available: https://proceedings.altex.org/?2017-01 (visited on 10/02/2022)
- R. Pasteka, M. Forjan, and S. Sauermann, "Development of a multidisciplinary and telemedicine focused system database", *Studies in Health Technology and Informatics*, vol. 236, pp. 144–151, 2017. DOI: 10.3233/978-1-61499-759-7-144
- R. Pasteka, M. Forjan, and V. David, "A single point of contact data platform for rehabilitative exercises and equipment: Development of the rehabitation database", *ACM International Conference Proceeding Series*, pp. 317–322, 2018. DOI: https://doi.org/10.1145/3218585.3218676
- V. David *et al.*, "Development of a multi-purpose easy-to-use set of tools for home based rehabilitation: Use cases and applications developed during the rehabitation project", *ACM International Conference Proceeding Series*, pp. 323–330, 2018. DOI: 10.1145/3218585.3218677
- M. Frohner *et al.*, "Smart grid interoperability profiles development", *2017 IEEE International Conference on Smart Grid Communications (SmartGridComm)*, pp. 189–194, October Oct. 2017. DOI: 10.1109/SmartGridComm.2017.8340674
- M. Gottschalk *et al.*, "Structured workflow achieving interoperable smart energy systems", *Energy Informatics*, vol. 1, p. 25, S1 Oct. 2018, ISSN: 2520-8942. DOI: 10.1186/s42162-018-0039-x

Book chapters

- J. Hrušková *et al.*, "Fyziologie – teorie k praktickým cvičením", 2021, Electronic book
- J. Hrušková *et al.*, *Workbook fyziologie protokoly - biomedicínská technika a nelékařské obory*. Masarykova univerzita, 2021, ISBN: 9788021098978

Invited lectures/presentations

- R. Pasteka, “Applications of human respiratory system modelling in the context of biomedical engineering”, Vienna University of Technology, Wien, 2021
- R. Pasteka “Applications of Biomedical Engineering in Respiratory Care”, University of Trás-os-Montes and Alto Douro, 2020
- R. Pasteka, “Hands-on learning and research applications”, International Week Turku, 2019
- R. Pasteka “Human Respiratory System Modelling”, University of Trás-os-Montes and Alto Douro, 2019

Reviewer activities

- Biomedical signal processing and control journal, Cell biology and toxicology journal, IEEE access journal,